NOTICE

The quality of this microfiche is heavily dependent upon the quality of the original thesis submitted for microfilming. Every effort has been made to ensure the highest quality of reproduction possible.

If pages are missing, contact the university which granted the degree.

Some pages may have indistinct print especially if the original pages were typed with a poor typewriter ribbon or if the university sent us a poor photocopy.

Previously copyrighted materials (journal articles, published tests, etc.) are not filmed.

Reproduction in full or in part of this film is governed by the Canadian Copyright Act, R.S.C. 1970, c. C-30. Please read the authorization forms which accompany this thesis.

THIS DISSERTATION
HAS BEEN MICROFILMED
EXACTLY AS RECEIVED

AVIS

La qualité de cette microfiche dépend grandement de la qualité de la thèse soumise au microfilmage. Nous avons tout fait pour assurer une qualité supérieure de reproduction.

S'il manque des pages, veuillez communiquer avec l'université qui a conféré le grade.

La qualité d'impression de certaines pages peut laisser à désirer, surtout si les pages originales ont été dactylographiées à l'aide d'un ruban usé ou si l'université nous a fait parvenir une photocopie de mauvaise qualité.

Les documents qui font déjà l'objet d'un droit d'auteur (articles de revue, examens publiés, etc.) ne sont pas microfilmés.

La reproduction, même partielle, de ce microfilm est soumise à la Loi canadienne sur le droit d'auteur, SRC 1970, c. C-30. Veuillez prendre connaissance des formules d'autorisation qui accompagnent cette thèse.

LA THÈSE A ÉTÉ
MICROFILMÉE TELLE QUE
NOUS L'AVONS REÇUE

A Laboratory Investigation of Possible Improvements in the Mixing of 90°-Confluence Flows at Box Culvert Outlets

by

Douglas M. Joy

A Thesis
presented to the University of Ottawa
in partial fulfillment of the
requirements for the degree of
Master of Applied Science
in
Department of Civil Engineering

Ottawa, Ontario, 1980

PREFACE

Intersecting channels is a situation that is often encountered in land drainage. For example, this is frequently the case with highway drainage culverts, where a culvert through a roadway embankment discharges into a receiving stream flowing parallel to the embankment. Quite often, because of the complex mixing processes at the confluence, many intersections of this type require special considerations. These special considerations may include protection of the natural channel boundaries against excessive erosion and the prediction of confluence energy losses. In the absence of special outlet structures (e.g. stilling basins) these problems are often solved by stabilizing the stream boundaries in the immediate vicinity of the junction (rip-rap protection, gabions, etc.) and/or reducing the angle of intersection between the two channels. However, these solutions can also be expensive, both in capital, and maintenance costs. On the other hand, little work has been done to improve culvert outlet geometry with a view to reducing confluence losses and abnormal scour in the junction area.

Knowledge of the flow conditions at a confluence can help the designer regarding two important design considerations. First they can assist the engineer in better evaluating the energy loss through the confluence, by knowing the

order of magnitude of the losses due to the confluence, and knowing the energy correction factors downstream of the confluence. Secondly, prior knowledge of boundary shear stresses that may occur will allow the engineer to provide the required protection needed to prevent erosion.

The goal of this study was to investigate, by means of a physical model, the effects of small changes in culvert outlet geometry on the flow conditions at and downstream of the confluence. This with the goal that an overall reduction in cost for a typical installation could be achieved by having a 90° intersection and yet providing minimal protection against scour in the receiving channel.

A laboratory model with 1.83 m and 12.3 m long channels (representing the lateral culvert and receiving channel respectively) was used in the study. Evaluation of the performance of each outlet geometry tested was over a range of flow rates and by measurement of several pertinent parameters. These parameters included boundary shear stresses, energy correction factors and the energy loss through the confluence over and above that loss due to friction.

It was found that the use of energy correction factors equal to unity, as has been routinely done in the past, would lead to errors as high as 95% in the estimation of

kinetic energy levels downstream of the confluence. In addition to this results showed that substantial improvement in the flow conditions downstream of the confluence could be achieved by beveling (flaring) the downstream corner of the culvert outlet.

The principal areas in which this geometric alteration showed improvement were as follows: (i) reduction in the energy correction factor (which can be used as an indicator of the degree of velocity distribution distortion); and (ii) reduction in the boundary shear stresses generated immediately downstream of the confluence. Although these reduced values (particularly the shear stresses) were not as small as those found for uniform flow conditions, the overall improvement over that for a square-edged outlet was none-the-less substantial. Finally, although related energy losses were determined, values were found to be quite erratic and since no identifiable trend was noted it was not possible to state, conclusively, the effects of these outlets change on confluence energy losses.

ACKNOWLEDGEMENTS

This work would not have been possible without the assistance of several members of the staff of the Civil Engineering Department at the University of Ottawa. Mr. R. Moore supplied countless hours of time during the laboratory work, both during the construction and testing of the model. Without his skills as a craftsman the apparatus would undoubtedly have been much less satisfactory than it was. Particular thanks are due to Dr. D.R. Townsend, whose encouragement and expertise in Hydraulics were invaluable to the author. Finally, acknowledgement is also given to the National Research Council of Canada, who supplied the funds for the construction of the model and a Scholarship to the author.

TABLE OF CONTENTS

LIST OF TABLES

LIST OF PLATES

LIST OF FIGURES

Figure page

NOMENCLATURE

d	- thickness of turbulent boundary layer
d_o	- diameter of pitot tube
e	- total energy/unit mass
e_p	- potential energy/unit mass
e_u	- energy/unit mass with respect to local temperature
e_v	- kinetic energy/unit mass $(v^2/2)$
g	- gravitational acceleration
h	- local elevation
n	- Manning roughness coefficient
n_b	- ratio of lateral channel width to main channel width (B_l/B_m)
n_q	- ratio of lateral channel flow to combined flow (Q_l/Q_t)
p	- local pressure
v	- local velocity
v_b	- local velocity measured with pitot tube against boundary
v_*	- shear velocity $(\tau/\rho)^{1/2}$
y	- distance from channel boundary
A	- area of channel cross section
$d\vec{A}$	- area vector, normal to surface
B_l	- lateral channel width
B_m	- main channel width
C	- Chezy roughness coefficient

E	- energy level in control volume
dE	- change in total energy in control volume
$H_{f_{1-2}}$	- friction loss from section 1 to 2
$H_{T_{1-2}}$	- turbulent energy loss/unit weight from section 1 to 2
H_{T_l}	- turbulent energy loss/unit weight of lateral channel flow
H_{T_m}	- turbulent energy loss/unit weight of main channel flow
H_{T_t}	- total turbulent energy loss
δH	- heat added to a system from its surroundings
K_e	- velocity head correction factor
N_R	- Reynolds number
P_w	- wetted perimeter of cross section
Q	- flow rate
Q_l	- flow rate in lateral channel
Q_m	- flow rate in main channel upstream of junction
Q_t	- combined flow rate ($Q_m + Q_l$)
R	- hydraulic radius of cross section
S_o	- channel bed slope
V	- average velocity over cross section (Q/A)
V_o	- free flow velocity
$\forall$	- control volume
$\vec{V}$	- velocity vector
$W_{pressure}$	- work done by fluid pressure
W_{shaft}	- work done by fluid on a rotating shaft
W_{shear}	- work done by fluid shear stress

δW - work done by a system on its surroundings

X - distance along main channel from channel junction (positive downstream)

X' - relative distance along main channel (X/B_m)

X_1 - distance from start of channel to origin of turbulent boundary layer

X_2 - distance from origin of turbulent boundary layer

X_{1-2} - distance from cross section 1 to 2

Y - distance from left wall

Y' - relative distance across channel (Y/B_m)

Z - distance from channel bed

Z_{o_t} - uniform flow depth for combined flow rates

Z' - relative depth in channel (Z/Z_{o_t})

γ - specific weight of water

θ - angle of intersection of two channels

ν - kinematic viscosity of water

ξ_l - turbulent energy loss coefficient for lateral channel flow

ξ_m - turbulent energy loss for main channel flow

ξ_t - total turbulent energy loss coefficient

ρ - density of water

τ - local boundary shear stress

$\bar{\tau}_o$ - average boundary shear stress

Chapter I

INTRODUCTION

1.1 INTRODUCTORY REMARKS

In the field of Open Channel Hydraulics situations sometimes occur which are often difficult, if not impossible, to describe using the conventional flow equations. This can be due to any number of reasons, including high degrees of turbulence and large numbers of flow field influencing variables. The complex flow field generated at the confluence of two intersecting channels is just such a situation.

Channel junctions are often encountered in highway culvert design, i.e. discharge through a roadway embankment into a larger (receiving) stream flowing parallel to the embankment. If the flow rate of the larger stream is much larger than that discharging from the culvert, this situation presents no particular hydraulic problems and can be adequately described using one-dimensional flow equations. If, however, the flow discharging from the culvert becomes substantial (relative to the receiving stream) the direct discharge of the lateral flows into the natural stream may cause significant problems. At the confluence of the two

streams the complex (and highly turbulent) mixing processes generate both an unstable and asymmetrical flow field in the vicinity of the intersection. This instability in the flow produces (secondary) surface waves which then propagate downstream for some distance. Also, a severely distorted velocity distribution results in high boundary shear stress concentrations which in turn can cause severe local scour of the natural channel. The occurrence of either of these two phenomena is generally considered unacceptable in culvert design. Thus for design purposes, the practicing engineer is concerned with minimizing these, as well as determining the magnitude of the confluence energy losses.

In present practise avoidance of local scour and downstream disturbances (surface waves) is usually accomplished in one of two ways. The first approach is to keep the angle of intersection of the two streams to an absolute minimum. Although this avoids the above mentioned problems very effectively (with some significant restrictions discussed in the next chapter) it requires very long culvert lengths at small angles of intersection. Also, in some cases this may not be possible, either because of 'right-of-way' limitations or because the culvert may already be in place before a problem is realized. The other solution quite often used is to provide protection to the boundaries of the natural stream, not only in the area of the intersection, but also

for some distance downstream. This, however, has the disadvantage of high cost and in addition the necessity of periodic maintenance.

While a considerable amount of work has been done in the past concerning highway culvert design, most investigators have concentrated their efforts on the reduction of head losses at the culvert inlet (8,10). Culvert outlets on the other hand have received little or no attention (except when they are designed like spillways) and are usually constructed as mirror images of the inlets. This is contrary to the fact that the design objective at the inlet is to minimize the energy losses and at the outlet the objective is quite often to maximize the losses.

1.2 STUDY GOALS

Given this paucity of information on intersecting channels in general and specifically for that where culvert outlets are concerned, it was the goal of this research project to investigate possibilities whereby the length of a culvert could be minimized (by having a 90° intersection) and the required scour protection lessened; all of these so that an overall cost savings could be realized for the typical installation. To be able to realize an economic benefit and yet have an inflow at large angles of intersection requires two things:

1. An improved outlet junction structure to promote a more efficient mixing of the two streams;

2. Rapid dissipation of the lateral momentum introduced by the lateral inflow.

These will first of all minimize the levels of turbulence and instability generated at the confluence which cause surface waves to propagate downstream. Secondly, and perhaps more importantly, high boundary shear stresses (caused by distorted velocity distributions) which encourage scour will be reduced. It is possible that by altering the geometry of the culvert outlet this can be accomplished at an overall cost savings.

Due to the aforementioned instability and complexity of the flow field, the hydraulic conditions at the channel confluence are difficult to describe accurately from a theoretical viewpoint. This situation then lends itself well to a scale model study to examine the mixing processes and monitor the effects produced by discrete changes in the junction geometry.

In studying the effectiveness of various proposed junction geometries several aspects of the flow field will be examined. First, dye studies will be made to determine, qualitatively, the mixing patterns of the two streams for a

wide range of flow conditions. Secondly, velocity profiles will be obtained at several locations downstream of the junction to examine the residual effects of the initial mixing process on the combined flow. Thirdly, actual boundary shear stress distributions (based on the resulting distorted flow field) will be determined to identify where scour may occur. Finally, energy balances will be made through the junction and the losses due to friction and turbulence determined.

In installations where very high velocities occur, say an average velocity of over 2.5 m/s, channel bed protection by itself will not necessarily prevent scour and thus sophisticated energy dissipators (e.g. stilling basins) must be employed. The present study was directed more towards installations which have average velocities below these high values. For example if the model scale was taken as 1:4, a typical average outlet velocity of 0.5 m/s would represent a prototype velocity of 1.0 m/s and therefore would be in the lower velocity range and would not require sophisticated dissipators.

Chapter II

LITERATURE REVIEW

The mixing of intersecting streams has been studied by many, and, as stated by Chow (p. 512) (6),

> "The conclusions of such studies indicate that generalization of the problem is not possible or even desirable. When the application of hydraulic theory to the problem encounters limitations, a model study will give the best solution for the flow characteristics involved."

These studies have been either analytical, analytical with experimental data or just experimental in nature. All approaches have met with some success but all have illustrated how complex the situation is. By far the most successful types of studies are those that are strictly experimental in nature. These are invariably designed to optimize one or a few specific situations with regard to some desired performance criteria and well defined constraints.

The first to study the intersection of two channels was Taylor (20). In his work Taylor developed an equation to determine the ratios of the upstream and downstream depths based on momentum theory. While the results were rather good for an angle of intersection of 45^{o}, at a higher angle of intersection (135^{o}) they became rather poor. This was

undoubtedly due to the fact that a more severe angle of intersection results in larger distortion of the downstream velocity distribution. This leads to a momentum correction factor[1] substantially greater than unity, (Taylor used unity in his formulations). It should be noted that all of the flows in this study were tranquil. In the discussion following, Palmer (14) suggested two things of interest:

1. Analysis should be on the basis of energy;

2. The shape of the junction would have a profound effect on the results and that rounding of the corners would improve the flow conditions.

This then defined the two theoretical approaches, one using momentum considerations (as Taylor used) and another using energy considerations (as Palmer suggested).

Work done by Bowers (4) is typical of those purely experimental in nature. This was one of the first publications indicating the problems which occur at junctions. Those indicated were:

1. Wave generation;

---

[1]Momentum and energy correction factors relate the momentum and energy calculated using the average flow velocity and the values calculated by integrating across the cross section. Generally these are taken to be equal to the minimum possible of unity.

2. High local scour;

3. Formation of hydraulic jumps in the channels.

The results of this study, after many trials, were the design of junction geometries which would work well over a range of flows for a specific location. An important aspect of this study is that the problem of scour was solved by lining the channels with non-erodable material.

Atalik (1) was the first to attempt a general study of the energy conditions at the confluence of two open channels. The author examined many of the parameters to be determined in the present study for one junction geometry and at one angle of intersection (90^{o}). This included determination of the distortion of the velocity profiles and their change downstream, as well as energy losses through the junction. However, probably the most significant contribution was his determination of the energy and momentum correction factors, which were found to be well above unity. In addition the author identified some locations of high velocity and the existence of a 'dead' zone just downstream of the junction.

Many investigators have examined the situation of sewer junctions, including Pardee (15), Sangster et al (17), Stev-

ens (19) and Lorah (13). Those that concern only pressure (or pipe full) flow (17,19) however, are of little significance to the present study.

Pardee (15) used a momentum balance approach applied to the particularities of a storm sewer junction to enable the designer to determine some of the parameters concerning the design of the junction. Of interest here are the assumptions used:

1. The momentum correction factors are equal to unity;

2. Normal depth occurs immediately downstream of the junction;

3. Friction effects can be ignored.

The author states that the accuracy of the formulas developed have been confirmed by numerous model tests, although no data is given to demonstrate this.

Using a totally empirical approach, Lorah (13) tried to develop equations to predict the power loss in a 'free-surface' pipe junction. The author studied two types of junctions, one which had intersecting pipes whose crown elevations were equal and another with equal invert elevations. The relationships developed were based soley on the

data without any regard for a theoretical basis. The author was able to obtain a good working relationship for the case where the inflow was at the upper inlet but not for the lower. Also of interest was the fact that an energy correction factor equal to unity was assumed and that the lower inlet always had less power loss than the upper inlet.

Although Barella (2) limited his model study to a series of very specific situations and thus the results cannot be generalized for all junctions, the conclusions are nonethe-less of interest. In the study optimum designs for several sites were determined based on minimizing wave heights and their propagation downstream. For all cases the flows were supercritical and the intersections consisted of spirals with the curves superelevated. Based on these criteria the conclusions were:

1. The water surface elevations of both incoming channels should be the same;

2. The angle of intersection should be almost 0°, and never greater than 12°;

3. Expansion of the width of the main channel downstream of the junction is favourable;

4. The velocities of the two channels should be nearly equal.

Finally, it should be noted that the final configurations were based on only one set of flow conditions.

Behlke and Pritchett (3) also concentrated their work on supercritical flows. The goals of their study were to reduce or eliminate the generation of wave pile-up. Although the authors looked at a wide range of flow conditions and junction geometries, they found that the problems could only be effectively solved for one set of design flow conditions and flow in only one channel. When the conditions deviated significantly from these, problems with wave pile-up occurred. Also of interest was the similarity in their conclusions with those of Barella (2).

By far the most comprehensive study of the energy losses to date was that done by Soong (18) and Lin and Soong (12). This was an attempt to determine the 'extra' energy loss in the junction due to the turbulence and to determine the streamwise variation of the energy correction factor. The authors found that the turbulent loss was in most cases larger than the friction loss and in all cases significant. In addition to measuring the streamwise variation of the energy correction factor, Soong developed an equation from first principles to predict this variation. Although the trends of the variation in the energy correction factor (determined by the author's equation and by actual measure-

ment) agree, the absolute values determined by the two methods differ significantly, and in addition the equation gives the obvious error of consistently giving some values of the energy correction factor less than unity.

Chapter III

NUMERICAL ANALYSIS

3.1 INTRODUCTION

The flow behaviour at the confluence of two channels has been studied numerically by many in the past. Mention has been made previously of the two different approaches to the analysis of the gross behaviour, those using energy and momentum considerations. In many of the analyses some assumptions have been used to simplify the problems. Some typical assumptions have been:

1. Uniform flow depth will occur downstream of the junction;

2. Frictional and other losses are negligible;

3. Energy and momentum coefficients are both equal to unity.

Most of these assumptions have not been found to be valid in the present study.

The analysis of any aspect except for the gross behaviour is made extremely difficult by the highly complex flow at the confluence. Because of this the analysis here has been limited to determining the energy loss through the confluence for the different junction structures tested. The

development of this is given in section 3.2.

Also of interest to the engineer are the distribution of boundary shear stresses, particularly the locations of the higher stresses. This, however, is usually difficult to determine and only an average value is obtainable. Use has been made of a technique using a pitot tube to determine these stresses and is presented in section 3.3.

3.2 ENERGY LOSSES

The analysis of the energy losses begins with the First Law of Thermodynamics, which states:

> "The difference between the heat added to a system of masses and the work done by the system depends only on the initial and final states of the system."

The difference in states is the change in energy (E), this can be expressed in equation form as:

$$dE = \delta H - \delta W \qquad 1.$$

Where:

dE = Increase in energy in the system;

δH = Heat added to the system from its surroundings;

δW = Work done by the system on its surroundings.

If this is then expressed as a rate of change in energy due to the rate of heat transfer and work done, Equation 1 becomes

$$\frac{dE}{dt} = \frac{\delta H}{dt} - \frac{\delta W}{dt} \qquad 2.$$

When this concept is applied to fluid mechanics, the work and energy terms are made up of several components. For work done by the fluid the components are:

$W_{pressure}$ - Work done by normal stresses (pressure) acting on the boundaries of the system;

W_{shear} - Work done by the tangential stresses (shear) acting on the boundaries;

W_{shaft} - Work done on a rotating element in the system transmitted outside the system by means of a shaft.

Thus:

$$\frac{\delta W}{dt} = \frac{\delta W_{pressure}}{dt} + \frac{\delta W_{shear}}{dt} + \frac{\delta W_{shaft}}{dt} \qquad 3.$$

For the energy term, if it is expressed as the energy/unit mass (e), the components are:

e_u - Internal energy/unit mass associated with the local temperature of the fluid;

e_p - Potential energy/unit mass associated with the position of the fluid. Equal to $g \cdot h$ where g is the gravitational acceleration and h is the local elevation to the fluid;

e_v - Kinetic energy/unit mass associated with the local velocity (v) of the fluid, (equal to $v^2/2$).

Thus the total energy/unit mass of the fluid can be expressed as:

$$e = e_u + e_p + e_v \qquad 4.$$

If this first law is now applied to some control volume, the rate of change of energy in the control volume is equal to the net rate of energy flux across the surface plus the rate of change within the volume. This is given in Equation 5.

$$\frac{dE}{dt} = -\oint_{cs} e\rho \, (\vec{V} \cdot d\vec{A}) + \frac{\partial}{\partial t} \int_{cv} (e\rho dV) \qquad 5.$$

in which:

$\vec{V}$ - Velocity vector;

$d\vec{A}$ - Unit area vector;

ρ - Density of the fluid;

$\forall$ - Control volume.

For a steady state condition the last term is zero, thus Equation 5 can be reduced to:

$$\frac{dE}{dt} = -\oint_{cs} e\rho(\vec{V}\cdot d\vec{A}) \qquad 6.$$

Now if the local pressure is given as p, the net rate at which work is being done by the pressure on the boundaries is:

$$\frac{\delta W_{pressure}}{dt} = -\oint_{cs} p(\vec{V}\cdot d\vec{A}) \qquad 7.$$

Combining equations 2, 3, 6 and 7 gives:

$$\frac{\delta H}{dt} - \frac{\delta W_{shaft}}{dt} - \frac{\delta W_{shear}}{dt} = -\oint_{cs} (\frac{p}{\rho} + e)\rho(\vec{V}\cdot d\vec{A}) \qquad 8.$$

For open channel hydraulics the second and third terms on the left side of the equation can be set equal to zero, thus this can be reduced to Equation 9.

$$\frac{\delta H}{dt} = -\oint \left(\frac{p}{\rho} + e\right) \rho \left(\vec{V} \cdot d\vec{A}\right) \qquad 9.$$

By choosing a control volume which has boundaries that are either a fixed surface, free surface or perpendicular to the velocity and by combining Equations 4 and 9, the following is obtained:

$$\frac{\delta H}{dt} = -\oint_{cs} \left(\frac{p}{\rho} + e_u + g \cdot h + \frac{v^2}{2}\right) \rho \left(\vec{V} \cdot d\vec{A}\right) \qquad 10.$$

This type of analysis can be found in most standard fluid mechanics texts, for example Daily and Harleman(7).

For open channel flows this can be applied between two cross sections (1 and 2) using average values and the following substitutions:

$\oint_{cs_1} \rho \left(\vec{V} \cdot d\vec{A}\right) = \rho Q$ = mass flow rate into control volume;

$\oint_{cs_2} \rho \left(\vec{V} \cdot d\vec{A}\right) = -\rho Q$ = mass flow rate out of control volume.

Making these substitutions into Equation 10 gives the following:

$$\frac{\delta H}{dt} = \left(\frac{p}{\rho} + e_u + g \cdot h + \frac{V^2}{2}\right)_2 \rho Q - \left(\frac{p}{\rho} + e_u + g \cdot h - \frac{V^2}{2}\right)_1 \rho Q \qquad 11.$$

Dividing by ρg and assuming that ρ and e_u remain constant reduces this still further to:

$$\frac{\delta H}{dt}/\gamma = \left(\frac{p}{\gamma} + h + \frac{V^2}{2g}\right)_2 Q - \left(\frac{p}{\gamma} + h + \frac{V^2}{2g}\right)_1 Q \qquad 12.$$

If the left side is neglected (or assumed to equal zero) and the right side of the equation is divided by the flow rate, Equation 12 becomes the familiar Bernoulli Equation. However, in situations where significant energy losses occur the $\frac{\delta H}{dt}/\gamma$ term must be retained to have a functional relationship. This term is then referred to as the 'losses' since the energy is not readily usable and is usually in the form of a boundary friction loss from cross section 1 to 2 ($-H_{f_{1-2}}$). Using this the general energy equation is written as:

$$\left(\frac{p}{\gamma} + h + \frac{V^2}{2g}\right)_1 Q - \left(\frac{p}{\gamma} + h + \frac{V^2}{2g}\right)_2 Q = QH_{f_{1-2}} \qquad 13.$$

In most uniform flow conditions Equation 13 adequately describes the flow and the boundary friction losses are usually determined using either the Manning (14) or the Chezy (15) equations (metric versions):

$$H_{f_{1-2}} = \frac{X_{1-2}\, n^2\, V^2}{R^{4/3}} \qquad 14.$$

$$H_{f_{1-2}} = \frac{X_{1-2}\, V^2}{R\, C^2} \qquad 15.$$

Where:

X_{1-2} - Distance between cross sections 1 and 2;

n,C - Roughness coefficients;

V - Average velocity (= Q/A);

R - Hydraulic radius (= A/P_w);

A - Cross sectional area;

P_w - Wetted perimeter.

However, in cases where high turbulence and distorted velocity distributions occur, Equation 13 fails to adequately describe the flow for two reasons:

1. Higher energy losses to internal fluid friction;

2. Substantial increases in the kinetic energy level over that given by $V^2/2$.

The assumption that:

$$\int \rho v^2 (\vec{V} \cdot d\vec{A}) = \rho \frac{Q^3}{A^2} = \rho V^2 Q \qquad 16a.$$

(which was used to obtain Equation 13) is true only when the velocity is constant across a cross section. However, when there is some variation in the local velocity within the cross section, this assumption leads to an underestimation of the kinetic energy. This then leads to the introduction of the energy correction factor (K_e) which is used to account for the discrepancy in Equation 16a.

$$\int \rho v^2 (\vec{V} \cdot d\vec{A}) = \rho K_e V^2 Q \qquad 16b.$$

Equation 13 is then rewritten using K_e:

$$(\frac{p}{\gamma} + h + K_e \frac{V^2}{2g})_1 Q - (\frac{p}{\gamma} + h + K_e \frac{V^2}{2g})_2 Q = Q H_{f_{1-2}} \qquad 13.$$

When energy losses due to internal friction, or turbulence, become significant a turbulent mixing loss ($H_{T_{1-2}}$) term must be included:

$$(\frac{p}{\gamma} + h + K_e \frac{V^2}{2g})_1 Q - (\frac{p}{\gamma} + h + K_e \frac{V^2}{2g})_2 Q = (H_{f_{1-2}} + H_{T_{1-2}}) Q \qquad 17.$$

Application of Equation 17 to combining flows first requires some modifications. Recalling that the subscripts 1 and 2 refer to the incoming (upstream) and outgoing (downstream) cross sections respectively, the subscripts m, l, t and j are introduced. These represent the various cross sections used to define the control volume and can be described as:

m - Main channel upstream of the junction;

l - Lateral channel upstream of the junction;

t - Main channel downstream of the junction

j - Junction of the two channel centerlines.

Using these, Equation 17 becomes:

$$(H_{T_{m-j}} + H_{f_{m-j}}) Q_m + (H_{T_{l-j}} + H_{f_{l-j}}) Q_l + (H_{T_{j-t}} + H_{f_{j-t}}) Q_t$$

$$= (\frac{p}{\gamma} + h + K_e \frac{V^2}{2g})_m Q_m + (\frac{p}{\gamma} + h + K_e \frac{V^2}{2g})_l Q_l$$

$$- (\frac{p}{\gamma} + h + K_e \frac{V^2}{2g})_t Q_t \qquad 18.$$

Isolating the turbulent mixing loss terms on the left and rewriting gives:

$$H_{T_{m-j}} Q_m + H_{T_{l-j}} Q_l + H_{T_{j-t}} Q_t$$

$$= \left[\left(\frac{p}{\gamma} + h + K_e \frac{V^2}{2g}\right)_m - \left(\frac{p}{\gamma} + h + K_e \frac{V^2}{2g}\right)_t - H_{f_{m-j}} - H_{f_{j-t}}\right] Q_m$$

$$+ \left[\left(\frac{p}{\gamma} + h + K_e \frac{V^2}{2g}\right)_l - \left(\frac{p}{\gamma} + h + K_e \frac{V^2}{2g}\right)_t - H_{f_{l-j}} - H_{f_{j-t}}\right] Q_l \qquad 19.$$

Further revision gives:

$$\left[H_{T_{m-j}} + H_{T_{j-t}}\right] Q_m + \left[H_{T_{l-j}} + H_{T_{j-t}}\right] Q_l$$

$$= \left[\left(\frac{p}{\gamma} + h + K_e \frac{V^2}{2g}\right)_m - \left(\frac{p}{\gamma} + h + K_e \frac{V^2}{2g}\right)_t - H_{f_{m-j}} - H_{f_{j-t}}\right] Q_m \qquad 20.$$

$$+ \left[\left(\frac{p}{\gamma} + h + K_e \frac{V^2}{2g}\right)_l - \left(\frac{p}{\gamma} + h + K_e \frac{V^2}{2g}\right)_t - H_{f_{l-j}} - H_{f_{j-t}}\right] Q_l$$

By examining the terms in Equation 20, it is apparent that the first [ ] term on the left and right of the equation represent the mixing loss/unit weight of the main channel flow (Q_m) and similarly the second [ ] terms represent the mixing loss/unit weight of the lateral channel flow (Q_l). Thus these two mixing loss terms can be defined as:

$$H_{T_{m-j}} + H_{T_{j-t}} = H_{T_m} = \left(\frac{p}{\gamma} + h + K_e \frac{V^2}{2g}\right)_m - \left(\frac{p}{\gamma} + h + K_e \frac{V^2}{2g}\right)_t$$

$$- H_{f_{m-j}} - H_{f_{j-t}} \qquad 21.$$

$$H_{T_{l-j}} + H_{T_{j-t}} = H_{T_l} = \left(\frac{p}{\gamma} + h + K_e \frac{V^2}{2g}\right) - \left(\frac{p}{\gamma} + h + K_e \frac{V^2}{2g}\right)$$

$$- H_{f_{l-j}} - H_{f_{j-t}} \qquad 22.$$

Also, the total mixing loss H_{T_t} can be defined as:

$$H_{T_t} = H_{T_m} \frac{Q_m}{Q_t} + H_{T_l} \frac{Q_l}{Q_t} \qquad 23.$$

This can now be non-dimensionalized by introducing n_q, the ratio of the lateral channel flow to the total flow (Q_l/Q_t) and by dividing the mixing loss terms by the kinetic energy level at the downstream cross section.

$$\frac{H_{T_t}}{K_e \frac{V_t^2}{2g}} = \frac{H_{T_m}}{K_e \frac{V_t^2}{2g}} (1 - n_q) + \frac{H_{T_l}}{K_e \frac{V_t^2}{2g}} n_q \qquad 24.$$

Further simplification is made by introducing the following coefficients:

$$\text{Overall mixing loss coefficient} = \xi_t = \frac{H_{T_t}}{K_e \frac{V_t^2}{2g}} \qquad 25.$$

Main channel mixing loss coefficient = $\xi_m = \dfrac{H_{T_m}}{K_e \dfrac{V_t^2}{2g}}$ 26.

Lateral channel mixing loss coefficient = $\xi_l = \dfrac{H_{T_l}}{K_e \dfrac{V_t^2}{2g}}$ 27.

Thus Equation 24 becomes:

$$\xi_t = \xi_m(1 - n_q) + \xi_l n_q \qquad 28.$$

This coefficient (ξ_t) is used in Chapter V to determine the magnitude of the mixing energy losses for each outlet geometry. These are presented graphically against n_q.

This development of the mixing loss coefficient is similar to that presented by Soong (18) with the exception of the inclusion of K_e when determining the kinetic energy level at the downstream cross section.

The determination of the energy losses just presented is of course based on energy principles. Mention has previously been made of two possible approaches to the problem, namely, using either momentum or energy considerations. In open channel flows, because of the large number of independent variables, no advantage is gained (without some of the assumptions in Chapter II) by adopting the momentum approach. Thus the energy approach was employed in this instance.

3.3 BOUNDARY SHEAR DETERMINATION

In open channel flows a shear force is exerted by the fluid on the channel boundaries. In channel design an estimation must be made of this to ensure that erosion of the channel boundaries doesn't occur. An average value for the shear stress ($\bar{\tau}_o$) in uniform flows is often determined using

Equation 29.

$$\bar{\tau}_o = \gamma R S_o \qquad 29.$$

Where:

$\bar{\tau}_o$ - Average shear stress;

γ - Specific weight of fluid;

R - Hydraulic radius;

S_o - Channel bed slope.

In uniform flows this is usually adequate, since the maximum shear stress in the section is very close to this average value. However, for situations where the shear stress varies significantly from this (e.g. those with distorted velocity distributions), recourse must be made to other means to determine the variation in τ_o across the channel. This is often difficult to measure.

Preston (16) introduced a simple method whereby the shear stress (or skin friction as the author referred to it) could be determined using a pitot tube in a wind tunnel. This method was based on the existence of a region near the surface where flow conditions are dependent only on the local skin friction, physical constants of the fluid and a

suitable length. This was later applied to open channel flows by Kartha and Leutheusser (11).

The 'Preston Technique' is based on the universal applicability of the Inner Law of Velocity Distribution, given in Equation 30.

$$\frac{v}{v_*} = \psi\left(\frac{v_* y}{\nu}\right) \qquad 30.$$

Where:

v - Local velocity at a distance y from the boundary;

v_* - Shear velocity $(\tau/\rho)^{1/2}$;

τ - Local shear stress;

ρ - Density of fluid;

ν - Kinematic viscosity of fluid;

ψ - Unknown function.

Kartha and Leutheusser state that for practical pusposes this can be assumed to be true for the following condition (where y is the distance from the boundary):

$$\frac{v_* y}{\nu} < 100 \qquad 31.$$

Since the technique requires that the pitot tube (diameter = d_o) be placed touching the boundary, Equation 31 can be rewritten (using $y = d_o/2$) as:

$$d_o < \frac{200\nu}{v_*} \qquad 32.$$

Thus a pitot tube must be used which satisfies this criterion in order to successfully use this technique.

The prescribed technique for calibration first requires that all the variables which influence the form of ψ be kept constant. These include:

1. Tip shape;
2. Pitot tube dimensions;
3. Distance from the boundary.

Thus by using a given pitot tube, touching the channel boundary, v can be replaced with the bed velocity (v_b) and y with $d_o/2$ in Equation 30 to give:

$$\frac{v_b}{v_*} = \psi\left(\frac{v_* d_o}{2\nu}\right) \qquad 33.$$

After some manipulation this can be rewritten as:

$$\frac{v_*}{v_b} = \psi'\left(\frac{v_b d_o}{2\nu}\right) \qquad 34.$$

Thus if ψ' is known v_* can be determined for known boundary velocities. This function (ψ') must be determined empirically.

To calibrate a pitot tube (i.e. to determine ψ') use is made of the logarithmic form of Equation 30 presented by both Preston (16) and Kartha and Leutheusser (11).

$$\frac{v}{v_*} = 5.75 \log\left(\frac{v_* y}{\gamma}\right) + 5.5 \qquad 35.$$

This equation (35), used in conjunction with pairs of v and y for different velocity profiles, is then used to determine the apparent shear stress (v_*') for each y value. These are then plotted and the best average is used as v_* for the given v_b (v measured at $y = d_o/2$). Any variation in v_*' can be explained by the complex effects of turbulence, viscosity, pitot tube shift and the closeness of the channel boundary. Following this a non-dimensional calibration curve is made by plotting v_*/v_b vs $v_b d_o/2\nu$ for all pairs of v_* and v_b.

Chapter IV

MODEL AND INSTRUMENTATION CONSIDERATIONS

4.1 EXPERIMENTAL APPARATUS AND INSTRUMENTATION

The experimental investigation was conducted in the hydraulics laboratory of the Department of Civil Engineering at the University of Ottawa. The apparatus used for the experimental work consisted of the following principal components: main channel, lateral channel, 'V' notch weir, manometer bank, pumps and header tanks. These are all shown schematically in Figure 1 and also in Plate 1.

The main channel had a rectangular cross section with a width of 0.305 m, height of 0.152 m and an overall length of 12.3 m. Supporting this was a variable slope platform which had its slope set to 0.001 throughout the study. Intersecting the main channel, 5.08 m from the entrance section, was the lateral channel. This also had a rectangular cross section and a wall height of 0.152 m. The overall length of the lateral channel was 1.83 m and its width could be set at either 0.102, 0.152 or 0.203 m. The angle of intersection of the two channels could be set at either 45.0°, 67.5° or 90.0°. Both channels and the various junction structures tested were constructed from clear plexiglass.

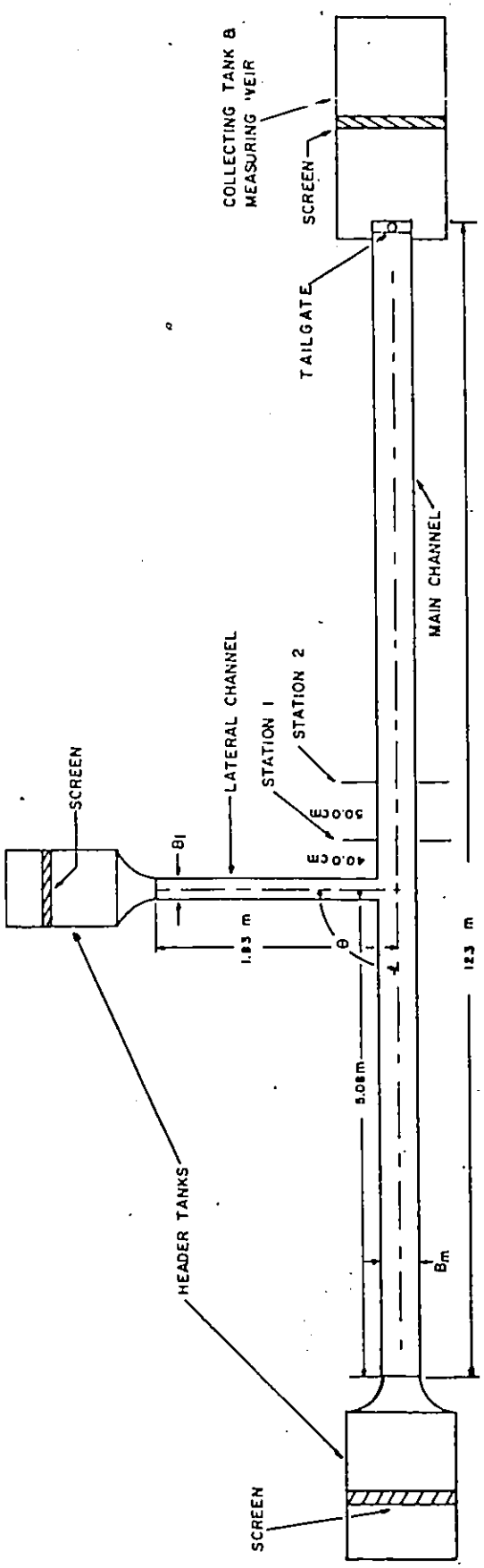

Figure 1: Schematic of Model Setup

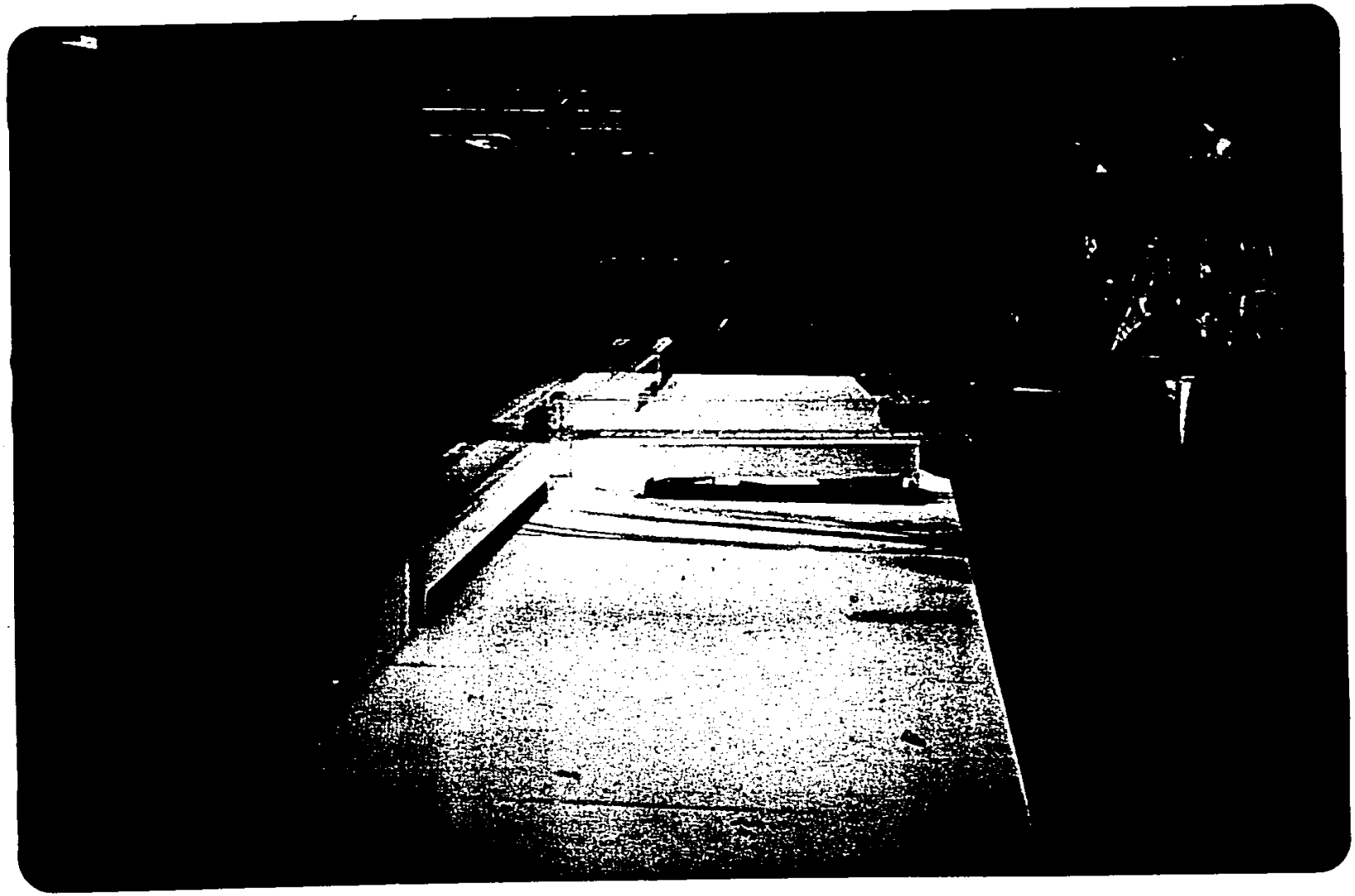

Plate 1: Model Layout
(Looking Upstream)

Each channel was equipped with a header tank designed to produce a smooth 'entrance' flow to the channels. The tanks were each supplied with a constant flow rate by separate pumps whose capacities were 0.010 and 0.007 m^3/s at heads of 18 and 28 m for the main and lateral channels respectively. Discharge from the main channel was into a collecting tank equipped with a pre-calibrated 90°, 'V' notch weir. The latter was used to accurately set the two flows in the channels.

Although open channel flow depths in a laboratory setting are usually measured using a point or a hook gauge, this was not possible in either the junction area nor immediately downstream of it. This was because of the rapid fluctuations in depth, due to the aforementioned instability and high degree of turbulence in this region, in spite of the quasi-steady state of the flows. It was therefore impossible to accurately measure the average depth with such conventional tools. To resolve this problem thirty piezometric tapping points were installed in the floor of the main channel to determine the average depths. These tapping points were connected to a manometer bank with 3.0 m long flexible hoses. Because of frictional effects along the hoses rapid fluctuations in depth due to turbulence were dampened out and a good estimation of the average depths was obtained.

Velocity measurements were primarily taken with a 'NIXON STREAMFLO PROBE' (type 543) current meter. This was capable of measuring velocities from 0.0 to 1.50 m/s. However, because of the current meter's size, it could only be placed to within 0.65 and 0.75 cm of the wall and bed respectively. To permit velocities closer to the boundaries to be measured, a 4.0 mm diameter pitot tube was used near the boundaries of interest to determine the velocities there.

Depth readings (other than those taken in the junction area) were measured with a point gauge having a minimum gradation of 1.0 mm. The pitot tube, current meter and the point gauge could all be interchangably mounted on a mobile carriage, which in turn was mounted on the channel walls.

A cathetometer was used to read the manometers (both those for the tapping points and the pitot tube). The instrument had a minimum gradation of 0.05 mm.

4.2 CALIBRATION PROCEDURES

Several aspects of the model and instrumentation had to be checked or calibrated before testing could begin. These aspects included calibration of the 'V' notch weir and pitot tube (with respect to shear stress measurement), determination of flow development length and channel roughness, check-

ing the manufacturer's calibration of the current meter, setting the channel slope and determining the energy and momentum correction factors for uniform flows.

The 90^{o} sharp-crested weir was constructed precisely according to standard specifications. This was then calibrated using the volumetric tank in the laboratory over the range of anticipated flows. The results were found to agree to within $\pm 1.5\%$ with other published data over the whole range of experimental flows.

The channel roughness coefficient was determined using the Manning equation. This was done by first establishing a steady flow rate in the main channel (with the lateral channel blocked off) and then establishing a uniform depth along the channel by adjusting the tailgate control on the channel. Following this the measured depth and flow rate were used in the Manning equation to determine 'n'. For a range of flow rates encompassing those used in the experiment 'n' was found to vary from 0.0110 to 0.0124. A value of 0.012 was then used throughout the study to determine uniform flow depths and related friction losses. The adopted value is a little higher than the value reported in standard hydraulic texts (5,6,9) for glass and plexiglass, but this was expected-considering the additional roughness effects due to the presence of joints between the channel sections.

With each set up for the 'n' determination, energy and momentum correction factors were also determined. These were found to vary from 1.017 to 1.024 and 1.005 to 1.008 respectively.

In prismatic laboratory flumes there is some distance from the channel entrance over which the flow field develops, past which it remains essentially constant. This is referred to as the 'development length' and can be defined as the length it takes for the turbulent boundary layer to reach the water surface. To ensure that the effects of the lateral inflow on the flow field were identified (and not confused with those effects originating from the entrance) it was necessary to determine that there were no residual effects from the entrance reaching the junction, i.e. that the flow field was fully developed before reaching the junction. For smooth surfaces Henderson (9) gives two criteria:

1. The turbulent boundary layer starts at a Reynolds number ($N_{r_{X_1}}$) equal to about 500,000;

2. The thickness of the boundary layer is given by:

$$d/X_2 = 0.38(N_{r_{X_2}})^{-1/5}$$

Where:

$N_{r_{X_1}} = V_o X_1/\nu$;

V_o = Free flow velocity;

X_1 = Distance from start of channel to origin of turbulent boundary layer;

X_2 = Distance along channel from origin of turbulent boundary layer;

ν = Kinematic viscosity;

d = Thickness of boundary layer at X_2.

For the present situation, typical values of depth (8.0 cm) and viscosity (1.31×10^{-6} m^2/s) give the turbulent boundary layer originating 3.2 m from the start of the channel and the layer reaching the water surface 6.0 m from the start of the channel. This, however, is unacceptable since the junction is only 5.1 m from the start of the channel. A close examination of the situation will resolve this problem, however. First, 0.5 m of bed in the header tank was ignored that would contribute to the onset of the turbulent layer, this will decrease X_1 to 2.7 and X_2 to 5.5 m. Secondly, it can be assumed that the turbulent boundary layer begins at the start of the channel if the channel is artificially roughened at its entrance section. Although the channel wasn't purposely roughened at the entrance, the joint between the channel and header tank does act, at least partially, in this manner. This will also have the effect of reducing X_1.

The above criteria are for idealized (smooth) surfaces and since the channel does have some measurable roughness, the actual value of X_1 will be reduced still further. Although most of these reductions in X_1 cannot be determined precisely, it is safe to assume that they will reduce it significantly enough to ensure that the flow is, in fact, fully developed upstream of the junction. Finally, this data was chosen to give the longest development length, thus for most cases it will be even less than that determined here.

To verify that the main channel flow was fully developed before the junction location, velocity profiles were measured along the upstream channel reach. These are shown in Figure 2 and indicate that the flow is fully developed upstream of the junction location.

Later, during the evaluation of the uniform flow conditions, evidence was found which indicated that the flow wasn't fully developed before the junction. During this part of the study two local maximum velocities were found to occur in the cross section 10.0 m from the entrance (this with the lateral channel blocked off). Since no mention of this phenomenon could be found in the literature further tests were conducted to determine the reason for their occurrence. The first of these was to measure a series of six velocity distributions between the entrance section and the

junction of the two channels. These showed that the two local maximum velocities developed at approximately 2.0 m after the entrance. Measurements were then repeated with a dense filter screen installed at the channel entrance, in addition to the screen already in the header tank. The result of this was the elimination of these local maximum velocities in the channel reach before the junction. It was assumed therefore, that these phenomena were probably indications of some entrance effect. These however were considered to be a secondary effect in the main channel and as such would have little influence on the flow field in and downstream of the confluence; this because of the highly turbulent nature and gross distortion of the flow field in this region.

The manufacturer of the current meter supplied a calibration curve for the instrument at the time of purchase, and, although it had been calibrated by the manufacturer prior to delivery, it was checked against the pitot tube to ensure that no damage had occurred during transit. The check was done over an appropriate range of velocities, the results of which are shown in Figure 3. It can be seen that there is reasonably good agreement between the two sets of data, with perhaps a tendency on the part of the current meter to give slightly higher values than the pitot tube. This is because the current meter is exposed to a much greater flow area than the pitot tube and has an inherent bias toward the

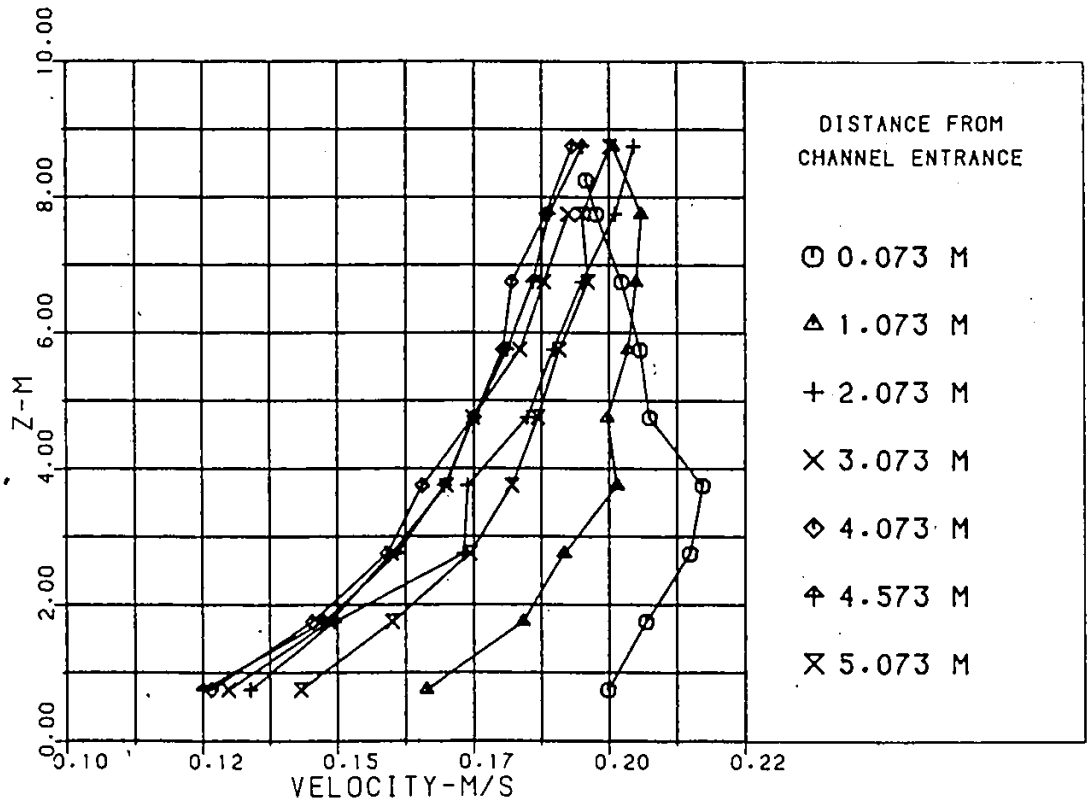

Figure 2: Development of Centreline Velocity

higher velocities in its domain. Upon examination of the velocity profiles it was found that this was indeed the case. By comparing the flow rate determined using the velocities measured and that using the weir, this bias was found to give an error of 2-3% over the whole cross section, and thus was considered acceptable.

The final calibration was that of the pitot tube to

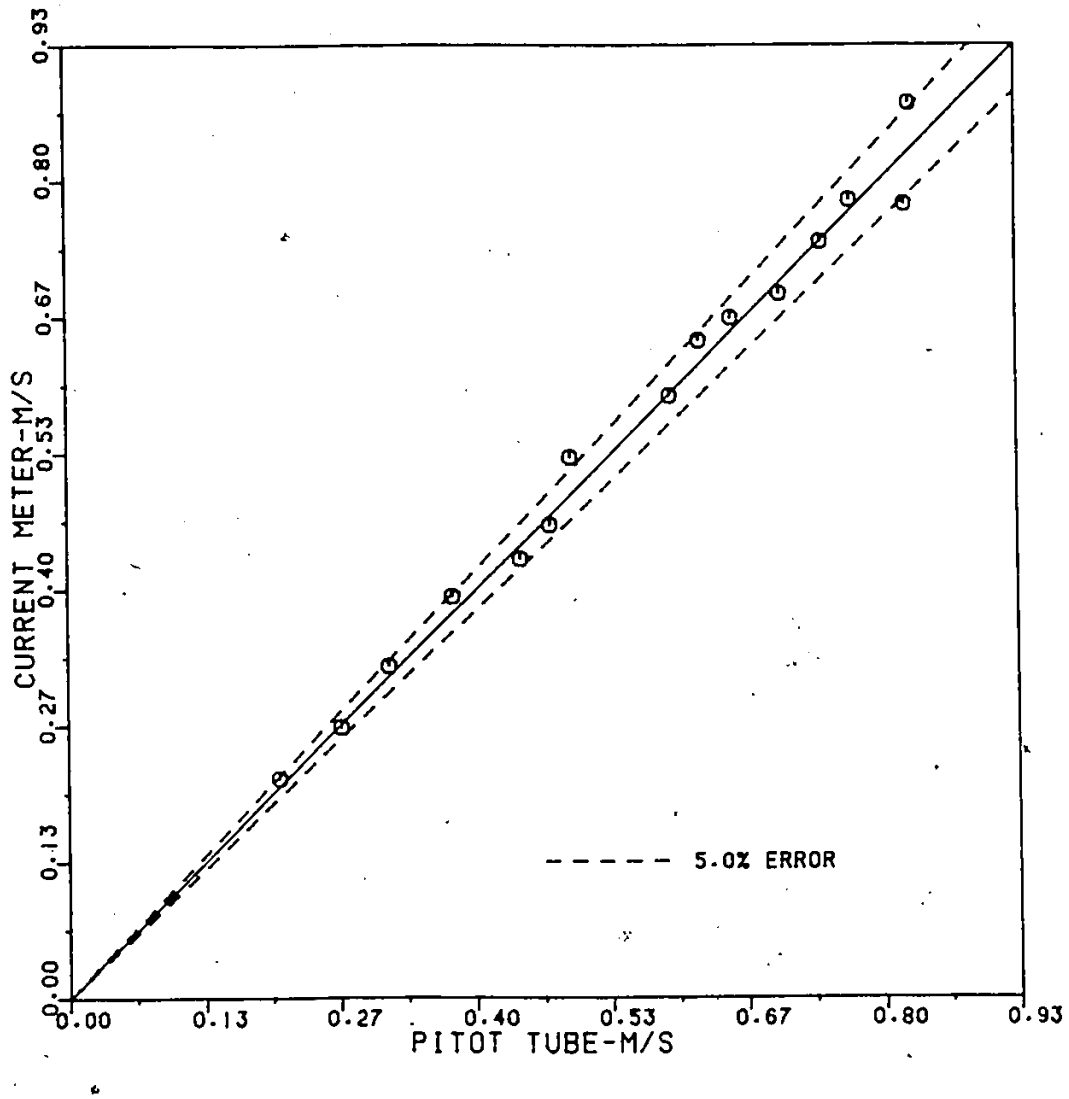

Figure 3: Comparison of Current Meter and Pitot Tube

ensure accurate determination of shear stress at the boundaries.

This was necessary because of the influence of the tip shape on the calibration curve. The method described by Kartha and Leutheusser (11) was used to perform the calibration. This method first requires measuring steady flow profiles for different bed velocities (bed velocities indicating the velocities measured with pitot tube while resting on the bed). Then the apparent shear velocity (v'_*) is determined using Equation 35. These are then plotted against the distance from the bed (y) and a 'best average' determined, (see Figure 4 a to i). Using this 'best average' as the shear velocity (v_*), v_*/v_b is plotted against $V_m d_o/2\nu$, as in Figure 5. Also shown in this figure is the calibration curve obtained by Kartha and Leutheusser (11) which shows good agreement with the present calibration. Based on this agreement over the range tested, the previous calibration curve was then used beyond the limits of the data obtained in the present calibration.

The main channel slope was set as close as possible to 0.001 with a precise level. This was done by first setting the platform slope as close as possible to the desired slope. However, because the channel is made up of 2.54 m long sections, it required further adjustment with shims to bring the elevations to within the desired accuracy of $\pm$0.5 mm. This was confirmed by measuring the stillwater depths and was also checked periodically throughout the testing programme; the results of one of these checks is shown in Figure 6.

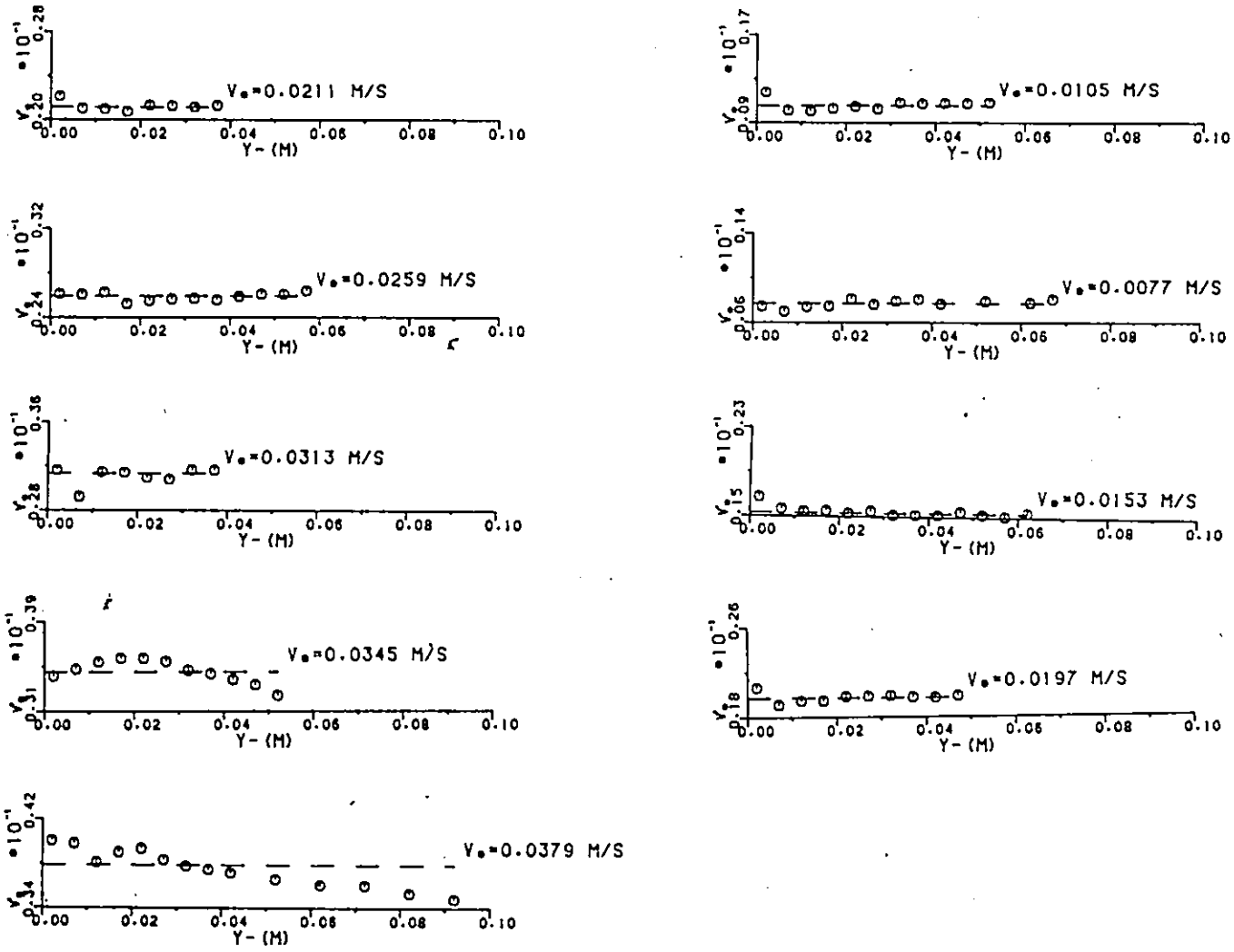

Figure 4: Apparent Shear Velocity vs Distance From Bed

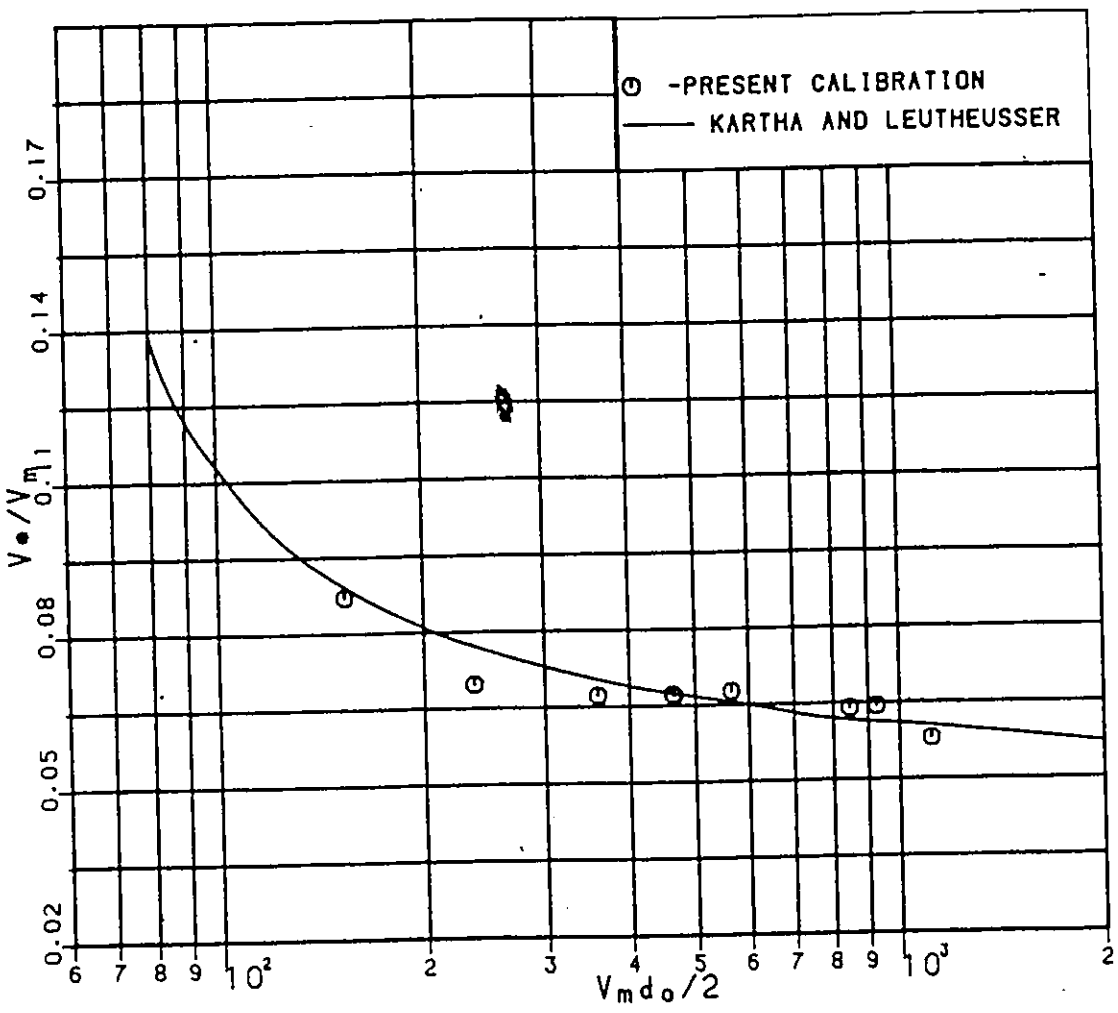

Figure 5: Shear Stress Calibration Curve

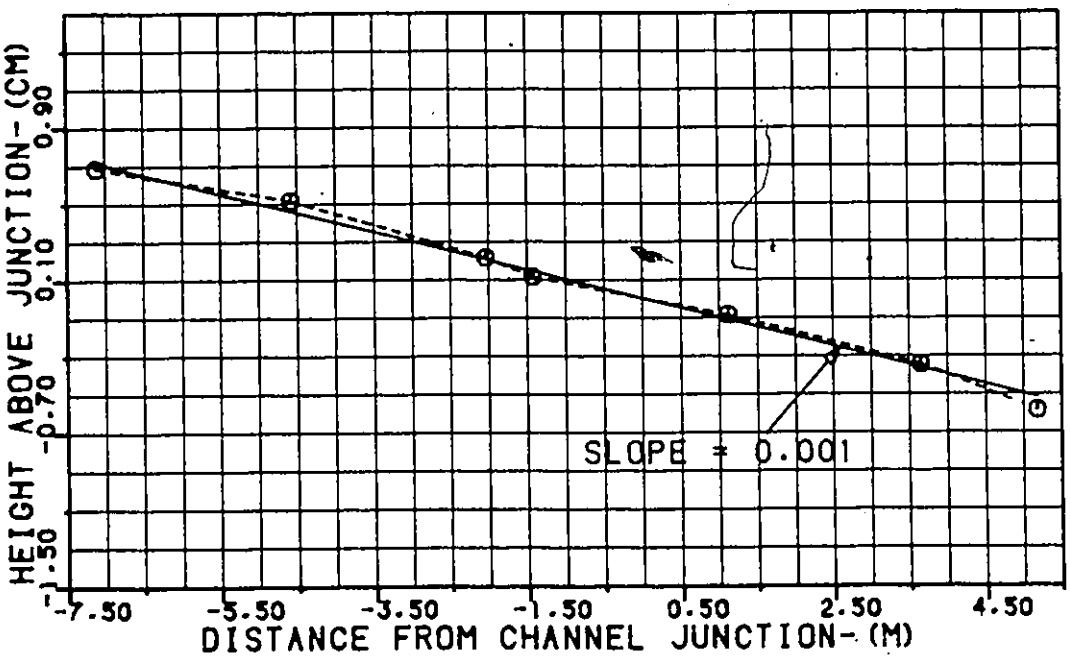

Figure 6: Channel Bed Slope

4.3 EXPERIMENTAL PROCEDURES

Each experiment began by setting the physical characteristics of the model. Those that were varied were the lateral channel width and slope, angle of intersection of the two channels and the geometry of the junction area. Following this the flow rates in each channel were individually set using the weir on the collecting tank at the end of the main channel. The main flow rate was kept constant throughout the experiment at $0.005m^3/s$. Once steady flows

were obtained the tailgate control was adjusted until uniform depth was established at approximately 5.0 m downstream of the junction. This was done to avoid the substantial drawdown caused by the free-overfall when the tailgate was open. It was noted that when the gate was fully open supercritical flows often occurred in the junction region, accompanied by a skewed hydraulic jump, which led to a much higher degree of turbulence in the junction area. The establishment of uniform flow depth is justified for two reasons:

1. It greatly reduced the level of turbulence (and local velocities) in the junction area;

2. This is probably closer to what could be expected in an actual field situation.

For each experiment several sets of velocity readings were taken, so that velocity contours (isovels) could be drawn. The latter were then used to determine the skewness of the flow field and velocities near the channel boundaries. Also, from the velocity measurements, energy correction factors could be determined. Not only were these factors used to quantify the velocity profile distortion, but also to calculate energies at various stations along the channel. The velocity readings were taken at two cross sections located 40.0 and 90.0 cm downstream from the junction centreline (hereafter referred to as stations 1 and 2 respectively).

The purpose of these (in addition of the above reasons) was to monitor the change in the velocity profiles with distance downstream of the junction. Although changes did take place further downstream than 90.0 cm from the junction, the object of the work was to return the flow field to near normal as soon as possible, and thus attention was focussed on the region immediately downstream of the junction.

The longitudinal locations of the velocity readings were kept constant throughout the study so that meaningful comparisons could be made between the different experiments. For each cross section approximately 60 velocity readings within the cross section were taken. These always included readings as near to the walls, bed and water surface as possible with the current meter. Readings were also taken next to the bed and wall opposite the lateral channel with the pitot tube. This gave a much better estimation of the boundary velocities and also permitted calculation of boundary shear stresses. No velocity readings were taken with the pitot tube on the wall next to the lateral channel (left side looking downstream) because these velocities were always less than those for normal conditions and thus of no concern with regard to shear stress. The balance of the velocity readings were taken with the current meter in the interior of the cross section and the locations were chosen so that the velocity distribution could be accurately determined.

In any flow field the local velocity is made up of three components, v_x - parallel to the channel, v_y - across the channel and v_z - perpendicular to the channel bottom. This is particularly true for combining flows. Thus to accurately determine the velocity all three components must be measured. However, based on a wealth of experimental evidence, the vertical components is small when compared with the other two components and thus can safely be ignored. It was originally attempted to find the horizontal direction of the velocity component in the region where the highest transverse velocity was located, i.e. at station 1, 40.0 cm downstream from the junction. This was done by measuring velocities at several angles to the x axis and determining the angle at which the velocity was the highest. Invariably this was found to be within $\pm$5% of the longitudinal velocity component.[2] Because of this, the velocity component parallel to the channel was assumed to accurately represent the total velocity.[3]

Initially some velocity readings were taken upstream of the junction in the main channel. These velocities were found to be very low (as expected) and yielded a value for the energy correction factor very close to that determined for uniform flow of 1.02. This was subsequently used for all subsequent energy calculations.

---

[2]The directional accuracy of the current meter is at best 5%.

[3]A 5.0% error in the direction of the velocity component over the entire cross section will give an error in the energy correction factor of less than 1.0%.

4.4 COORDINATE SYSTEM

The coordinate system used, in addition to right and left refering to looking downstream, is as follows:

X' - Longitudinal dimension parallel to the channel, equal to the distance downstream from the channel junction centrelines over the main channel width (X/B_m);

Y' - Lateral dimension across the channel, equal to the distance from the left wall of the channel over the main channel width (Y/B_m);

Z' - Vertical dimension perpendicular to the channel bottom, equal to the distance from the channel bottom over the uniform flow depth of the combined flows (Z/Z_{o_t}).

Chapter V

RESULTS

5.1 INTRODUCTION

Initially a series of tests were conducted on a set of plain junctions to determine the effects of the incoming flow on the flow conditions in and downstream of the confluence. This was done for four different physical arrangements, each over a range of flow rates,[4] and are summarized in Table 1. Following this various junction geometries and appurtenances were tried, all with S_1, B_1, and θ set at 0.015, 0.102 m and 90.0° (so that a meaningful comparison between each could be obtained).

On the basis of the initial 'plain' junction tests, it was decided that what was needed was a more effective redirection of the lateral channel discharge jet once it had entered the main channel. Several appurtenances[5] in the main channel were tried and evaluated visually. Of those tried this way, a set of four guide vanes, 15.1 cm in height, were found to work best. The arrangement tested is shown in Figure 7.

---

[4] Throughout the testing programme the main channel flow rate, slope and width were kept constant at 0.005 m^3/s, 0.001 and 0.305 m respectively.

[5] These included various sizes, shapes and numbers of both guide vanes and solid walls.

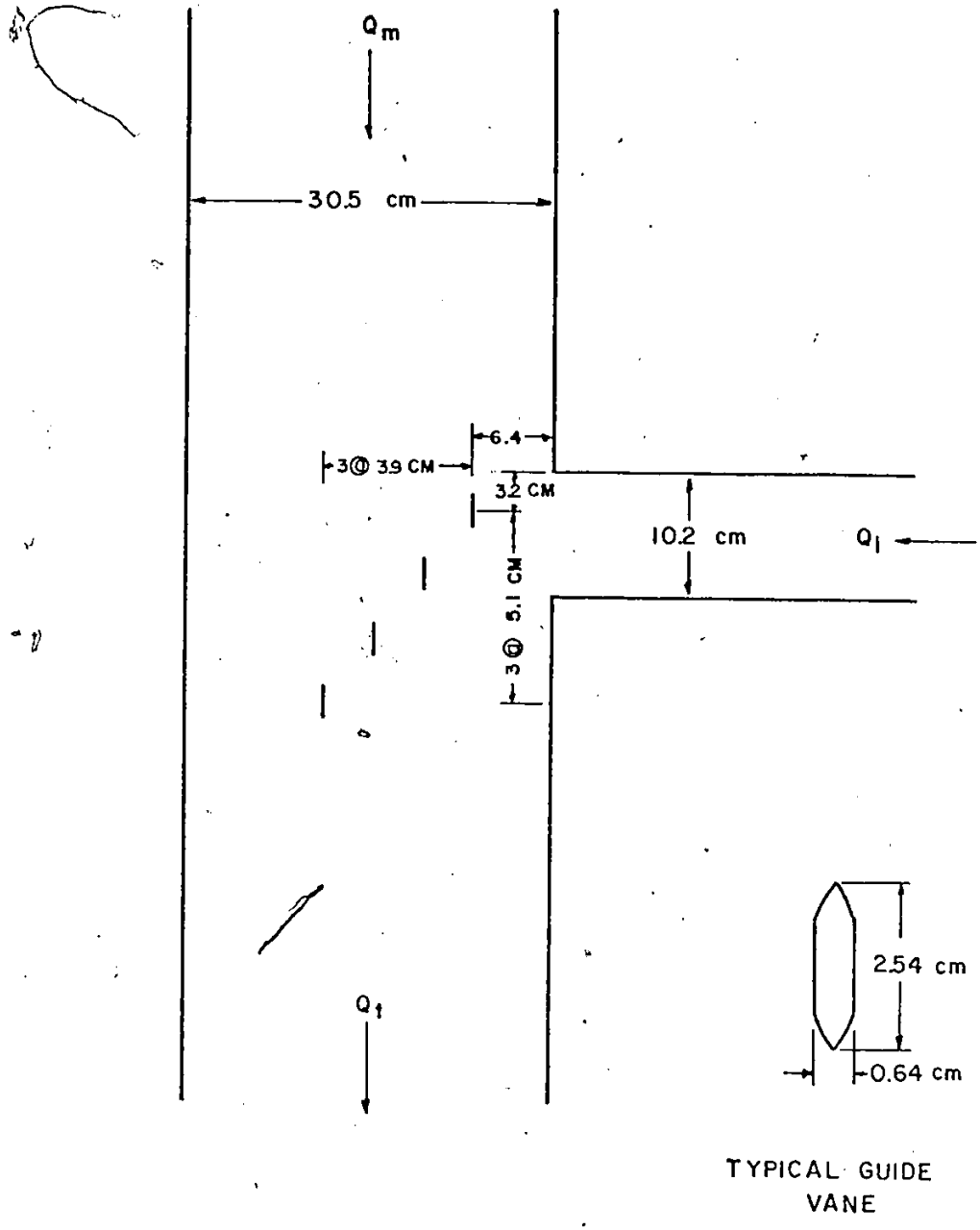

Figure 7: Plan View of Guide Vanes in Main Channel

TABLE 1

Lateral Channel Characteristics For Plain Junctions

TEST#	S_1	B_1 (m)	θ	Q_1 (m^3/s)
D1C-1	0.015	0.102	90.0	0.005
-2	0.015	0.102	90.0	0.00375
-3	0.015	0.102	90.0	0.0025
-4	0.015	0.102	90.0	0.00125
-5	0.015	0.102	90.0	0.0000625
D3C-2	0.015	0.102	45.0	0.00375
-3	0.015	0.102	45.0	0.0025
-4	0.015	0.102	45.0	0.00125
A1C-1	0.0	0.102	90.0	0.00125
-3	0.0	0.102	90.0	0.00375
-4	0.0	0.102	90.0	0.005
-5	0.0	0.102	90.0	0.000625
A1A-1	0.0	0.203	90.0	0..005
-2	0.0	0.203	90.0	0.00375
-3	0.0	0.203	90.0	0.0025
-4	0.0	0.203	90.0	0.00125

This was then fully tested over a range of Q_1 and also using different vane heights (15.1, 7.6 and 3.8 cm) to test the effects of vane submergence.

The results of these tests, as well as practical considerations, suggested that attention should be focussed on the outlet geometry of the lateral channel (or culvert). Based on the superior overall performance of a 45° intersection, and the need to redirect the lateral flow component,

the downstream corner of the outlet was beveled at 45° (see Figure 8) and the effect of this structural modification on junction performance was tested over a range of (lateral) flows. To further redirect the lateral flows, two different deflection walls were installed on the upstream corner of the outlet and tested under similar conditions, these are shown in Figures 9 and 10.

It was noted that, whereas most flow characteristics were substantially improved as a result of these modified outlet geometries, high (scour producing) velocities were still occuring at the channel bed. To alleviate this problem two additional appurtenances were tested. The first was a localized reverse slope at the end of the lateral channel to direct the flow upward and away from the bed. Secondly, because of possible sedimentation problems with the former, a superelevation type of reverse slope was tried (it was also felt that this second device would help, at least somewhat, in redirecting the lateral flow downstream). These last two are shown in Figures 11 and 12 and the test conditions for these and all other outlet devices are summarized in Table 2.

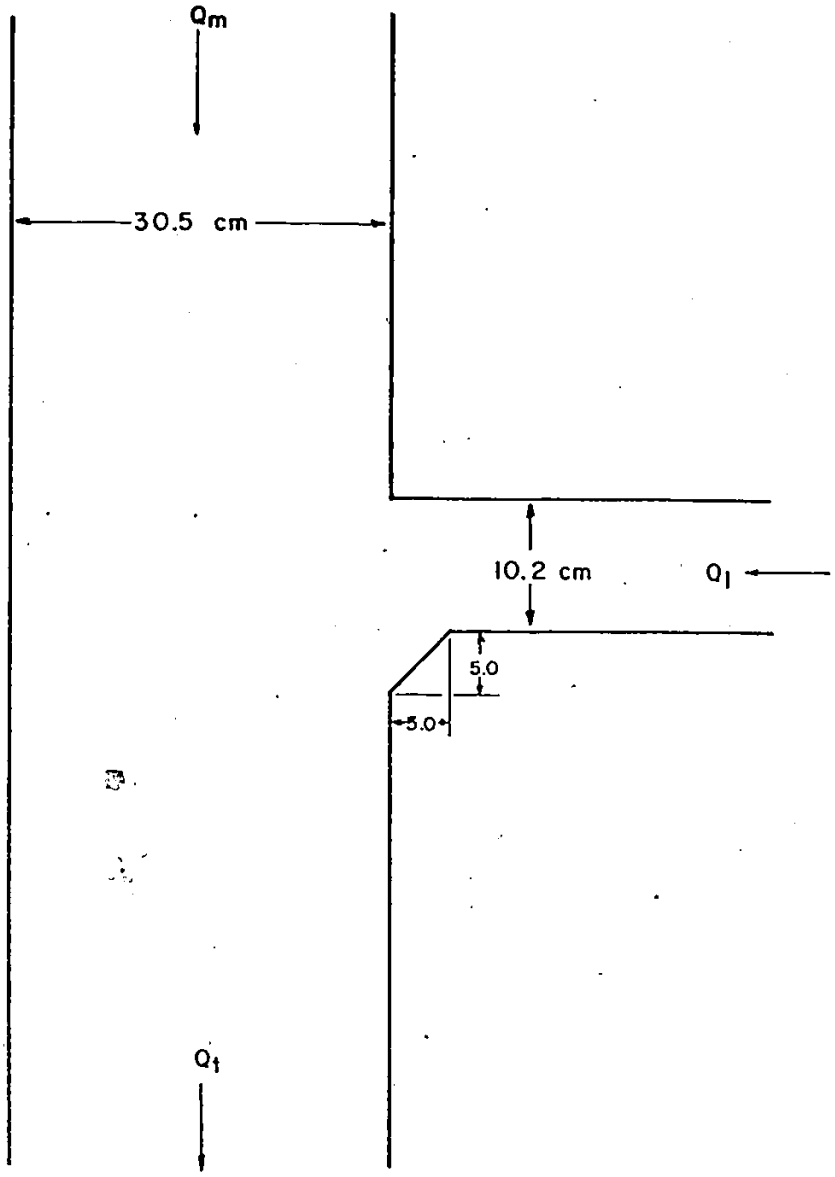

Figure 8: Plan view of Beveled Outlet

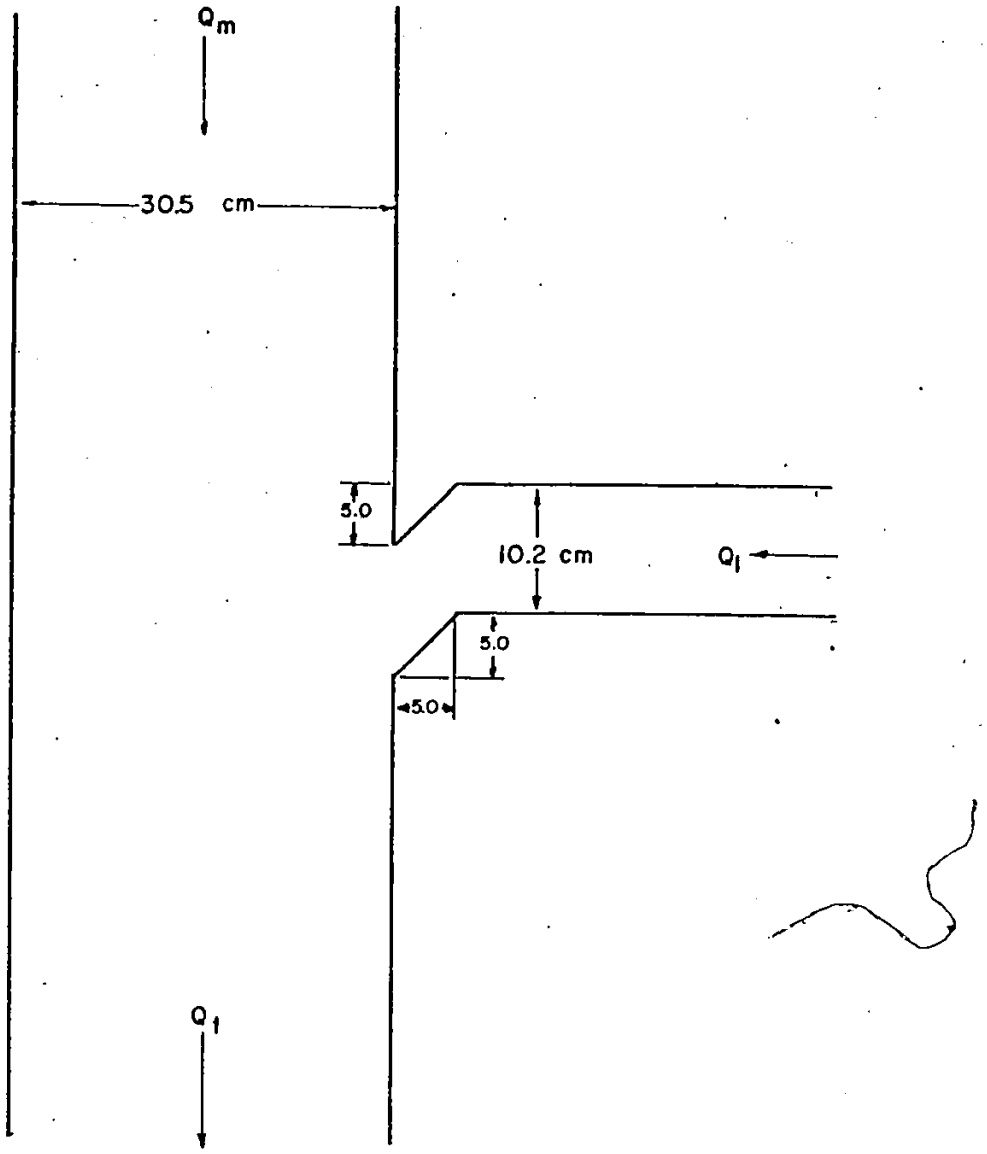

Figure 9: Plan View of Beveled Outlet with Large Deflection Wall

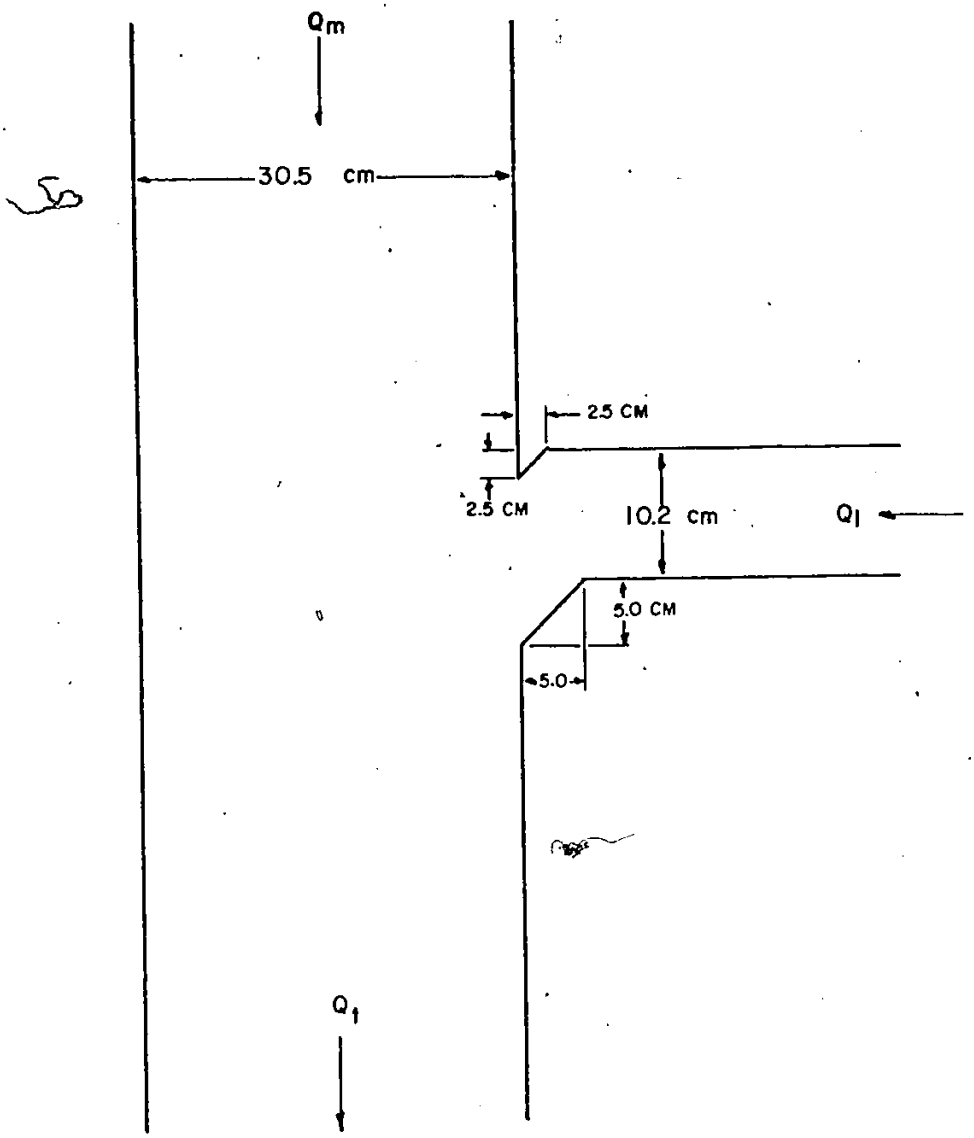

Figure 10: Plan View of Beveled Outlet with Small Deflection Wall

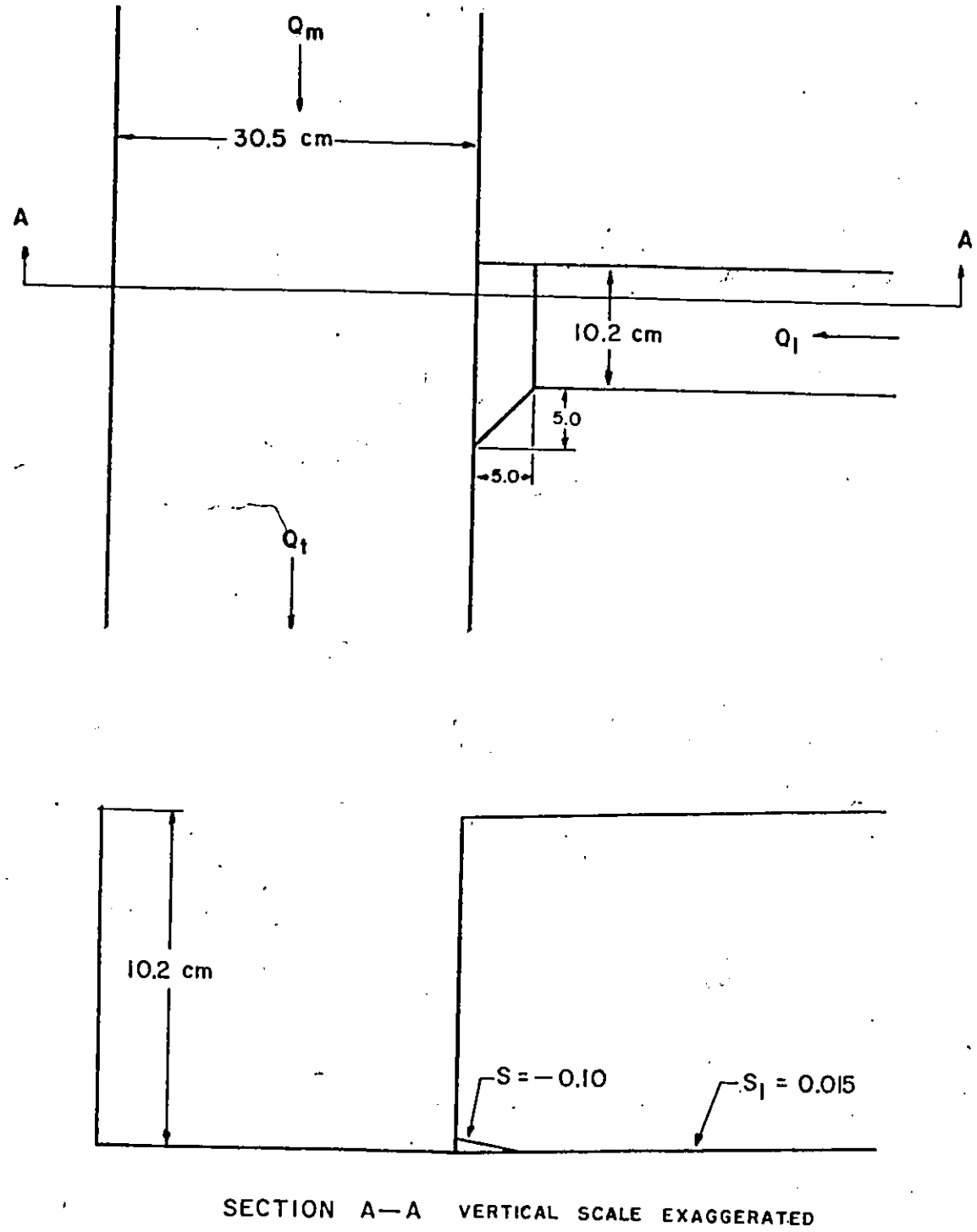

Figure 11: Plan and Profile of Reverse Slope with Bevel

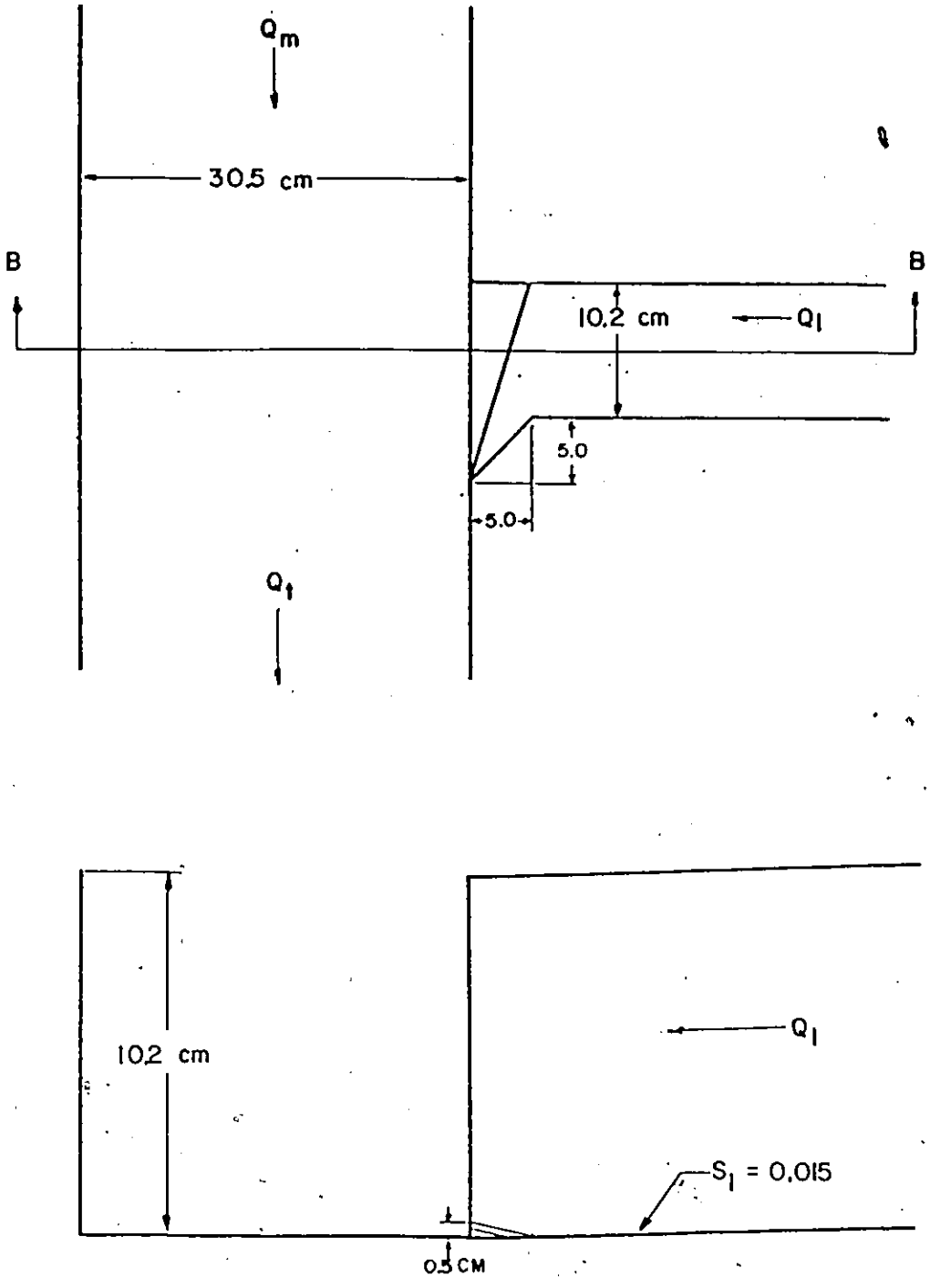

Figure 12: Plan and Profile of Superelevated Reverse Slope with Bevel

TABLE 2

Summary of Geometries and Appurtenances Tested

TEST	Q_1	GEOMETRY	FIGURE
D1C-11	.00500		
-12	.00375	Four vanes in main channel	
-13	.00250	to redirect flow, 15.1 cm	7
-14	.00125	in height.	
-15	.000625		
D1C-21	.00500		
-22	.00375	Same as above, except vanes	7
-23	.00250	7.6 cm in height.	
-24	.00125		
D1C-31	.00500		
-32	.00375	Same as above, except vanes	
-33	.00250	3.8 cm in height.	7
-34	.00125		
-35	.000625		
D1C-41	.00500		
-42	.00375	Downstream corner of outlet	
-43	.00250	channel given 45° bevel.	8
-44	.00125		
-45	.000625		
D1C-51	.00500		
-52	.00375	Similar to above, except with	
-53	.00250	large deflection wall added	9
-54	.00125	to the outlet.	
-55	.000625		
D1C-61	.00500		
-62	.00375	Similar to above, except with	
-63	.00250	smaller deflection wall.	10
-64	.00125		
-65	.000625		
D1C-72	.00375	Similar to D1C-42/44 except	
-73	.00250	with reverse slope at end of	11
-74	.00125	lateral channel.	
D1C-82	.00375	Similar to D1C-72/74 except	
-83	.00250	reverse slope superelevated.	12
-84	.00125		

5.2 UNIFORM FLOW CONDITIONS

Prior to examining the flow field characteristics at and below the confluence these same properties were evaluated for a 'uniform' flow condition in the main channel only. These results were then used as a basis for comparison in the tests that followed. Those flow properties of particular interest were:

1. Velocity Distributions;
2. Shear Stress Distributions;
3. Energy Correction Factors.

Isovel patterns (which show lines of equal velocity expressed as the measured velocity divided by the average velocity in the section) for uniform flows of 0.010, 0.00875, 0.0075, 0.00625 and 0.005625 m^3/s are shown in Figure 13. These show a relatively constant profile (non-dimensional), with the velocity varying across the section from .7/.8 to 1.1/1.2 of the average flow velocity. Local high velocities in all but the lowest flow rate occur at approximately 20% of the width from the channel sides and 50% of the depth. The occurrence of these local maximum velocities have previously been discussed in Chapter 3 in the section concerning development and therefore are not discussed here.

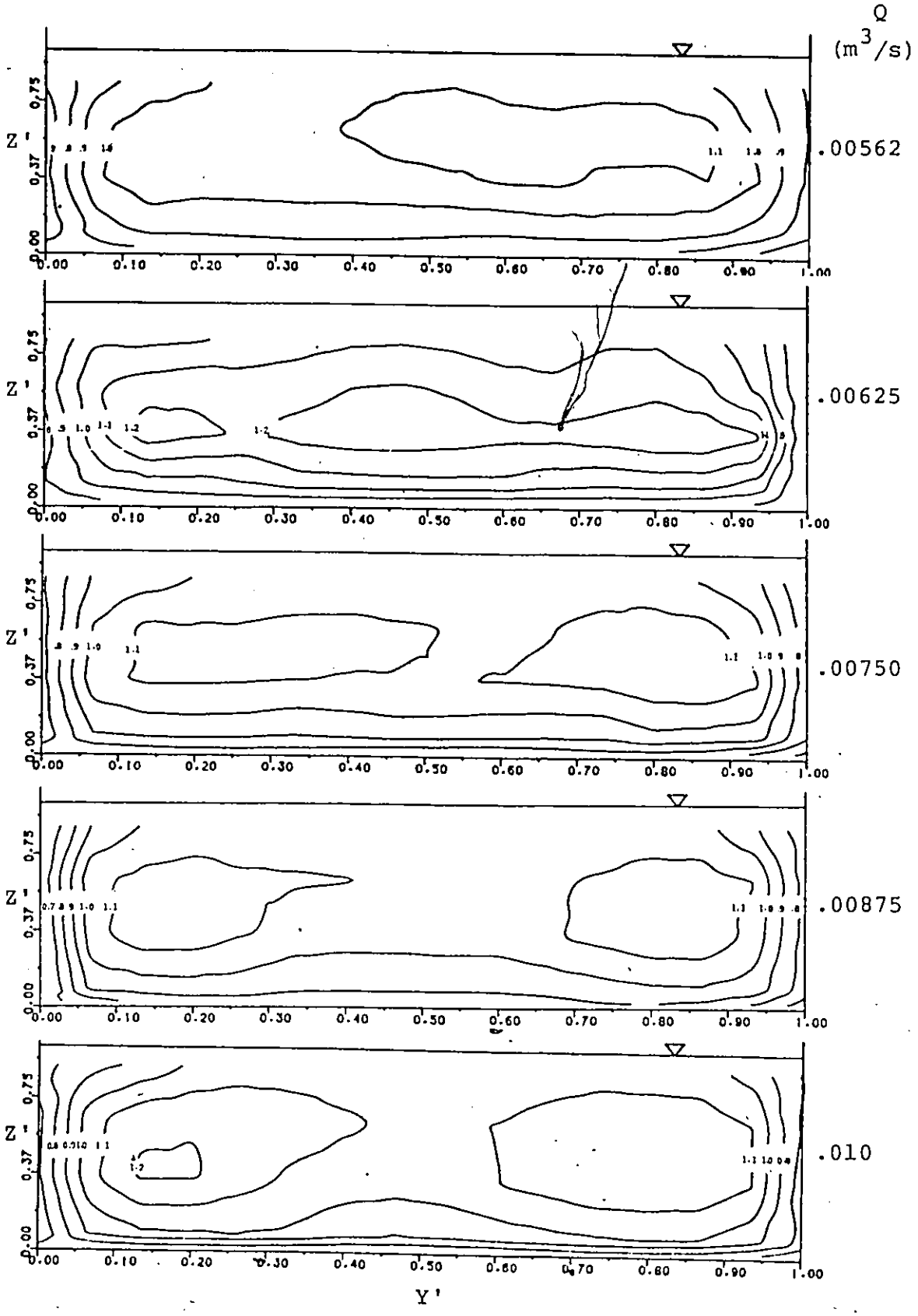

Figure 13: Isovel Patterns for Uniform Flow
(10 m from Channel Entrance)

The shear stress distributions (expressed non-dimensionally as the measured shear stress divided by the shear stress calculated using Equation 29) shown in Figure 14, all show a marked similarity. These show a maximum bed stress ranging from 0.69 to 0.91 and relatively constant across the section-with a slight reduction near the walls. Right and left wall results show that for a given flow they are identical (within experimental accuracy) and that they are also very similar for different flow rates (maximum values from 0.68 to 0.78).

The energy correction factors determined for uniform flow conditions were found to be greater than unity-as is usually assumed. These were found to be within $\pm$0.5% of the 1.02 value previously mentioned.

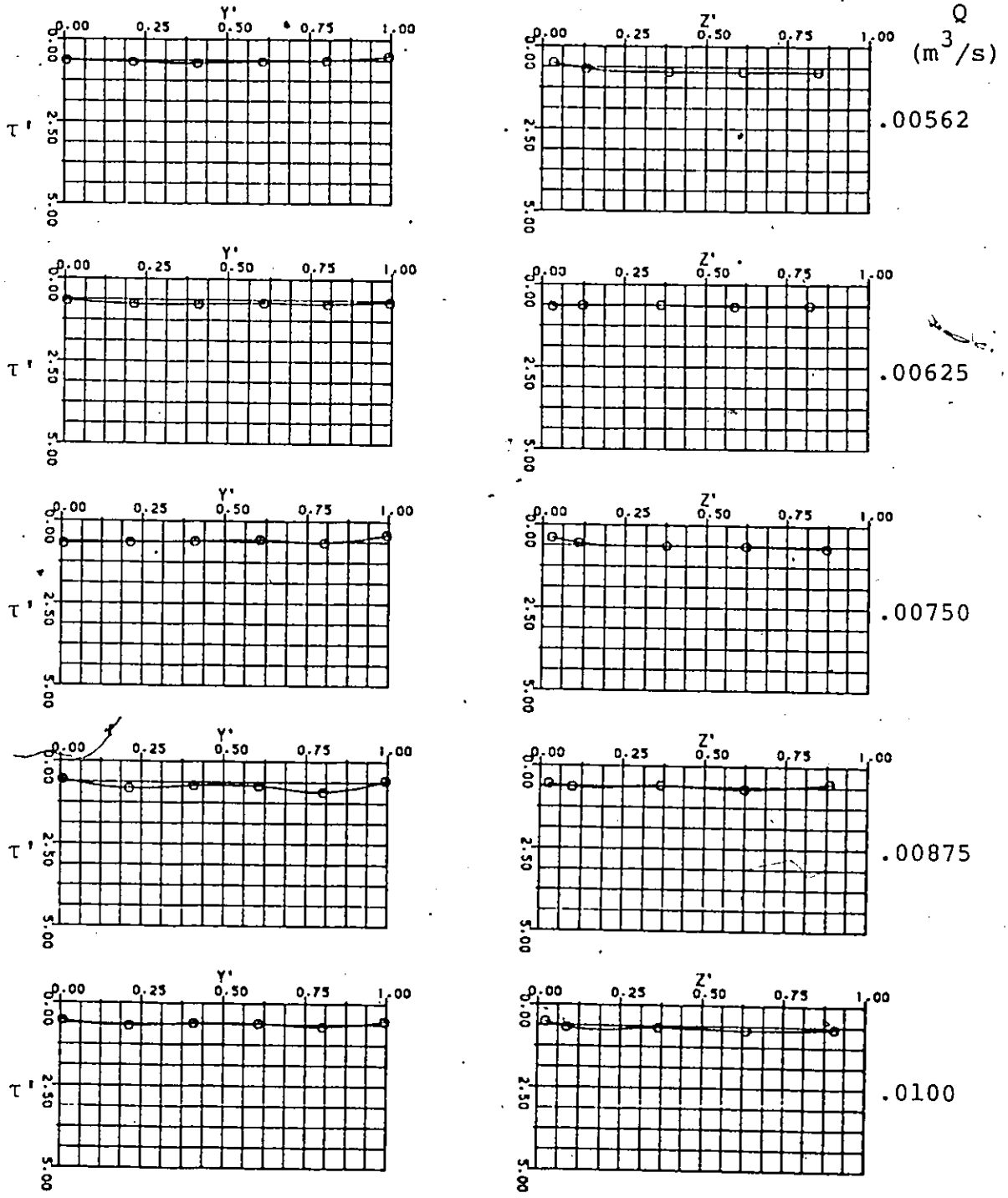

Figure 14: Shear Stress Distributions for Uniform Flow

5.3 PLAIN CHANNEL JUNCTION

Plain channel junctions were studied to determine the effects of changes in the lateral channel characteristics (width, slope and angle of intersection). The inference of 'plain' is that no appurtenances were added in the junction area and nor was any alteration made to the outlet of the lateral channel.

5.3.1 90^{o} Plain Channel Junctions

Three series of tests were conducted on a 90^{o} plain channel junction. These tests were designed to illustrate the effects of changing the slope, width and discharge of the lateral channel. The characteristics of these are summarized in Table 1.

5.3.1.1 Effect of Decreasing Lateral Discharge

To study the effects of changing the lateral discharge, the results of Tests D1C-1 to 5 are examined here. As the discharge decreases in the lateral channel, relative to the total flow, the overall level of turbulence decreases in the junction area and downstream of it.

Dye Studies

Plate 2 shows photographs of three of the plain channel junctions for a flow ratio of 0.33. The bottom two photographs, which are for similar conditions except for the channel into which the dye was injected, show that although there would appear to be a clear demarcation between the two flows, the line of demarcation is not the same when the dye is in different channels. This is due to the cross mixing of the dye between the two flows, and thus the line of demarcation between the two flows must be taken as somewhere between the two.

The results of the dye study for the 90^{o} junction showed that as n_q decreased the degree of penetration by the lateral inflow into the main channel flow decreased. Also, it could be seen that the area of reverse currents just downstream of the confluence also decreased with n_q.

Velocity Profiles

Isovel patterns are shown in Figures 15 and 16 for both downstream stations (X'=1.31 and 2.95) to illustrate the effect of decreasing n_q on the velocity distribution in the section. The isovels in these are again the measured velocity relative to the uniform velocity for that section.

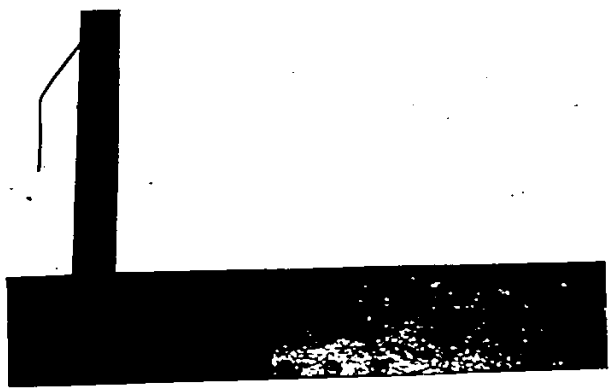

$S_1 = 0.0$

$S_1 = 0.015$

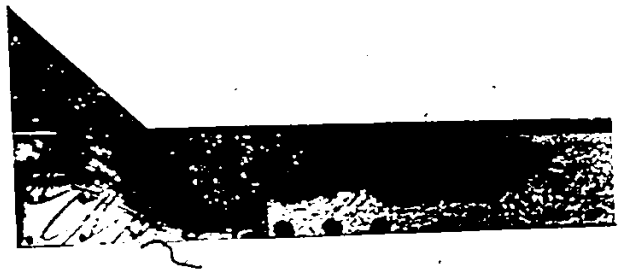

$\theta = 45^{o}$

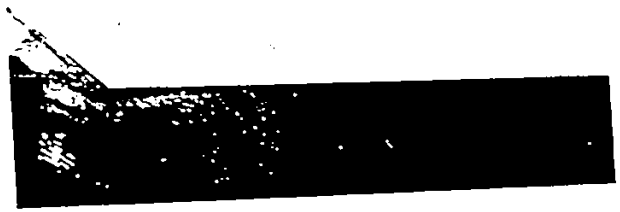

$\theta = 45^{o}$

Plate 2: Dye Results for Plain Junctions ($n_q = 0.33$)

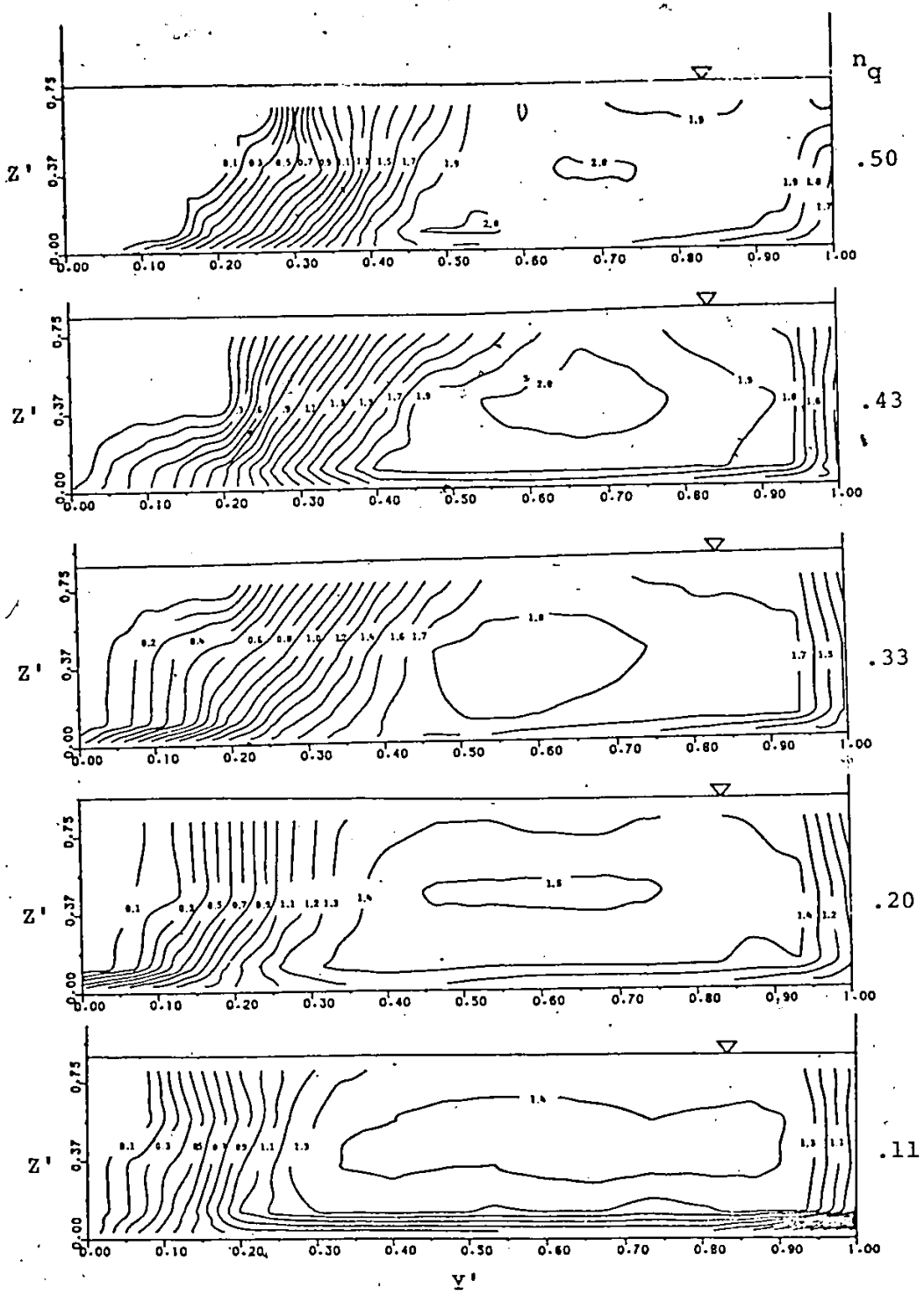

Figure 15: Isovels of 90° Channel Junction (X' = 1.31)

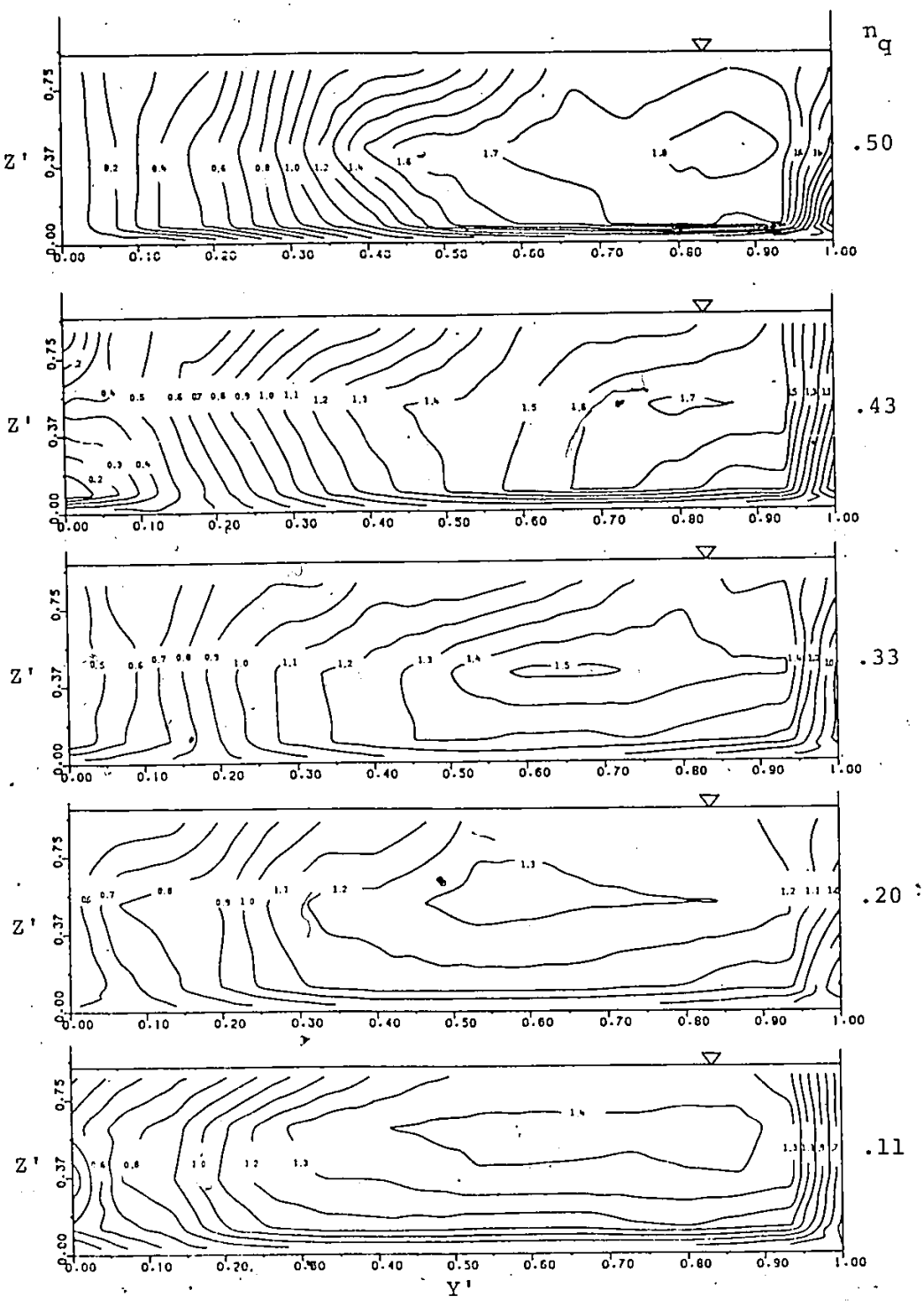

Figure 16: Isovels of 90° Channel Junction (X' = 2.95)

These show the region of unutilized flow area[5] diminishes from about 20% to 5% and from 4% to 0% at stations 1 and 2 respectively, as n_q decreases from 0.50 to 0.11. This unutilized area is of course the 'dead zone' which Atalik (1) referred to in his work.

The pertinent data concerning these velocity distributions are shown in Table 5-a[6] and Figure 17. The table shows the location of the maximum velocity filament gradually moving away from the bed and its value decreasing as n_q decreases. This trend is of course not one that is strictly followed, as can be seen from the data. A result of the turbulent nature of the flow is that the maximum velocity is changing, both its location and magnitude, quite rapidly with time and therefore its location, within the highest isovel, cannot be pinpointed exactly. Also, the maximum velocities measured on the bed and right wall decrease with n_q. Figure 17 shows the change in K_e with n_q at the two stations and this can be used as a measure of the distortion of the flow field. Recalling that if the velocity was constant across the section K_e would be

---

[5]The unutilized flow area is defined here as that area where the velocity is less than 10% of the average in the cross section.

[6]All tables and figures numbered with an '-a' are found in the appendix.

equal to unity and that for uniform flows this has been found to be 1.02, the increase in K_e due to the confluence was found to be substantial, ranging from 1.95 to 1.14 (an increase of 91 and 12%). This graph also shows the marked decrease in K_e with n_q and with distance downstream of the confluence.

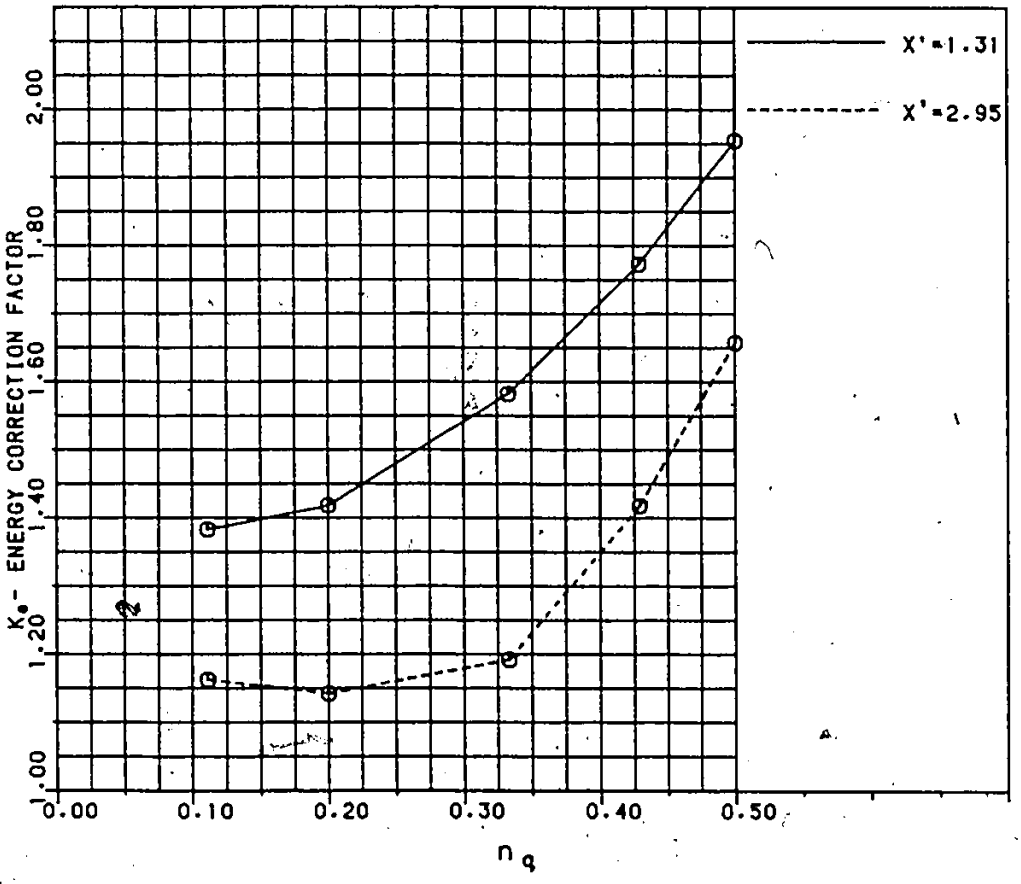

Figure 17: Energy Correction Factor vs Flow Ratio for Plain Junction

Shear Stress Distribution

Shear stress distributions are shown in Figure 18 for the plain junction and maximum shear stresses, for all tests, are summarized in Table 3-a. These clearly illustrate several important aspects:

1. Much higher shear stress than that given by γRS and also that measured for uniform flow (these increases were as high as 200% and 330% respectively);

2. Decrease in the maximum bed shear stress with n_q and distance from the confluence;

3. Shifting of the location of the maximum bed shear stress from right to left with decreasing n_q;

4. Decrease in maximum right wall stress with n_q;

5. Raising location of maximum right wall shear stress with distance downstream.

These figures become particularly significant when they are compared with the results obtained for uniform flow conditions shown in Figure 14.

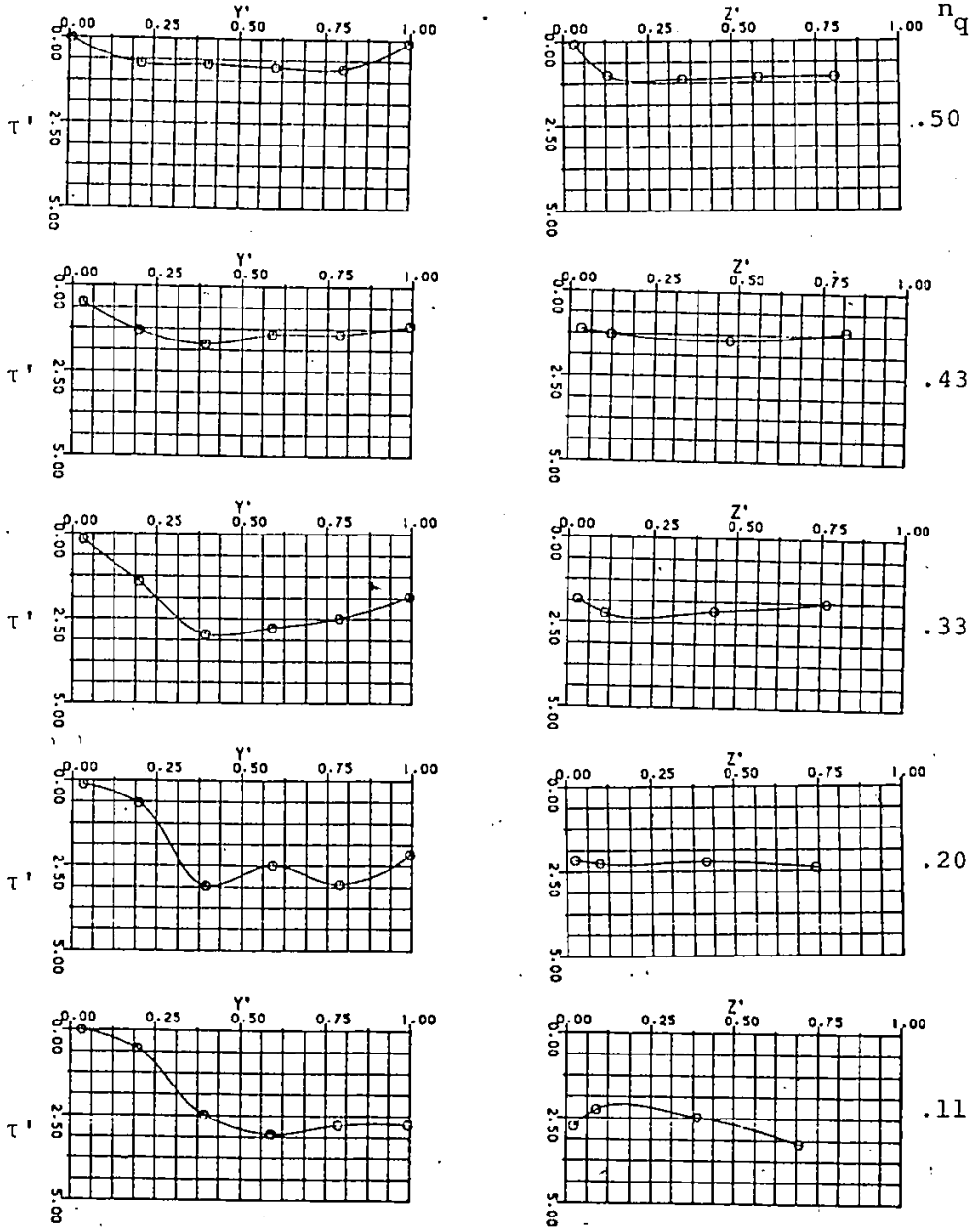

Figure 18: Bed Shear Stress Distributions for Plain Junction (X' = 1.31)

Mixing Energy Losses

Figure 19 shows the variation of the turbulent mixing loss coefficient (calculated using Equation 28) with n_q for both downstream stations (these are also shown in Table 4-a). It is seen that both decrease with n_q and that ξ_t at the further downstream station is generally higher than at the station closer to the lateral channel, with the exception of n_q at 0.20. Both of these observations are consistent with what would be expected to occur, namely: as loss

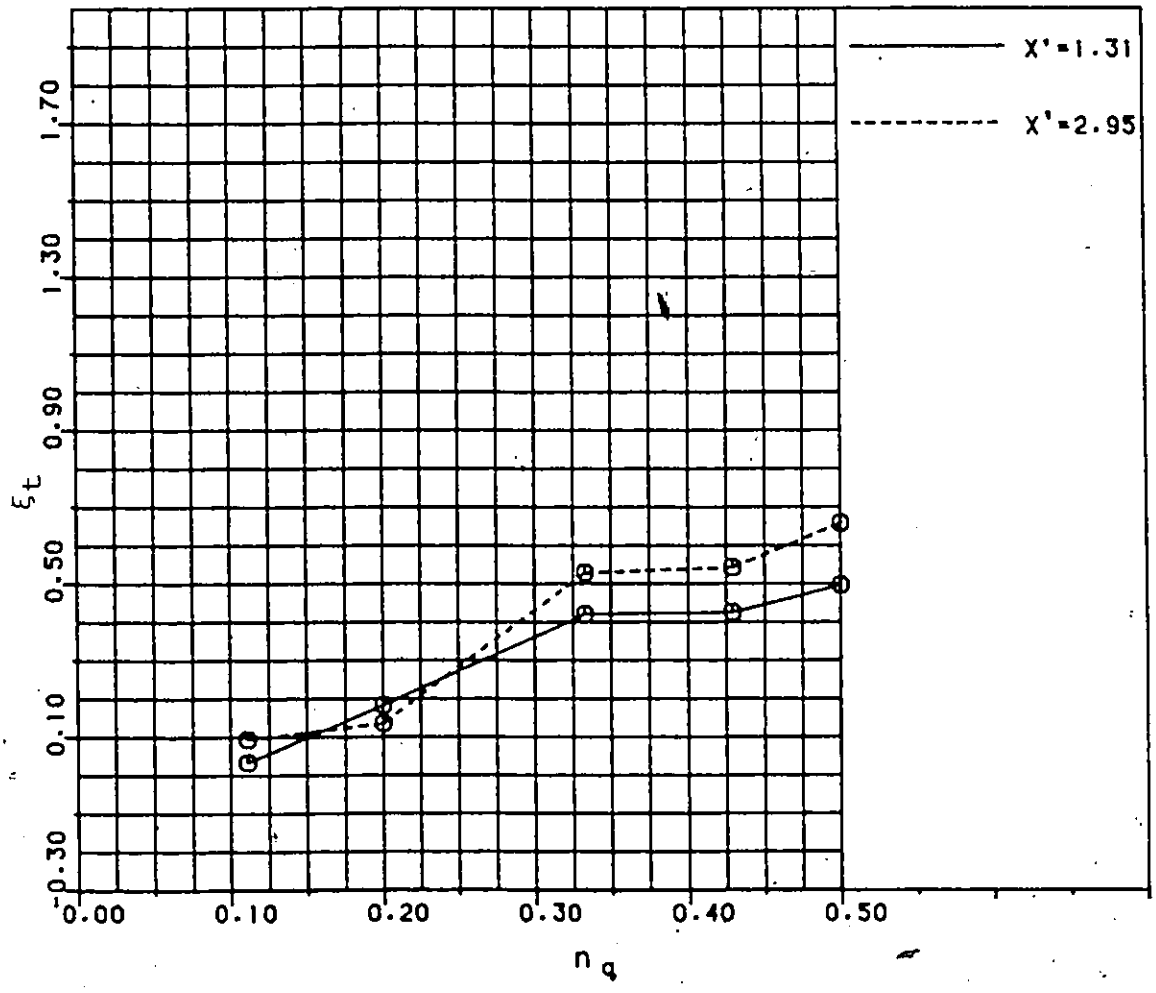

Figure 19: Mixing Loss Coefficient vs n_q for Plain Junction

lateral flow is introduced, less turbulence is generated and thus less energy is lost to mixing. Also, since there is still a relatively high level of turbulence in the flow field between the two stations sampled, there will be some energy loss to turbulence between them. This is borne out by the fact that ξ_t is larger at 2.95 channel widths downstream of the junction than at 1.31.

The fact that ξ_t is lower further downstream for n_q equal 0.20 is of course inconsistent with the above discussion. The reasons for this inconsistency, and others, are many and complex. Most important of these is the use of a uniform flow equation to determine the friction losses. Also important is the omission of the turbulent energy, i.e. the energy contained in the high frequency turbulence. Since the instruments used to measure velocities (pitot tube and current meter) had a very low frequency response and were therefore only capable of measuring average velocities this energy component could not be determined. To do so would have required using much more sophisticated instrumentation such as the hot-wire or laser doppler anemometers. It was felt that this was not necessary since interest was largely concerned with large scale turbulence.

5.3.1.2 Effect of Changing Lateral Channel Slope

The effect of the lateral channel slope on the flow conditions can be evaluated by examining the results of tests D1C-1 to 5 and A1C-1 to 5, which are identical except the lateral channel invert slopes of 0.015 and 0.00 respectively. It was found that by changing the slope of the lateral channel little or no significant change in the flow conditions was caused. Both the dye, shear stress and velocity profile results show little difference between the two slope conditions. K_e values are very close over the range of n_q tested, with the lesser slope having slightly smaller values (see Figure 20).

The reason that the lateral channel slope has such an insignificant effect on the flow field is due to the fact that the incoming velocity, which is primarily responsible for the effect on the flow, is dependent on the depth of the flow in the junction area, which in turn is primarily controlled by the downstream conditions. This of course is contrary to uniform flows where (in long channels) the flow depth, and thus velocity, is only dependent on the slope of the channel (all other things being equal). Thus it can be

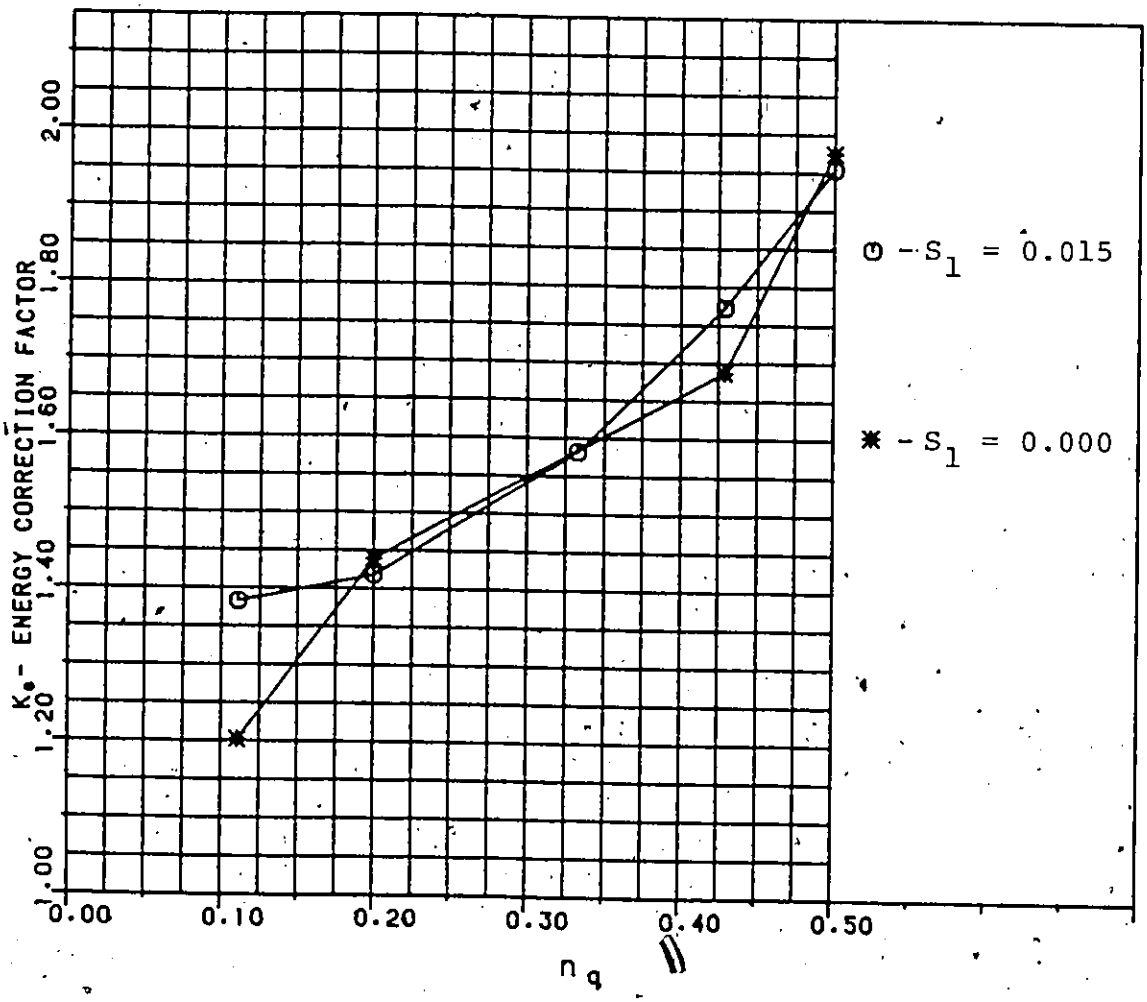

Figure 20: K_e vs n_q for Different Lateral Channel Slopes

assumed that if the lateral channel slope was allowed to be the determining factor concerning the outlet velocity (i.e. if the depth in the junction was less than uniform depth for the lateral) conditions would be worse with higher lateral channel slopes. This was seen to be the case.

5.3.1.3 Effect of Lateral Channel Width

Increasing the lateral channel width had the predictable result of improving the overall performance of the confluence. This is no doubt due to the decrease in the incoming flow velocity and thus momentum. This comparison is made by comparing the results of tests A1C-1 to 5 and A1A-1 to 4, which have channel widths of 10.2 and 20.3 respectively. Figure 21, which shows K_e for both width conditions, illustrates this improvement by a reduction in K_e, particularly at the further downstream station, with the wider channel of up to 19 and 28% at the upstream and downstream stations respectively. This difference, however, is not quite so apparent when the isovel patterns for the two channels (Figures 22 and 23) are examined.

5.3.2 45° vs 90° OUTLETS

As expected reducing the angle of intersection of the two channels from 90° to 45° significantly improved the results. This was illustrated by a marked reduction in K_e

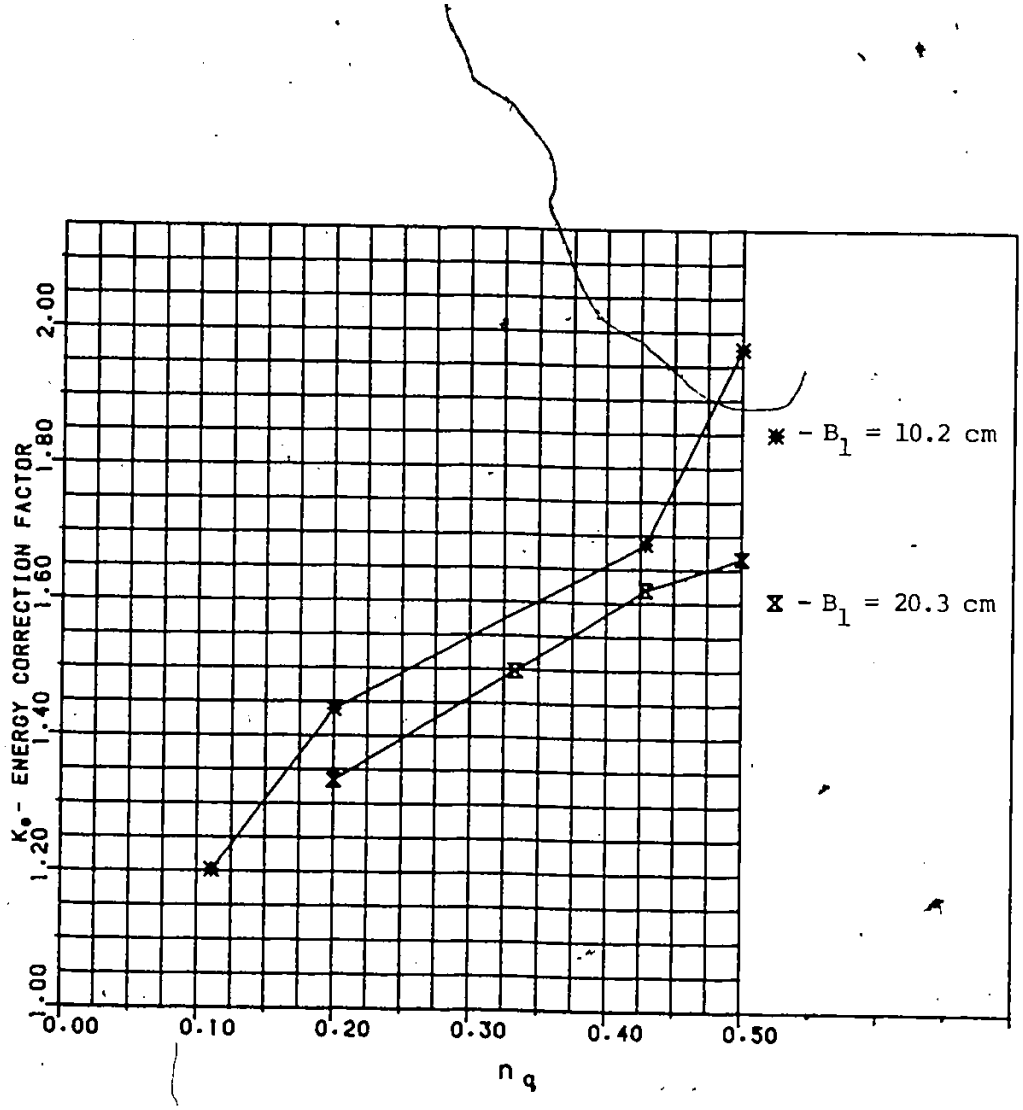

Figure 21: K_e vs n_q for Different Lateral Channel Width

(Figure 24), and a less significant yet noticeable reduction in ξ_t (Figure 25) over the whole range of n_q. Also, examination of Plate 2 showed that for equal flow rates, the 45° junction produced much less flow penetration into the main channel than that for the 90° arrangement. Finally, the isovel patterns (Figure 26) showed that the 45° configuration had a much better centered and a more uniform velocity

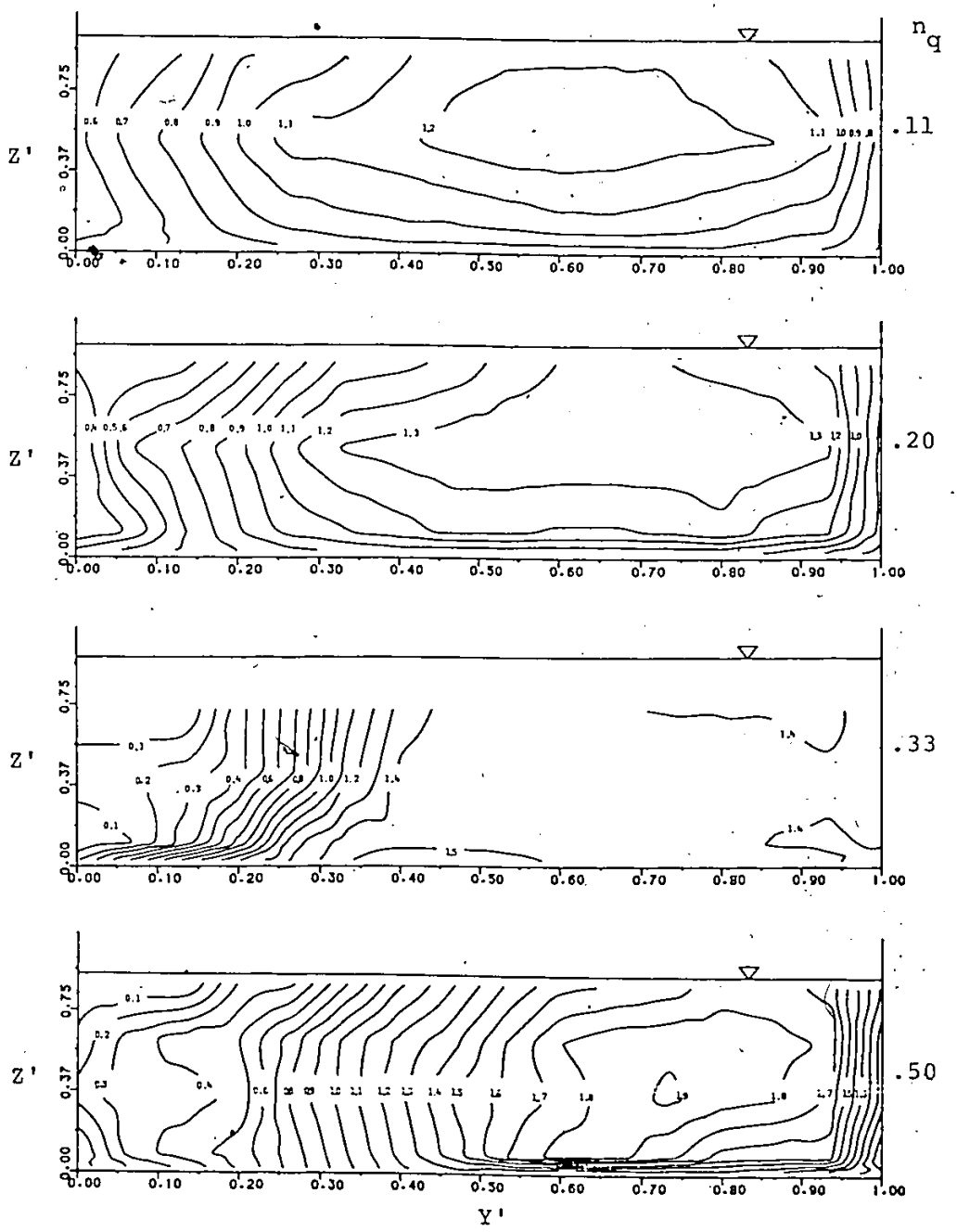

Figure 22: Isovel Patterns for Lateral Channel Width = 10.2 cm (X' = 2.95)

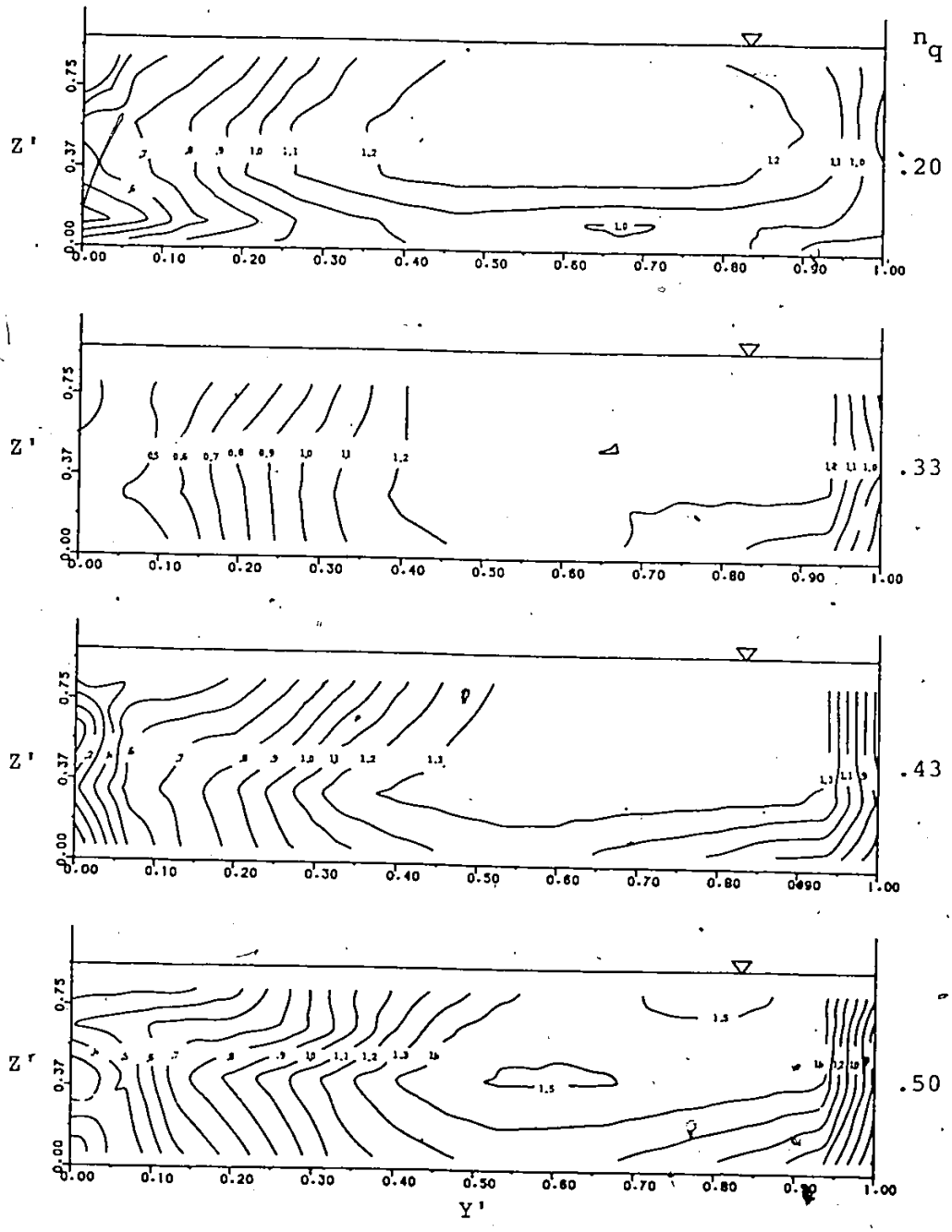

Figure 23: Isovel Patterns for Lateral Channel Width = 20.3 cm (X' = 2.95)

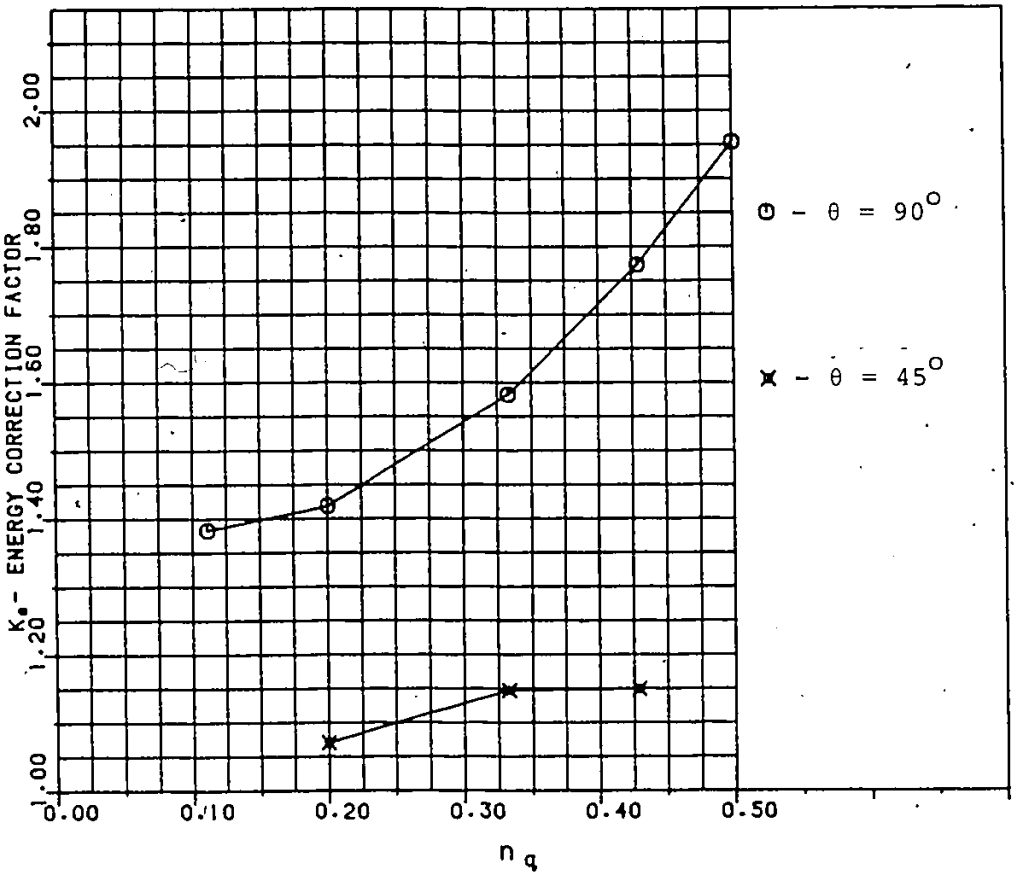

Figure 24: K_e vs n_q for 45° and 90°

profile as well as smaller velocity gradients, maximum velocities and boundary velocities. This was also found to be true further downstream (X' = 2.95) as can be seen in the appendix. In all aspects then the 45° intersection gave a much better result, with of course the only disadvantage being that to adopt such an arrangement would result in a culvert 41% longer than that required for a 90° junction.

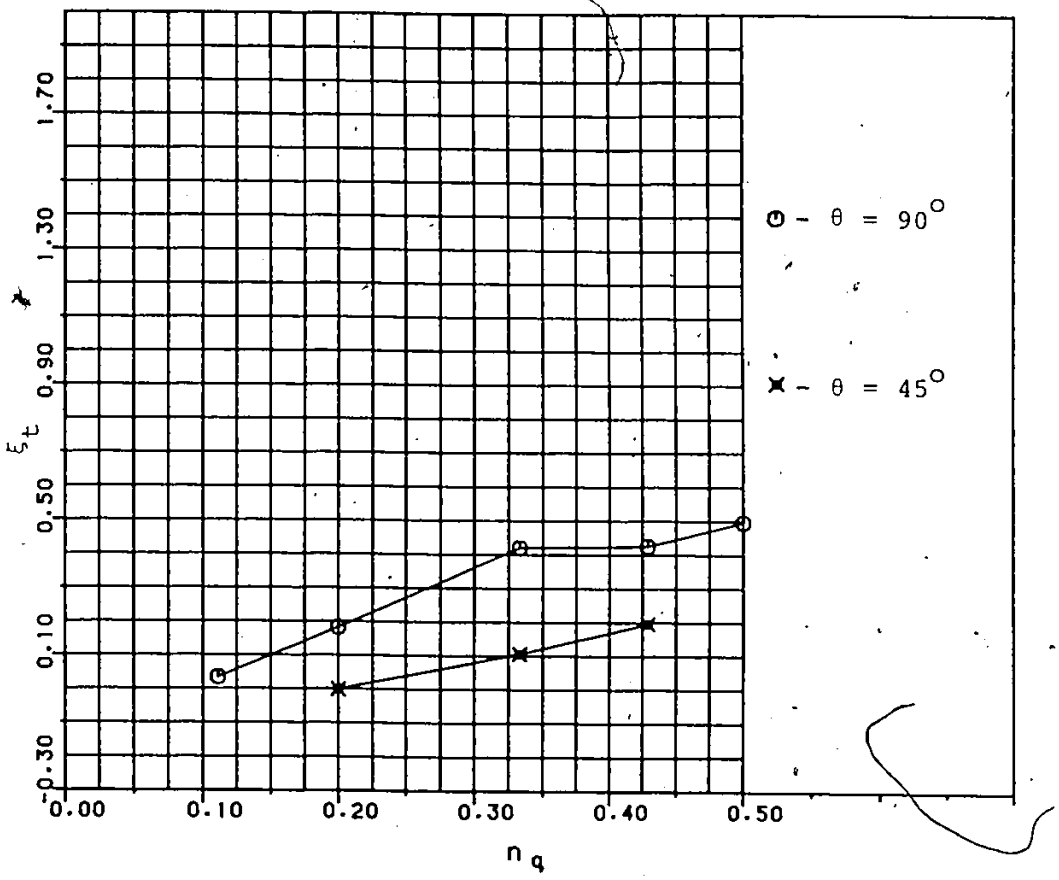

Figure 25: ξ_t vs n_q for 45° and 90°

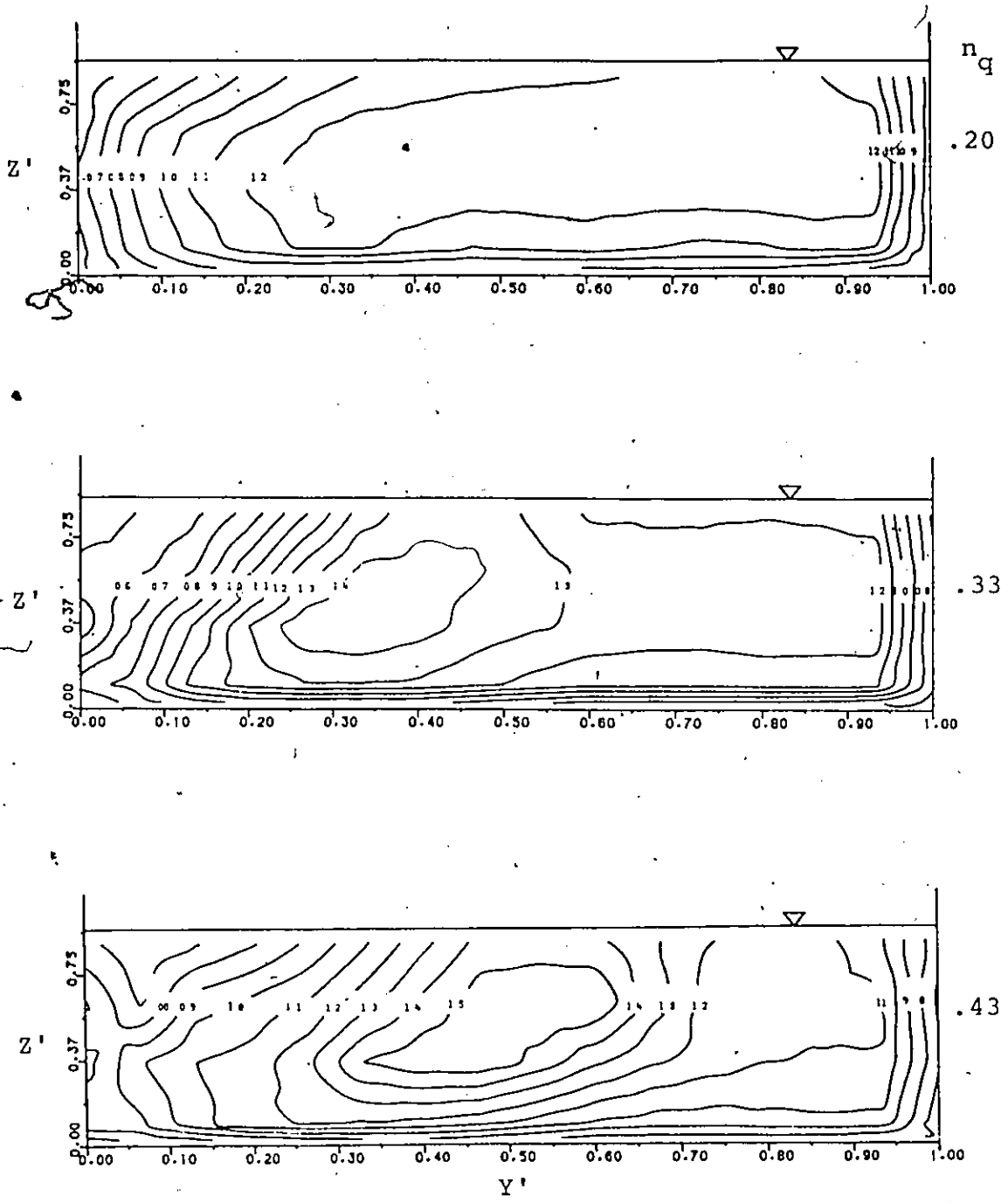

Figure 26: Isovel Patterns for 45° (X' = 1.31)

5.4 GUIDE VANES

As stated previously the use of guide vanes was an attempt to provide a mechanism whereby the lateral momentum would be more quickly dissipated and the incoming flows redirected with less adverse effects on the main flow. The configuration rigorously tested was one of several first evaluated visually. These included various walls and vanes of different sizes and shapes. This final configuration (shown in Figure 7) was then tested over a range of flow ratios and vane heights, the results of which are summarized here according to the following four methods of evaluation.

5.4.1 Dye Study

The 'dye' results showed that the gross redirection of the flow as a result of the presence of vanes was small, and became even less significant when the vanes became submerged.[7] This is shown in Plate 3 for all three vane sizes at $n_q = 0.33$.

5.4.2 Velocity Profile

For all three vane heights used there was a general reduction in the maximum velocity both in the cross section as

---

[7] No submergence occurred for the largest vanes, however it did occur for the 7.6 cm high vanes at and above $n_q = 0.33$ and for all flows for the smallest vanes.

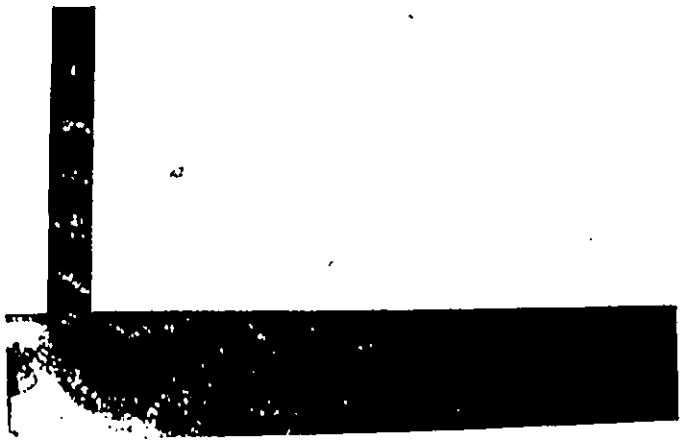

15.1 cm Vanes

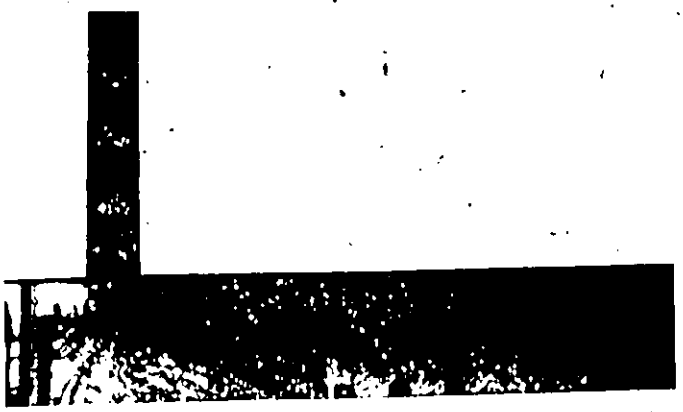

7.6 cm Vanes

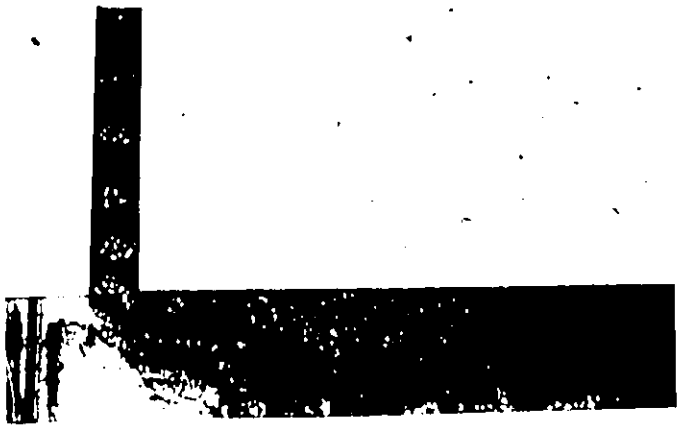

3.8 cm Vanes

Plate 3: Dye Results for Junctions with Guide Vanes (n_q = 0.33)

a whole and at the boundaries. This was small though, and the reduction was usually less than 10% and in some instances the velocity was even larger than with no vanes. These profiles are shown in Figures 27 to 32-a for stations 1 and 2 and the maximum velocities are summarized in Tables 6-a and 7-a.

With regard to the location of the maximum velocity it was generally shifted more toward the center of the channel with the vanes than without. This effect was seen to diminish with the reduction in vane height. Again this effect was generally small and in several instances the maximum velocity is closer to the right wall without the vanes than with. The unutilized cross sectional area was the aspect where most improvement was realized with the presence of guide vanes. This area was always reduced and more so with the larger vanes than with the smaller ones. This then is the reason for the significant reduction in K_e with guide vanes being present. Figure 33 shows the variation in K_e vs n_q for both the plain junction and all the vanes at station 1. Over the whole range (of n_q) this was reduced by the presence of the vanes, normally between 8 and 12%, although the vane height would appear to have a small or negligible effect on the reduction.

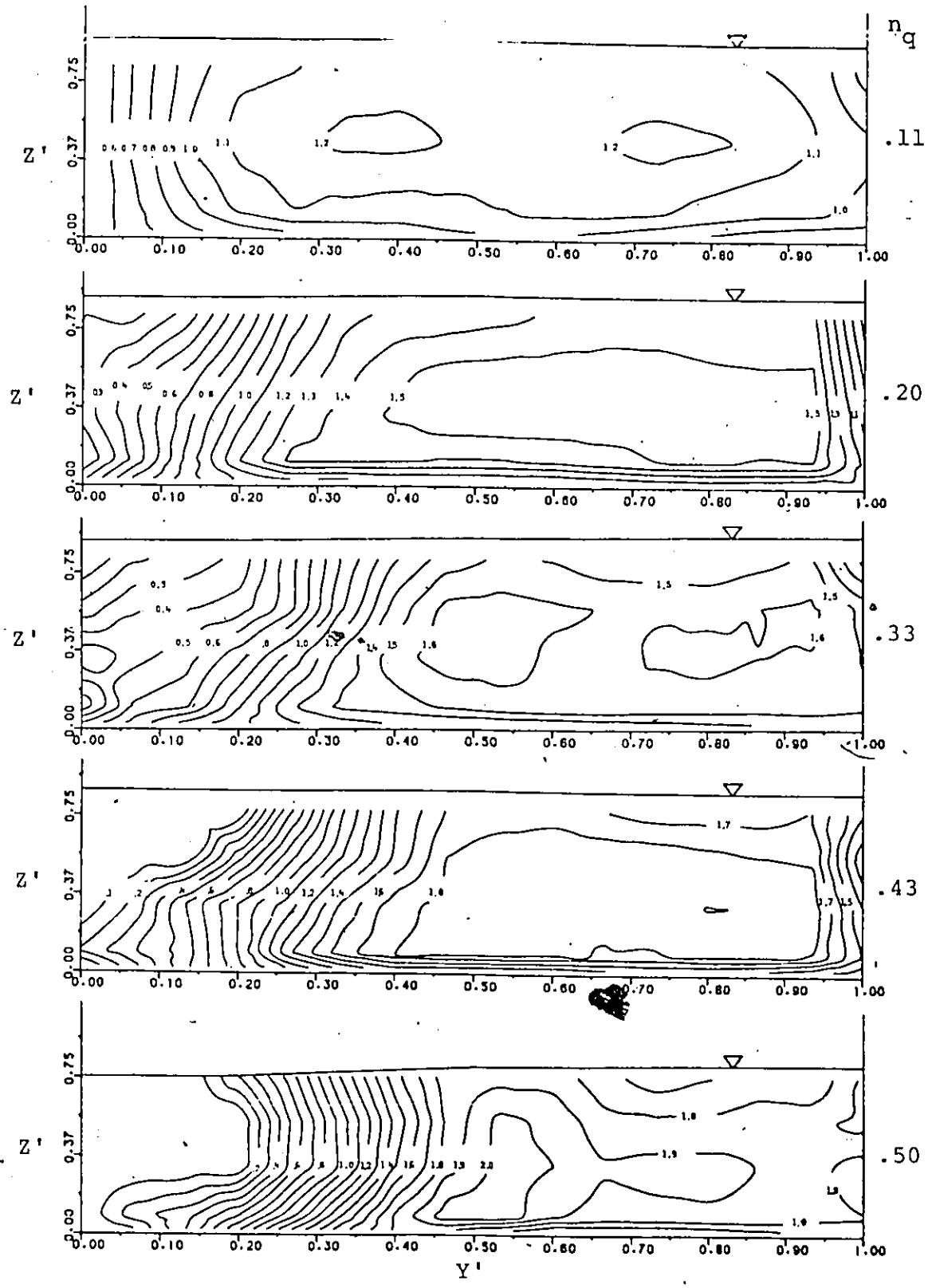

Figure 27: Isovel Patterns for 15.1 cm Guide Vanes (X' = 1.31)

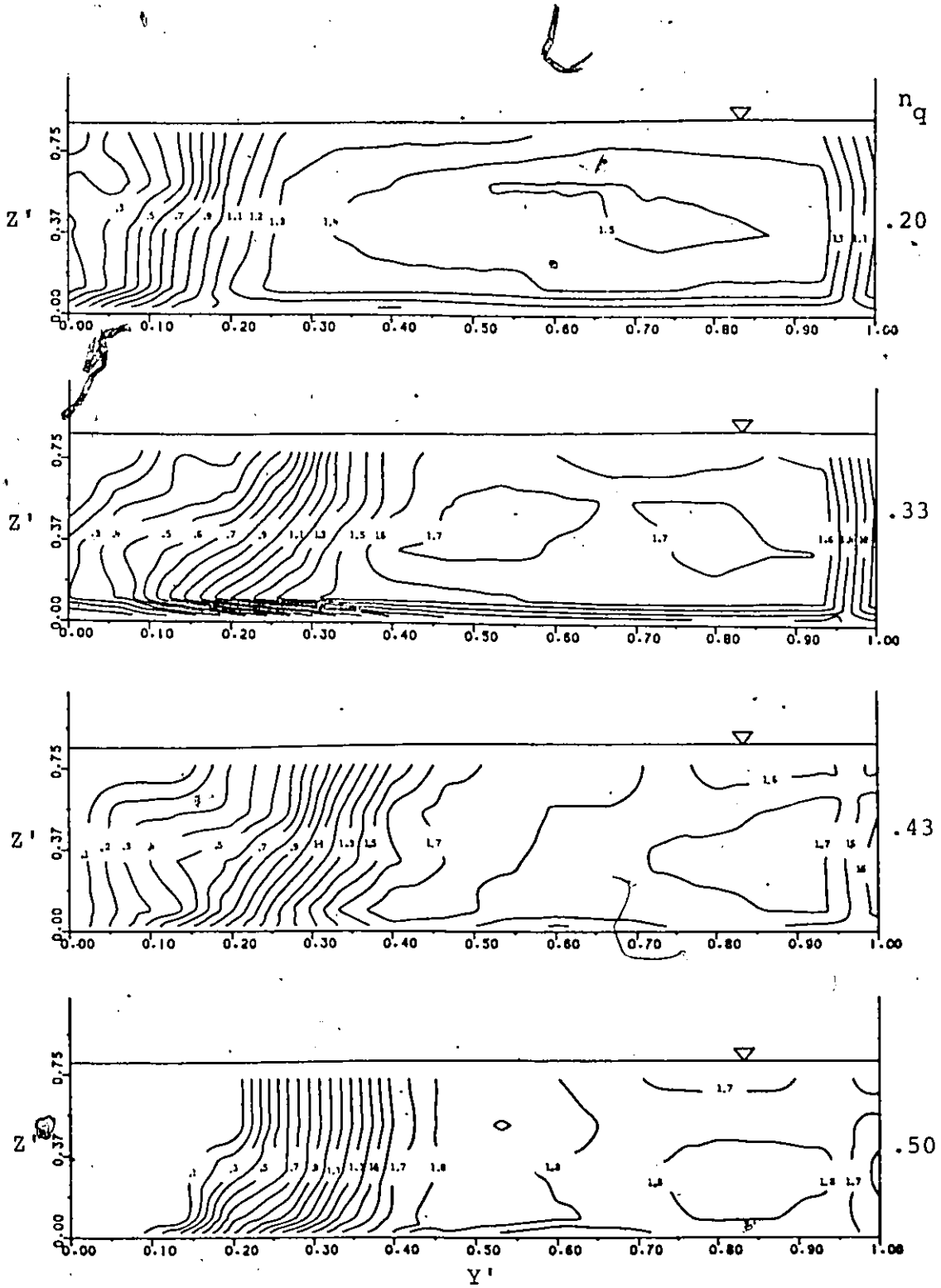

Figure 28: Isovel Patterns for 7.6 cm Guide Vanes (X' = 1.31)

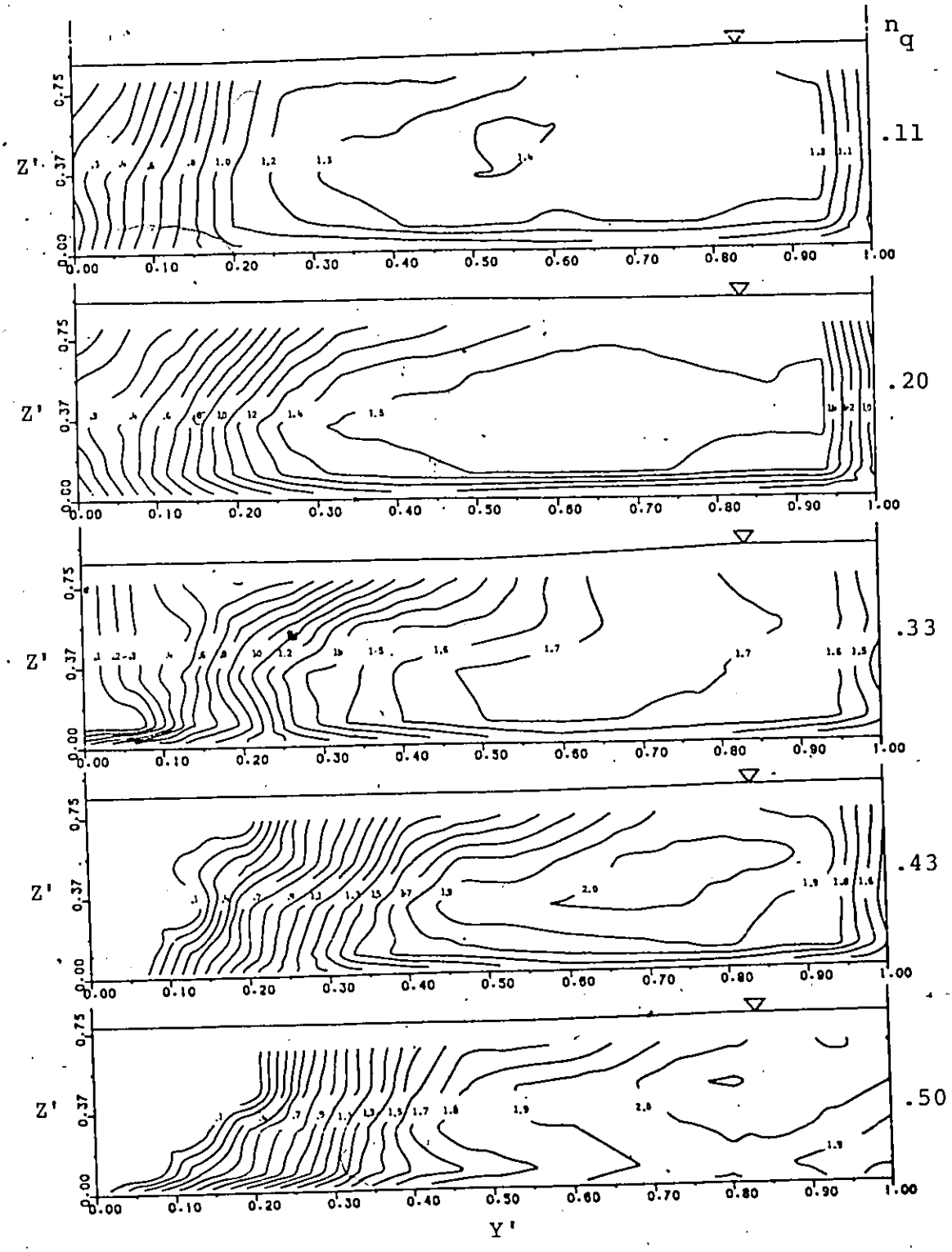

Figure 29: Isovel Patterns for 3.8 cm Guide Vanes (X' = 1.31)

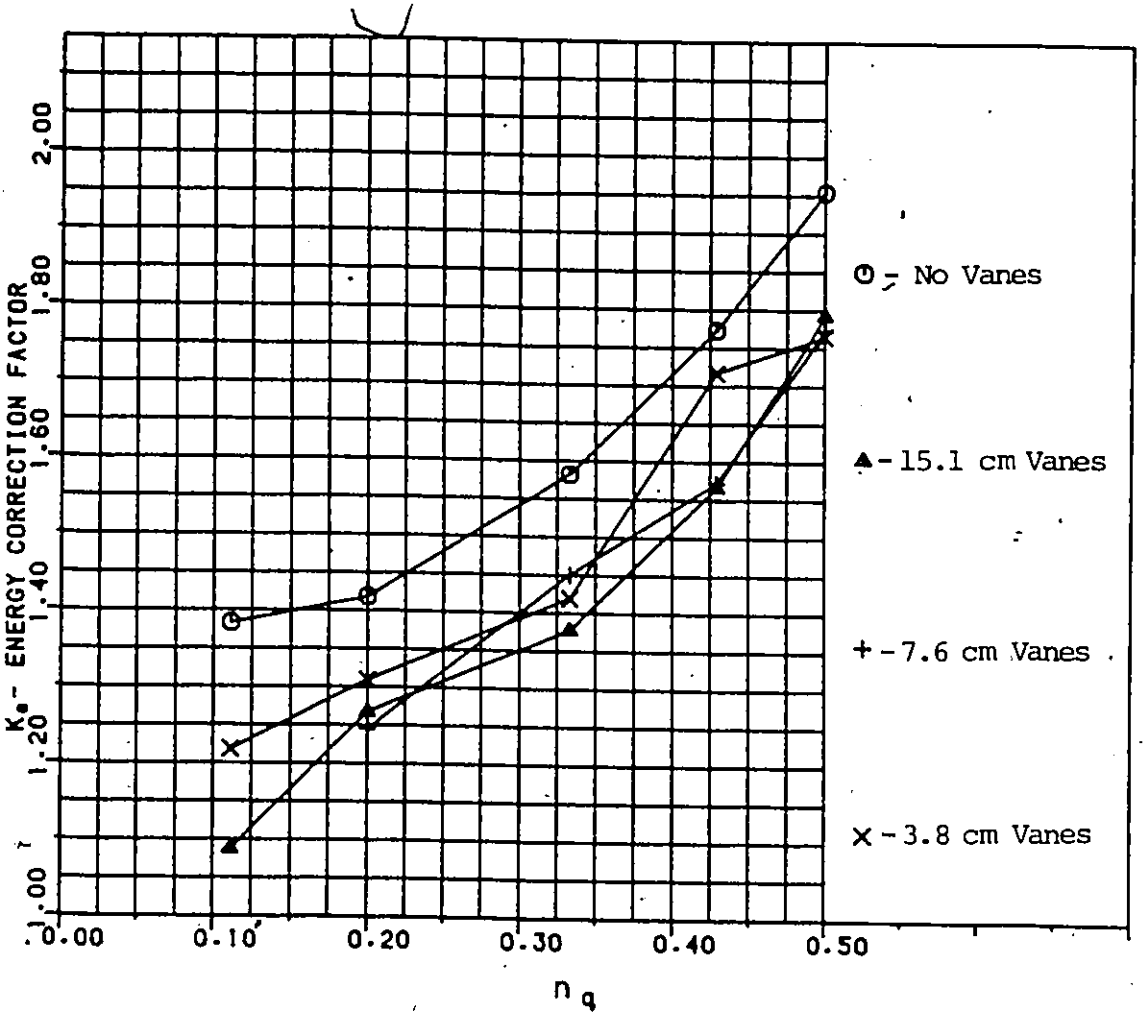

Figure 33: K_e vs n_q for Plain Junction and Guide Vanes (X' = 1.31)

In summary, then, the effects of the guide vanes were to give some marginal reduction in the maximum velocities and significant reductions in the unutilized flow area and the kinetic energy factor.

5.4.3 Shear Stress

The shear stress distributions for the guide vanes at station 1 are shown in Figures 34 to 36. These show that

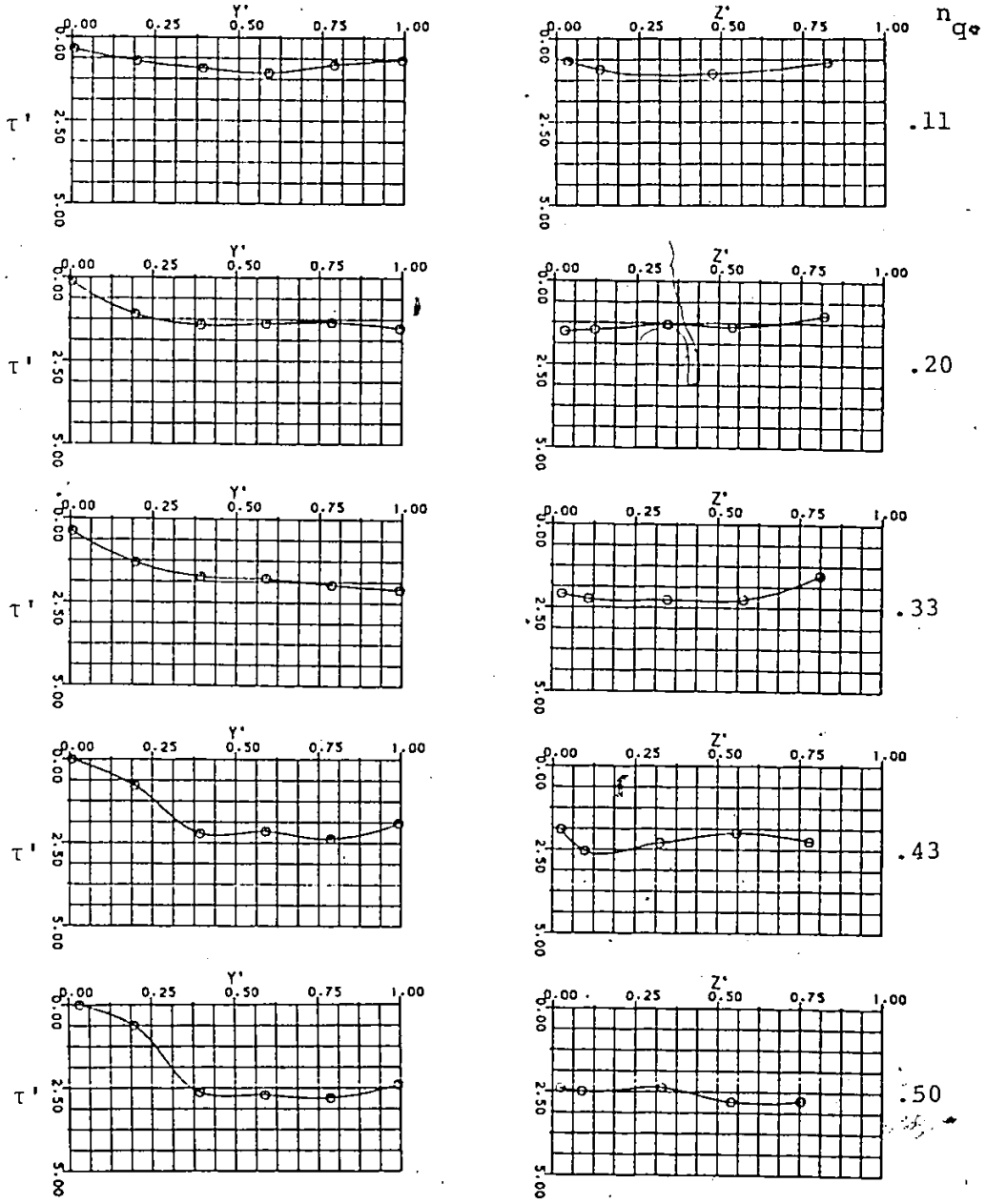

Figure 34: Shear Stress Distributions for 15.1 cm Guide Vanes (X' = 1.31)

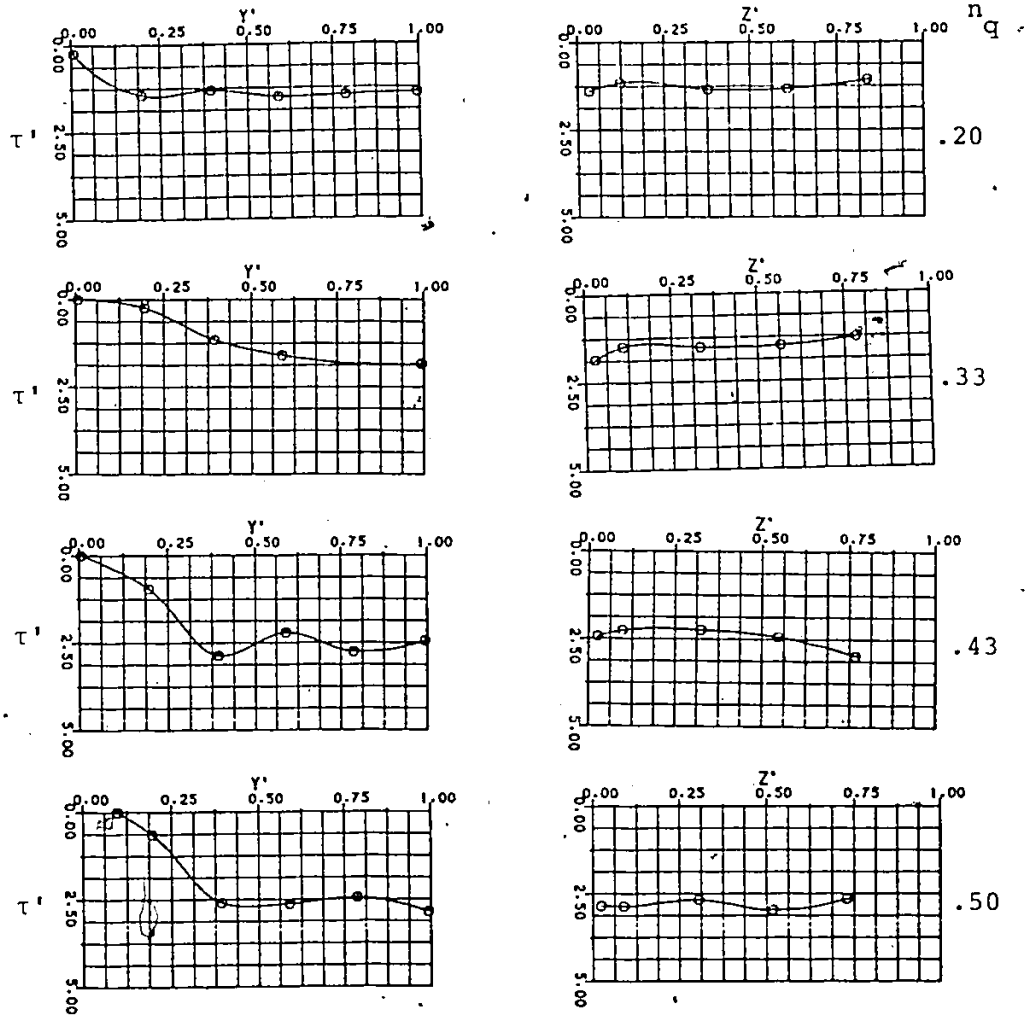

Figure 35: Shear Stress Distributions for 7.6 cm Guide Vanes (X' = 1.31)

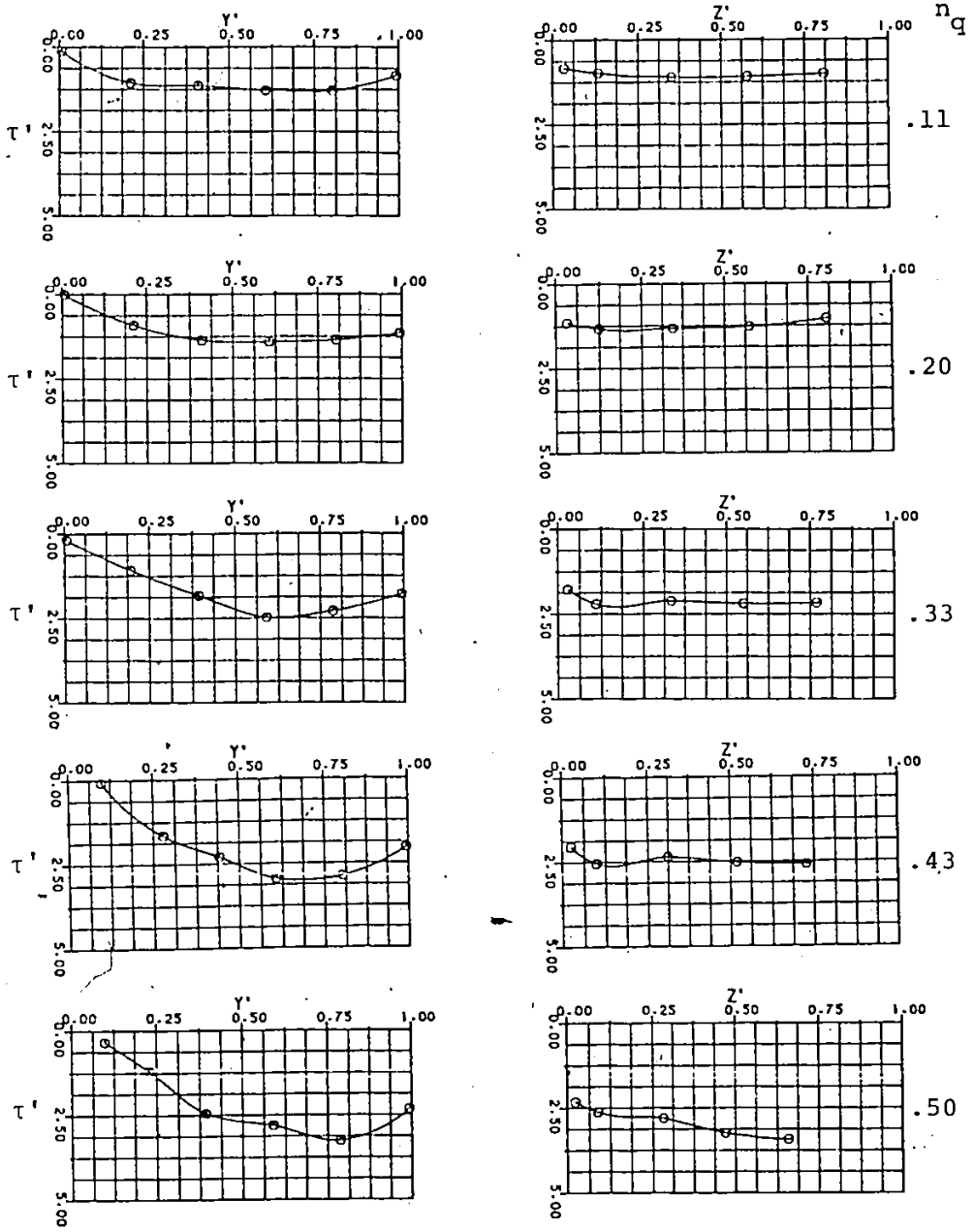

Figure 36: Shear Stress Distributions for 3.8 cm Guide Vanes ($\dot{X}'$ = 1.31)

the change in stresses as a result of the guide vanes being present was a general reduction of the bed stresses and little or no change in the wall shear stresses. This change became less as the height of the vanes decreased. Reference to Figures 37-a to 39-a shows that the change in the bed and right wall stresses from those measured for no guide vanes was marginal at station 2.

Although the vanes did reduce the maximum bed stresses slightly, it must be kept in mind that this change is small, and that the maximum stress is still substantially greater than that measured for uniform flow and that calculated using the theoretical expression $\gamma R S$ (as much as 360% and 320% respectively). Thus this area of the natural channel would undoubtedly still require some protection to prevent excessive erosion.

5.4.4 Mixing Energy Losses

The results of the determination of the mixing energy loss coefficient were interesting for two reasons. The first was that this was usually larger with the vanes than without (see Figure 40), although the difference is small. Secondly, in several instances this was determined to be less than zero-implying that the turbulence added energy rather than consumed it. This is of course erroneous and the problem again lies in the determination of the friction

losses with a uniform flow equation.

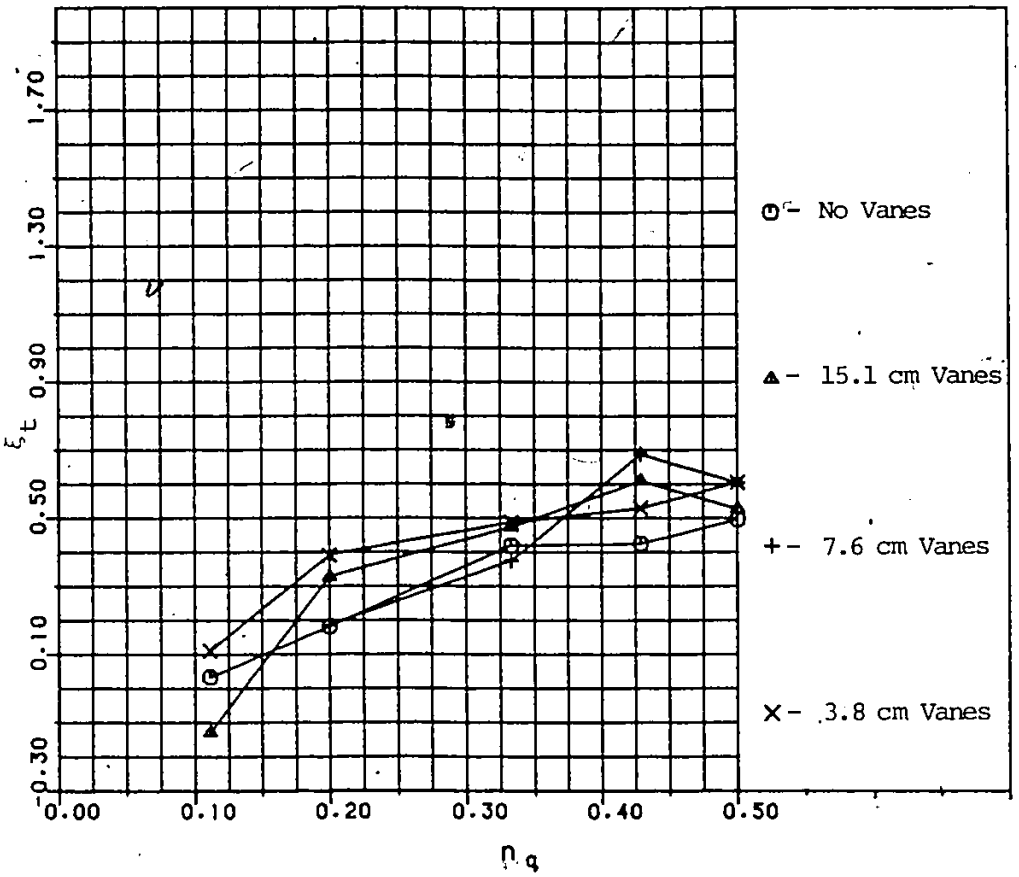

Figure 40: ξ_t vs η_q for Guide Vanes

5.5 OUTLET GEOMETRY CHANGES

Practical considerations concerning the construction and maintenance of guide vanes (as well as their poor performance) suggested that, to effectively improve flow performance, attention should be focussed on improving the outlet geometry of the culvert, or lateral channel. Several changes were tried and are discussed here separately.

5.5.1 Beveled Outlet Corner

The first change made was to bevel the downstream corner of the outlet according to Figure 8. This was found to cause a substantial change on the flow characteristics of the confluence.

5.5.1.1 Dye Results

Results of the preliminary dye studies showed that, since the flow was encouraged to turn downstream sooner, the dye, when injected into the lateral channel, took a much longer distance to reach the right wall of the receiving channel. Also, it reduced the 'dead zone' where the circulatory motions occur. This is illustrated in Plate 4 for n_q equal 0.33.

5.5.1.2 Velocity Distribution

The isovel patterns shown in Figure 41 for the beveled outlet over a range of flow rates show a profound change in the velocity distribution at station 1 over those for a plain junction. With the beveled outlet maximum velocities were reduced and the location of same rose and moved more toward the center of the section. However, further downstream at station 2 these improvements were much less pronounced, although the distributions were much more uniform

Beveled Outlet

Large Deflection Wall

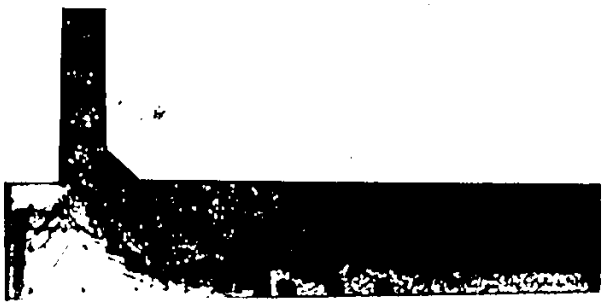

Small Deflection Wall

Plate 4: Dye Results for Outlet Geometry Changes (n_q = 0.33)

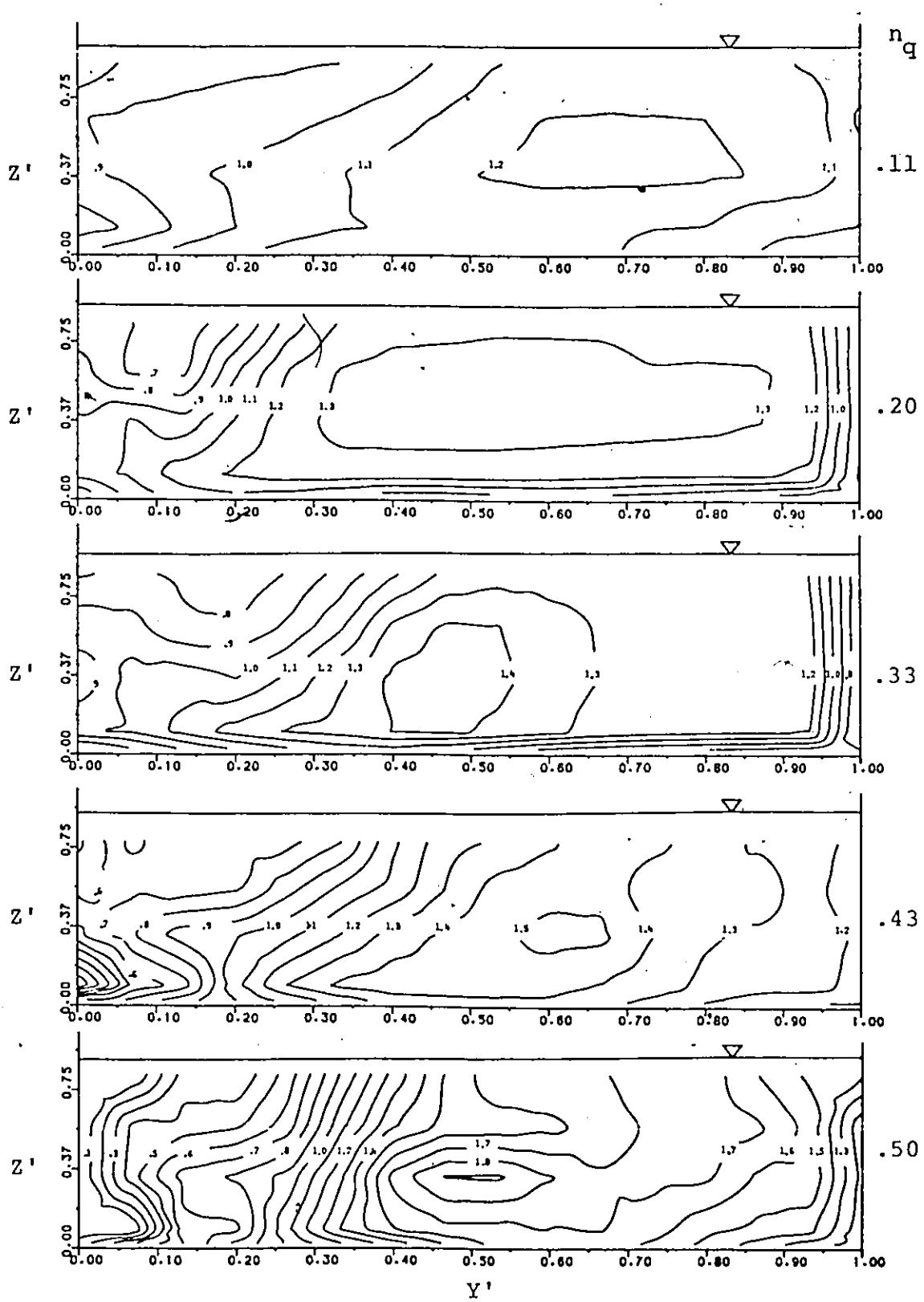

Figure 41: Isovel Patterns for Beveled Outlet (X'=1.31)

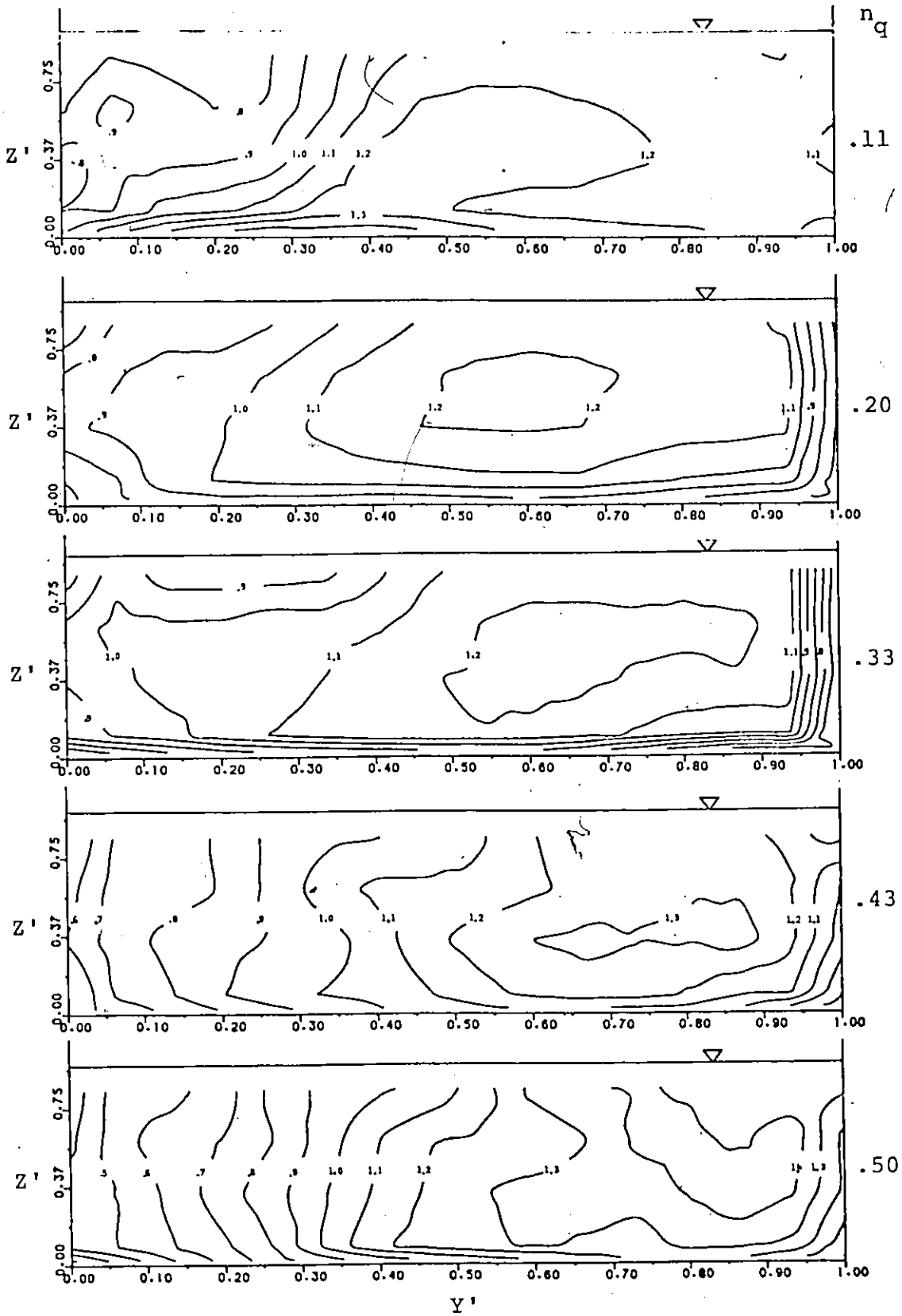

Figure 42: Isovel Patterns for Beveled Outlet (X' = 2.95)

and regular with the beveled outlet in place (see Figure 42). This is further illustrated by Tables 8-a and 9-a. The reason for this improvement at the upstream station was that although some redirection of the lateral inflow occurred sooner because of the bevel, there was nothing introduced to reduce its lateral momentum and thus it still, eventually, penetrated the main channel profile and shifted it by the same amount.

This improvement in the velocity distributions is also dramatically illustrated by the reduction in the energy correction factors shown in Figure 43. These showed a substantial decrease both at stations 1 and 2 (as much as 33 and 24% respectively) over the whole range of flows and at the lower flow ratios (n_q less than 0.33) the factor became nearly independent of the distance from the confluence and n_q. As well as this, K_e was found to be very nearly equal to that for uniform flow (1.06 vs 1.02).

5.5.1.3 Shear Stress Distributions

The shear stress distributions shown in Figure 44 showed some improvement over those obtained for a plain junction, most especially for flow ratios of 0.43, 0.33 and 0.20. These, however, were still both high and well above those distributions obtained for uniform flow (from

75 to 320% above). This was due to the relatively high bed and wall velocities still present.

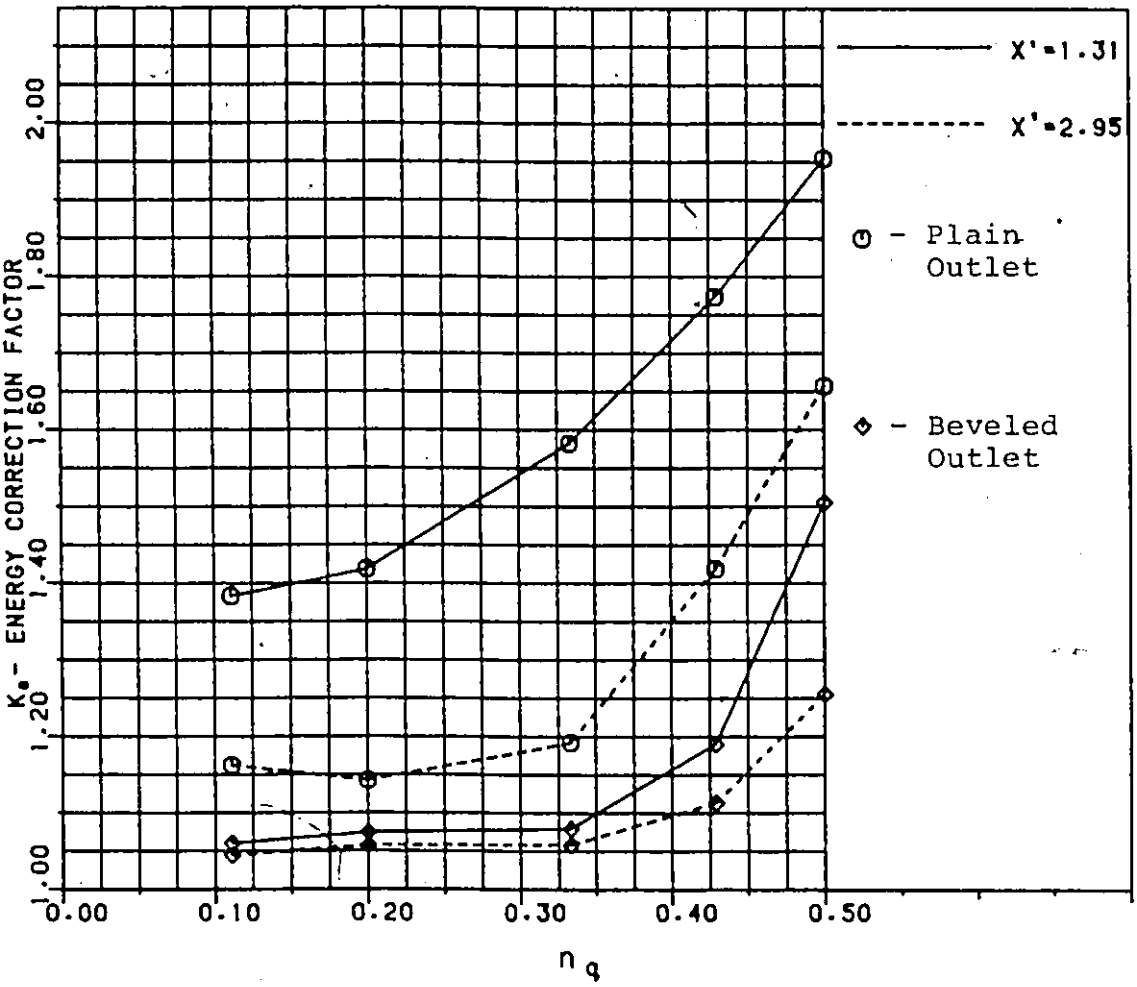

Figure 43: K_e vs n_q for Beveled Outlet

5.5.1.4 Mixing Energy Losses

The mixing energy losses for the beveled outlet (shown in Figure 45), although usually less than those for the plain junction, appeared to be quite unstable. Several values at station 2 were less than zero, and also all values (at station 2) were less than those upstream, indicating en-

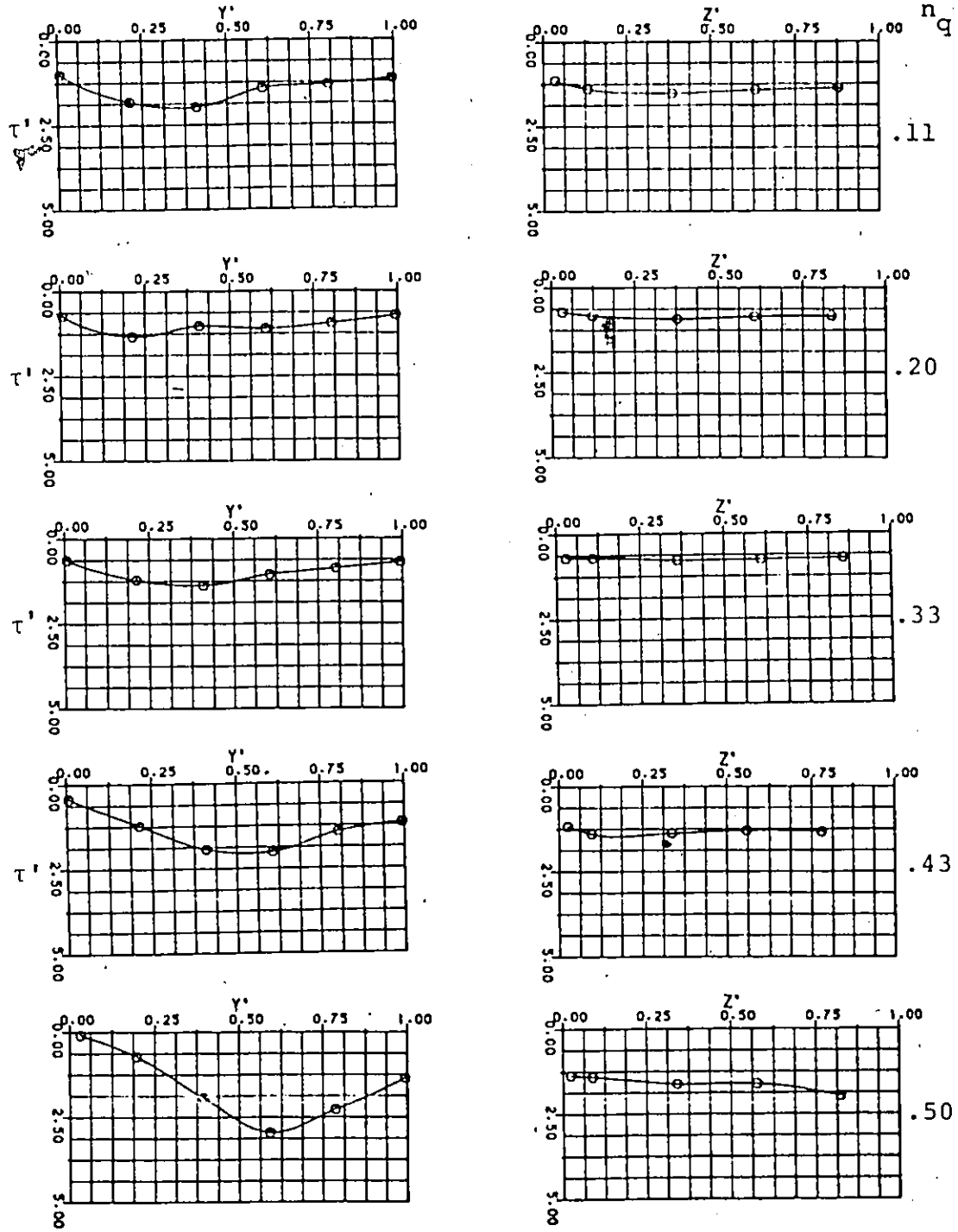

Figure 44: Shear Stress Distributions for Beveled Outlet (X' = 1.31)

energy was being added from station 1 to 2. This anomaly was due to the aforementioned problems concerning the calculation of the friction losses.

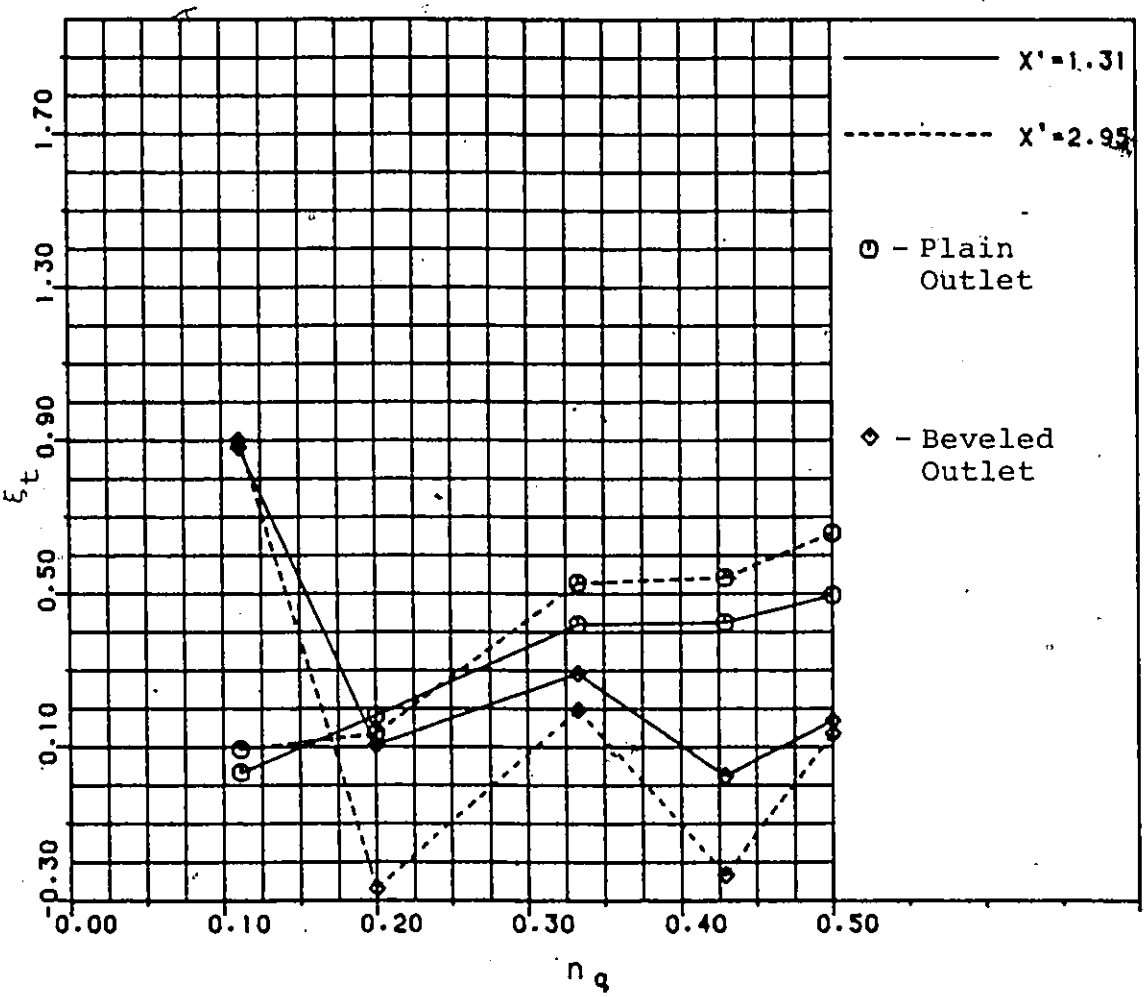

Figure 45 : ξ_t vs n_q for Beveled Outlet

5.5.2 Deflection Wall

To further assist the redirection of the incoming lateral flows, two different 'deflection walls' were installed at the upstream corner of the outlet (with the downstream corner still beveled). This was done not only because it would redirect the flow, but also because it would help to

reduce the lateral momentum, and thus prevent the flow field from shifting to the right further downstream. These deflection walls were of two sizes, shown in Figures 9 and 10.

5.5.2.1 Dye Results

The injection of the dye into the incoming flow showed clearly that deflection walls helped to redirect the flows downstream, this of course was less for the smaller wall. However, further downstream it can be seen (Plate 4) that there was still substantial penetration of the main channel flow field by the lateral inflow.

5.5.2.2 Velocity Distributions

The isovel patterns in Figures 46 to 49 clearly showed the dramatic effects of the deflection walls at the downstream stations 1 and 2. The most obvious change is the shifting of the profile to the left, with the maximum velocity filament either at or to the left of center. This effect again was reduced with the smaller deflection wall. The maximum velocities, however, were larger than with the beveled outlet using the larger wall, and as well, there was less utilized flow area. This however, was not true for the smaller deflection wall, which showed maximum velocities very near those of the beveled outlet but much better centered in the cross section. In addition, the isovel patterns at

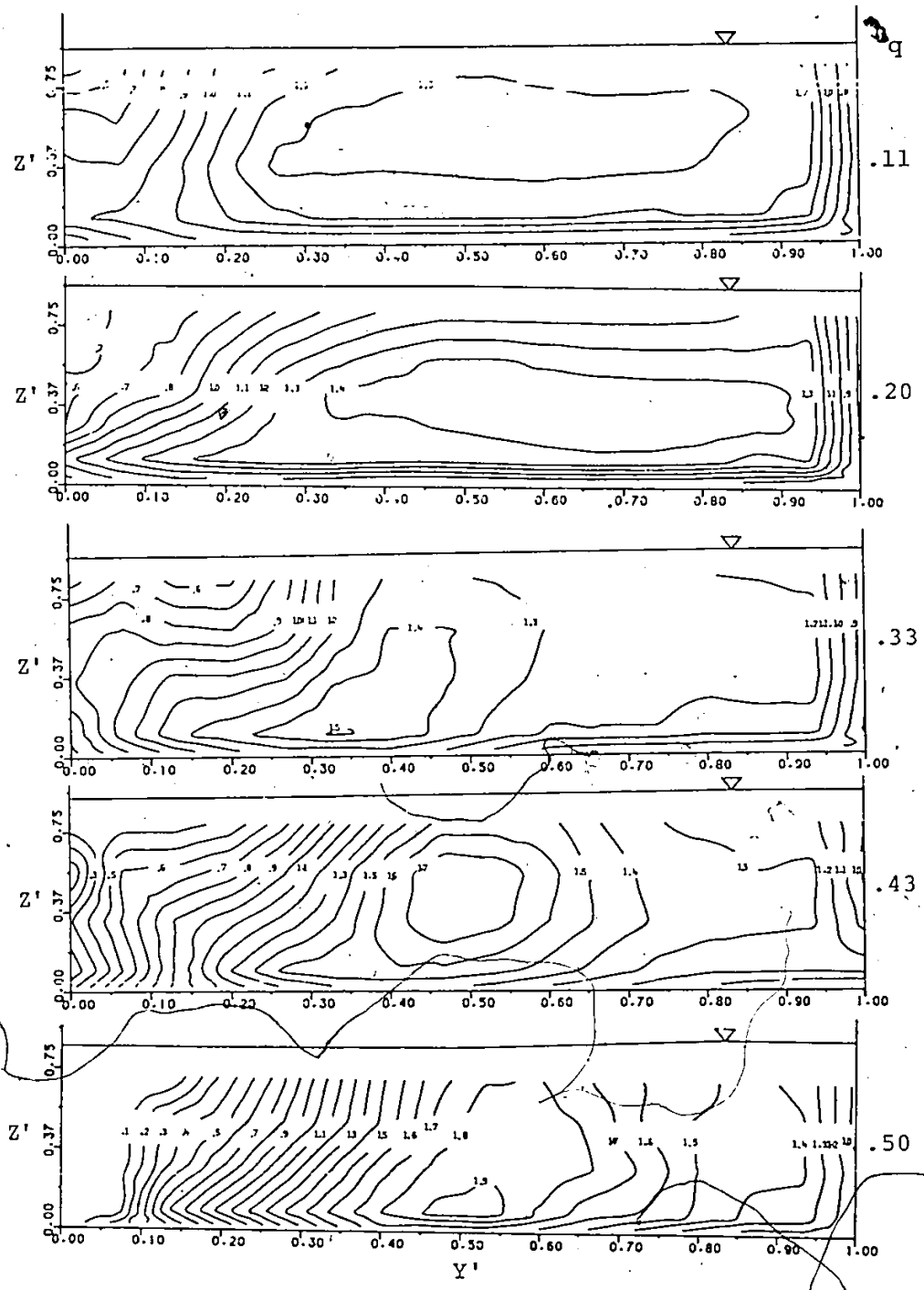

Figure 46: Isovel Patterns for Small Deflection Wall (X' = 1.31)

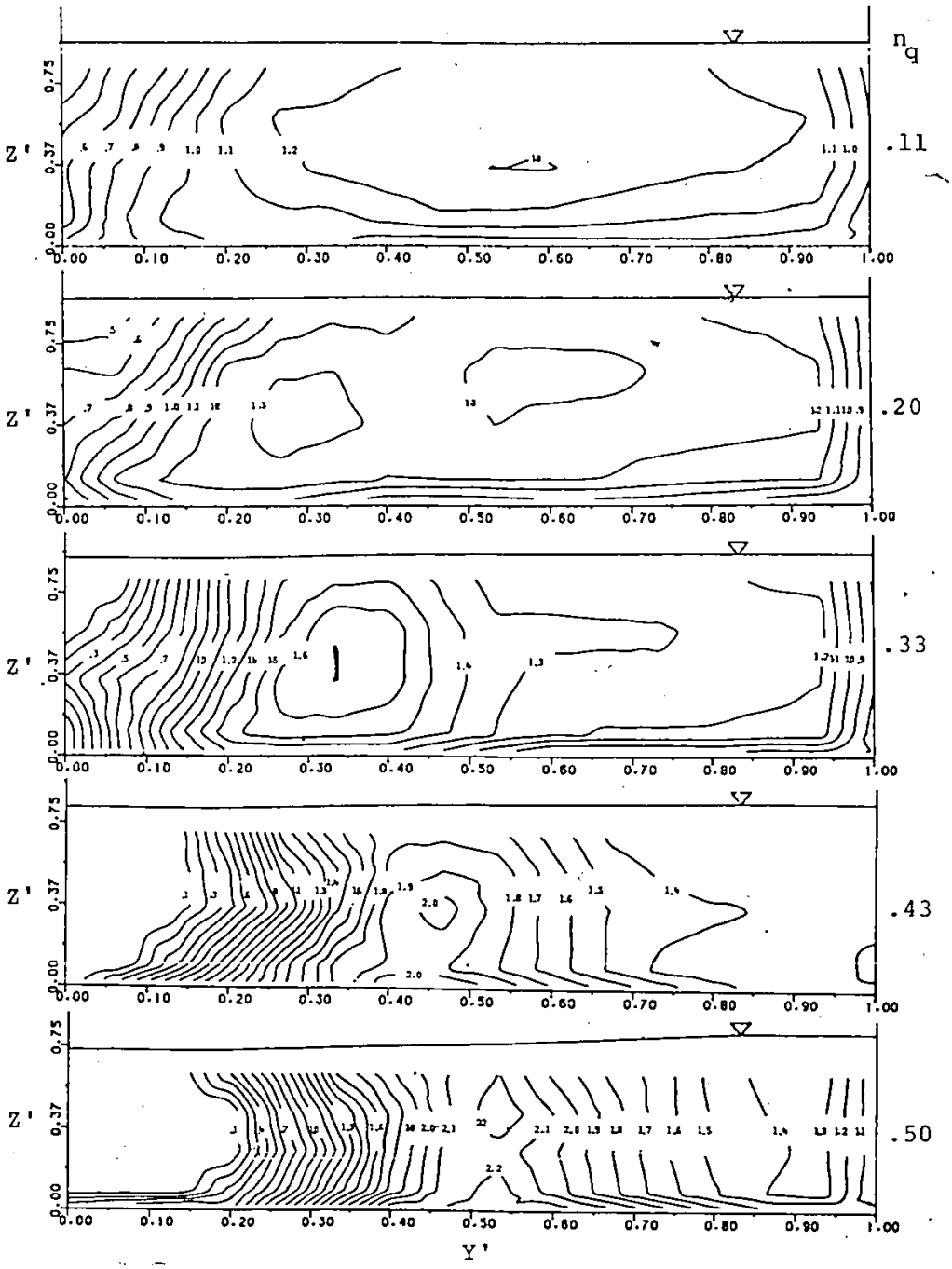

Figure 47: Isovel Patterns for Large Deflection Wall (X' = 1.31)

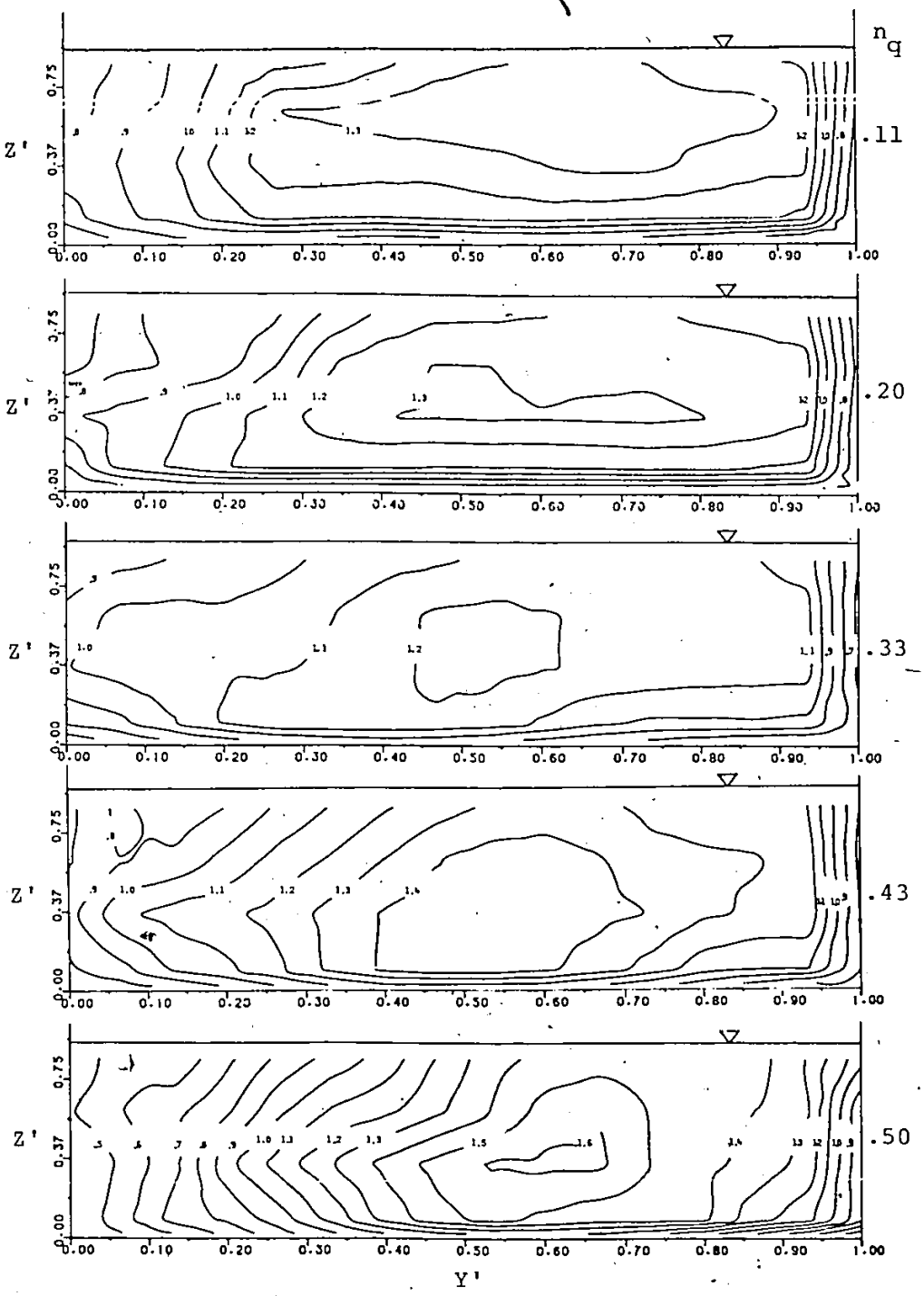

Figure 48: Isovel Patterns for Small Deflection Wall (X' = 2.95)

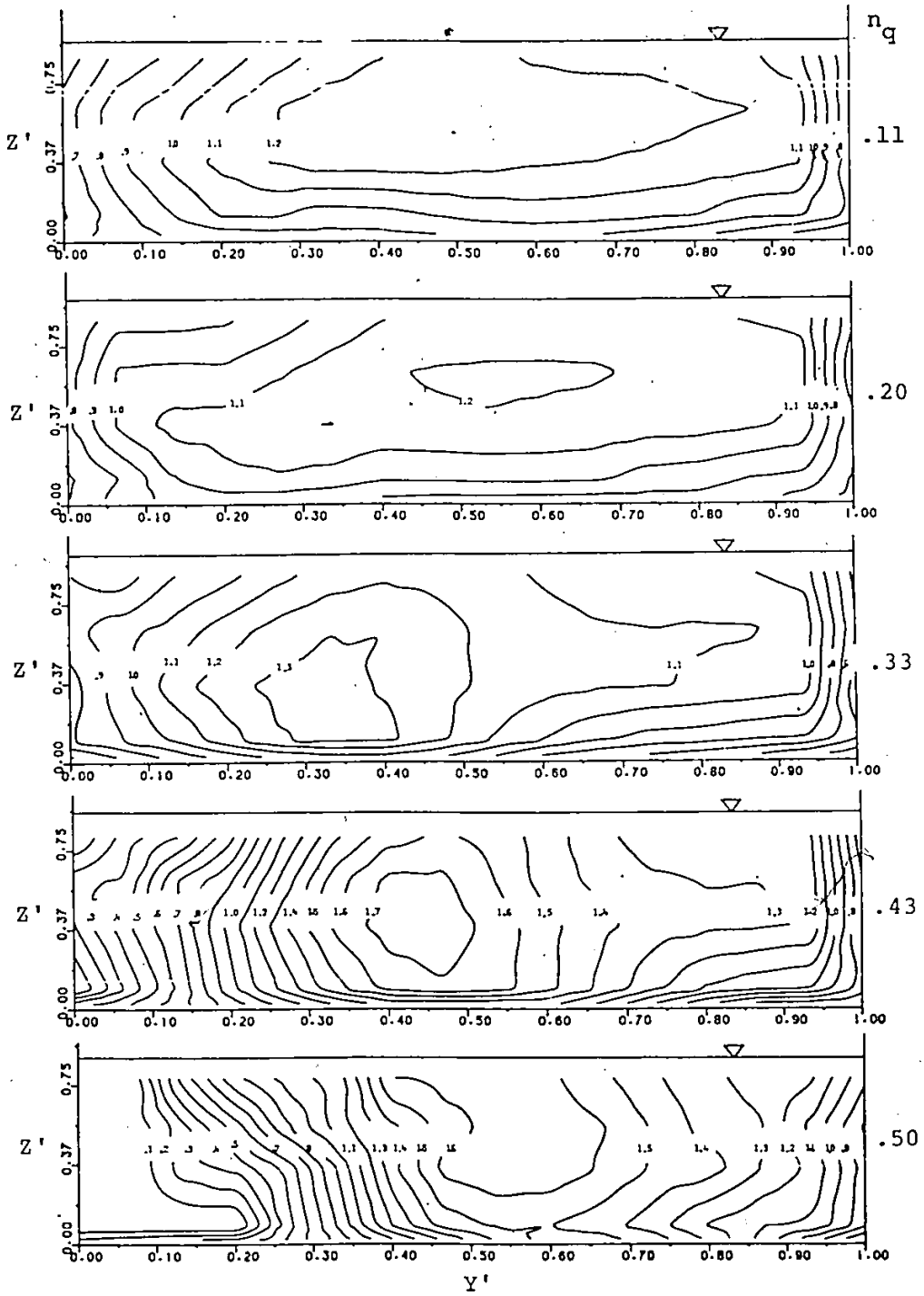

Figure 49: Isovel Patterns for Large Deflection Wall (X' = 2.95)

station 2 were very regular and were often approaching those for uniform flow conditions, particularly for the small deflection wall.

The reason for the reduced improvement with the large deflection wall can be attributed to the effect of the wall on the conditions in the lateral channel. Since the depth of flow in the lateral channel is controlled by the conditions at the exit, the presence of the wall at the end of the lateral channel created a 'ponding' effect in the channel. Thus for n_q equal to 0.50 the depth in the channel just before the confluence was found to increase by 33% and 10% for the large and small walls respectively. This had two effects:

1. Raising the incoming energy;

2. Raising the incoming depth over that in the junction.

The result of this latter effect was that upon entering the main channel, the incoming flow velocity had a significant downward component which forced the maximum velocity toward the bed. Obviously this could cause erosion problems in the receiving channel if left unchecked. In addition to this problem, the 'ponding' effect would necessitate a larger culvert to pass the required flow-if the energy level at the

culvert inlet was to remain the same (under outlet control conditions).

The energy correction factors shown in Figure 50 for station 1 show that although there was a substantial decrease over that for a plain junction, (up to 33%) they were still larger than that for the beveled outlet-at least at the higher flow ratios. For example at $n_q = 0.50$, K_e values were 24 and 7% greater with the large and small deflection walls respectively. This increase over the beveled outlet condition was due to the increase in the incoming energy, and was futher illustrated by the fact that K_e values for the larger wall in place were always greater than those for the

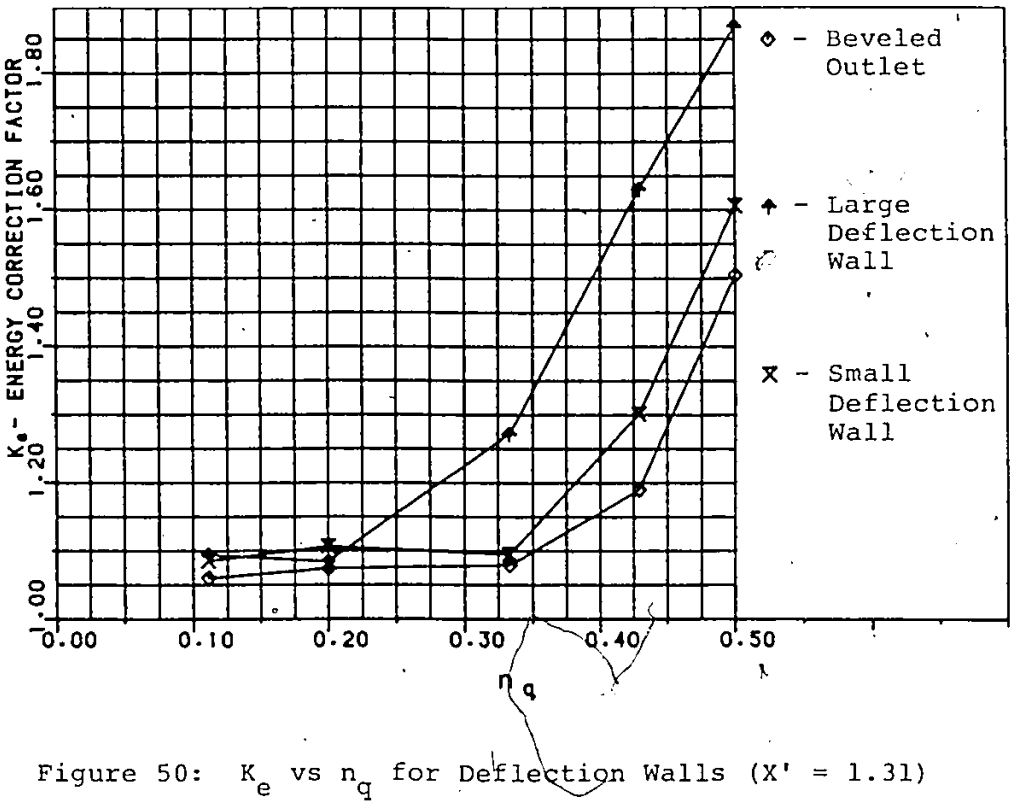

Figure 50: K_e vs n_q for Deflection Walls (X' = 1.31)

smaller wall. At station 2 these factors again followed these tendencies and approached uniform flow values at the lower flow ratios (see Figure 51).

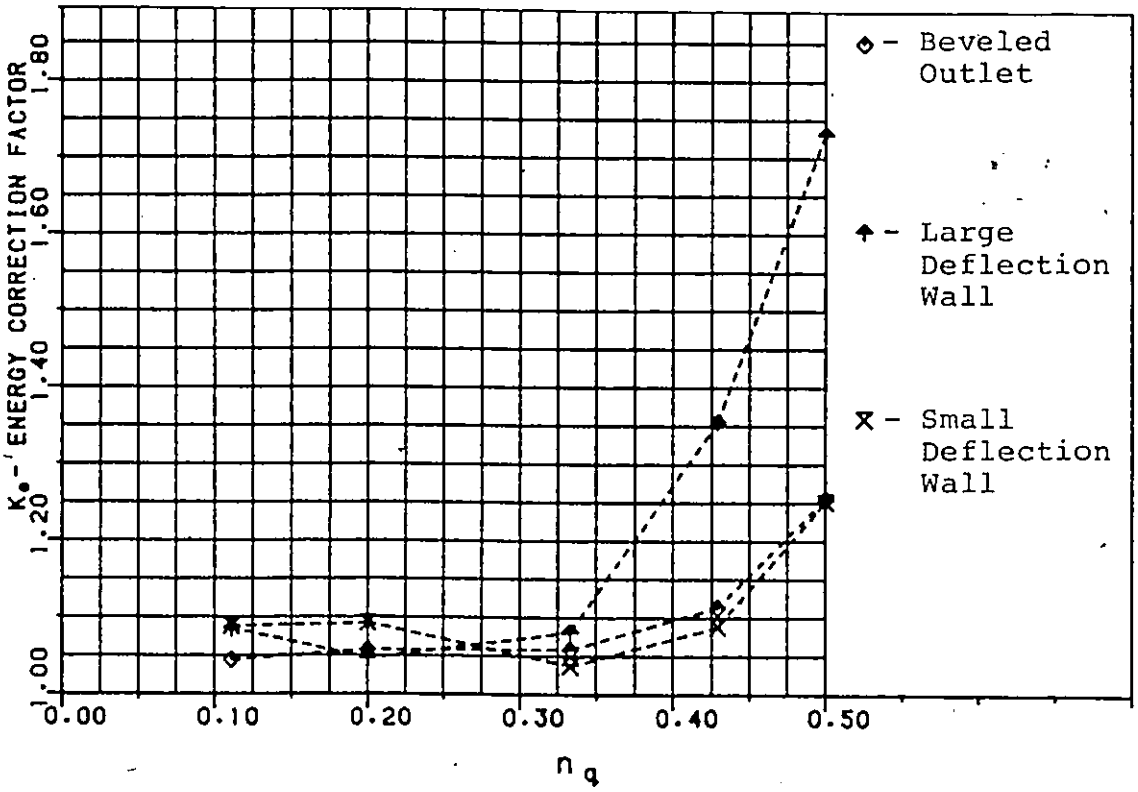

Figure 51: K_e vs n_q for Deflection Wall (X' = 2.95)

5.5.2.3 Shear Stress Distributions

The shear stress distributions in Figures 52 and 53 for station 1 show the effects of redirection of the flow and of backwater in the lateral channel. In most cases the maximum bed shear stress shifted substantially to the left and also increased in value. This was more noticeable with the larger

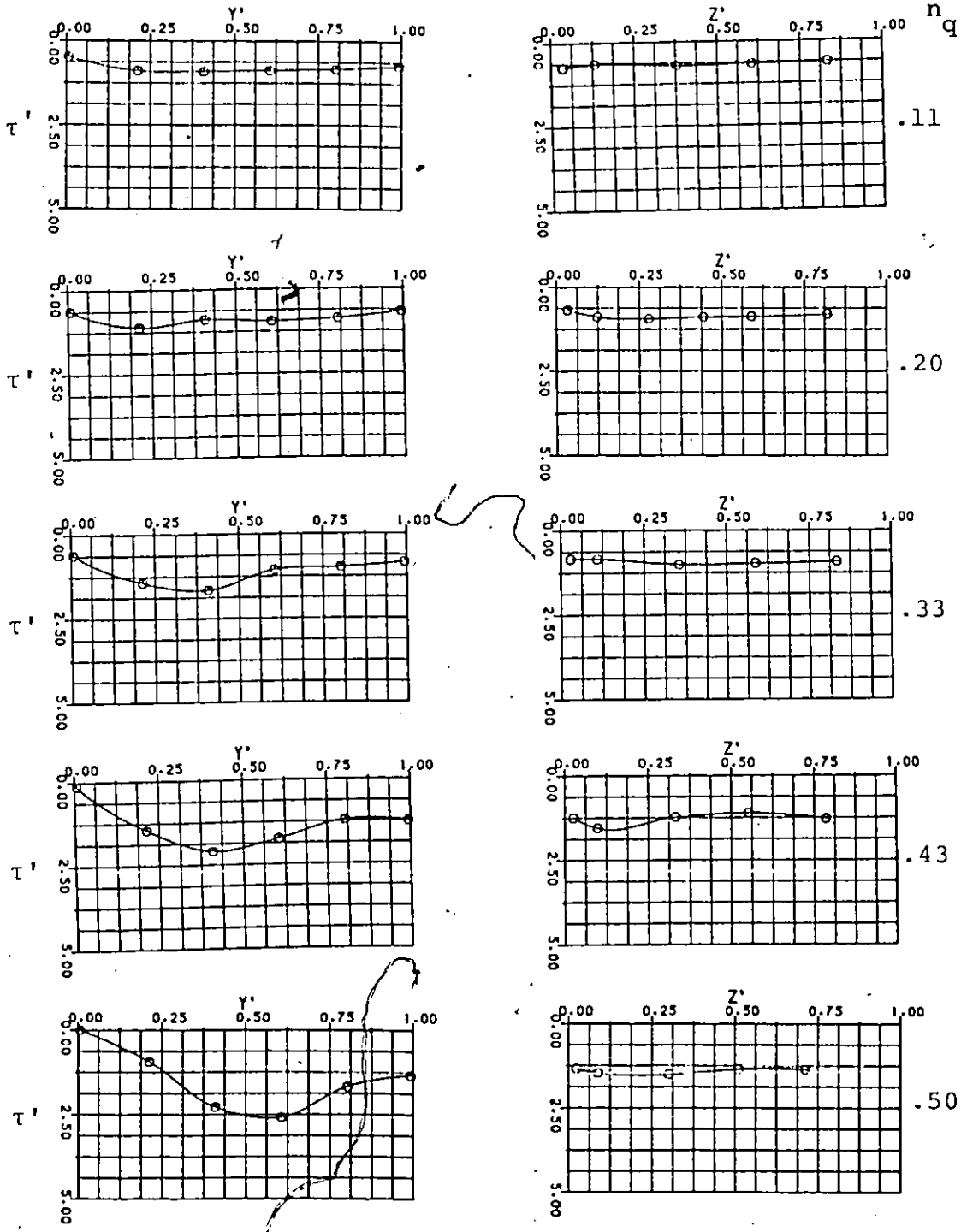

Figure 52: Shear Stress Distributions for Small Deflection Wall (X' = 1.31)

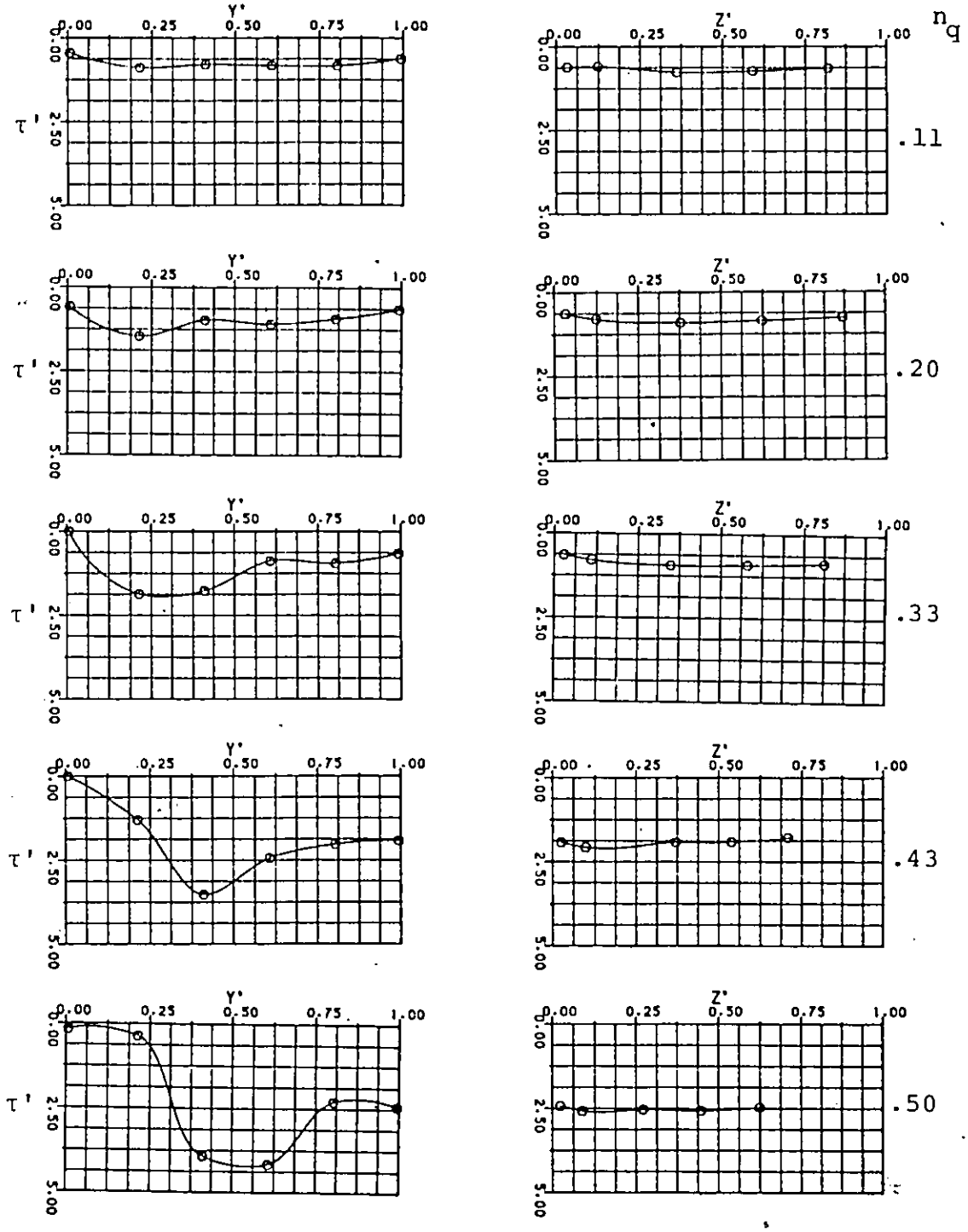

Figure 53: Shear Stress Distributions for Large Deflection Walls (X' = 1.31)

deflection wall. The shift to the left was of course due to the additional flow redirection as a result of the wall. The deleterious effect of the increase in the values of the shear stress (up to 4 times that determined using γ R S) was a result of the downward velocity component of the inflow, which in turn forced the higher velocities toward the bed. This effect was seen to diminish as the flow ratio (and thus the backwater effect) decreased. Similar results to these are also found in Figures 54-a and 55-a for station 2.

5.5.2.4 Mixing Energy Losses

The results of the determination of the mixing energy loss coefficient (shown in Figure 56) were again inconclusive. Although these were found to be larger than those for the beveled outlet at the higher flow ratios, the values were again erratic and no definable trend appeared.

5.5.3 Reverse Slopes

As a result of the high bed shear stress experienced with the beveled outlet (with and without the deflection walls), two attempts were made to give the incoming flow an upward velocity component to reduce the bed velocities. Because of the aforementioned problems with the backwater caused by the deflection walls, these attempts were in addition to the beveled outlet only. The first solution was to give the outlet a reverse

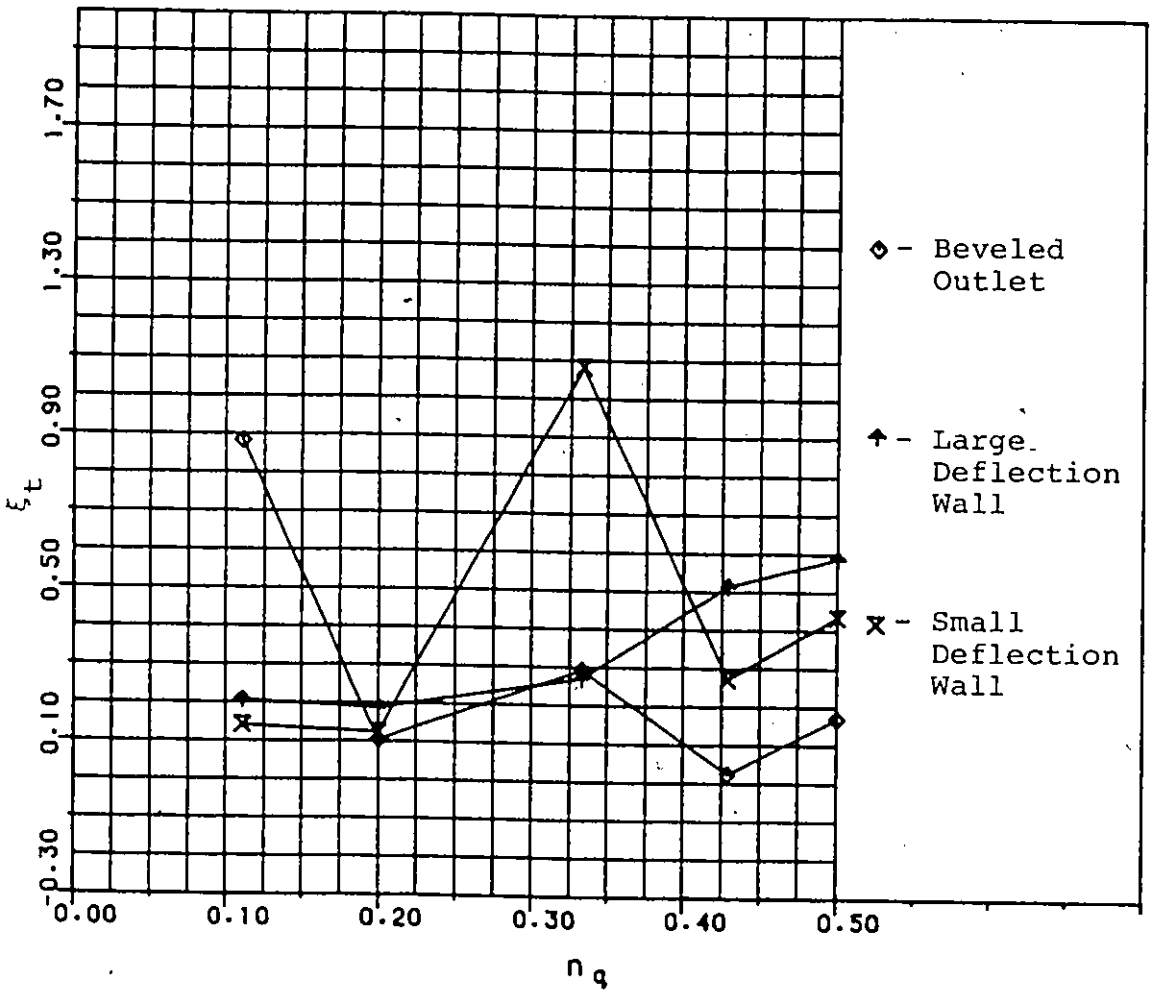

Figure 56: Mixing Energy Loss Coefficient for Deflection Walls (X' = 1.31)

invert slope as shown in Figure 11. Secondly, since the former might experience reduced beneficial effects if the culvert outlet were to be partially covered by sediment (which may occur at low flows), a superelevated reverse slope was tried which would allow both low flows and sediments to pass unimpeded into the receiving channel. Also, it was felt that this latter attempt might also help to redirect the lateral flows downstream.

5.5.3.1 Velocity Distributions

The isovel patterns in Figures 57 to 60 for both downstream stations show the effects of the reverse and superelevated reverse slope on the flow field. As noted, although there was some raising of the maximum velocity at station 1, this was lost by station 2. These velocities are also summarized in Tables 8-a and 9-a. The maximum bed velocities would also appear to be slightly less with these modifications in place, although the superelevated reverse slope is less effective in this regard, again this effect was lost by station 2. The same was also true for the right wall velocities. The energy correction factors shown in Figure 61 also indicated that these slope modifications had little or no effect on the flow field at station 1 by the less than 2% change in K_e. This was also found to be true at station 2.

5.5.3.2 Shear Stress Distribution

The shear stress distributions shown in Figures 62 and 64 showed some, marginal, reduction in the boundary shear stresses. As with the other effects the superelevated reverse slope would appear to be less effective. Also, these effects were negligible both at station 2 (Figures 63 and 65) and at the lower flow ratios.

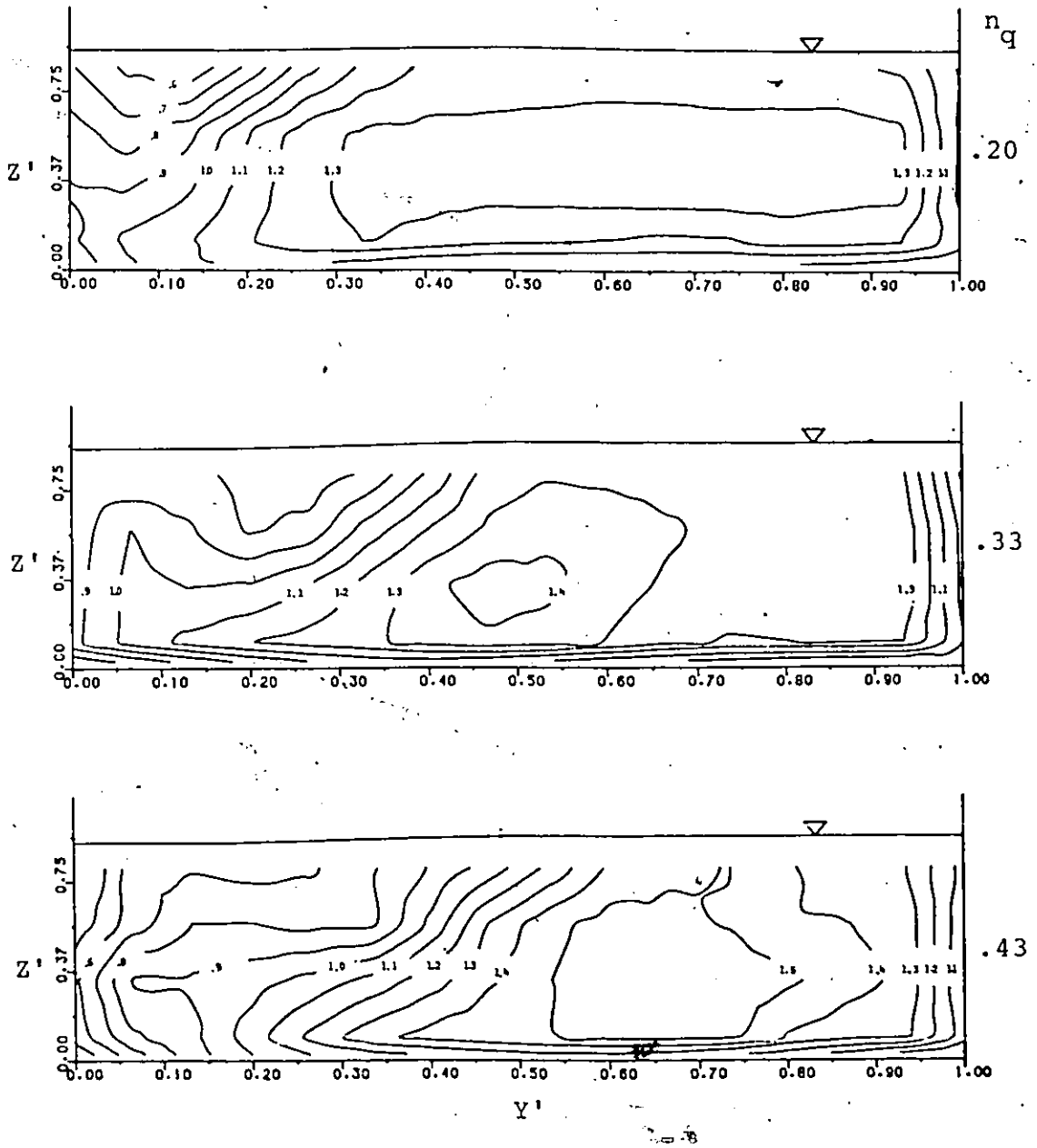

Figure 57: Isovel Patterns for Reverse Slope (X' = 1.31)

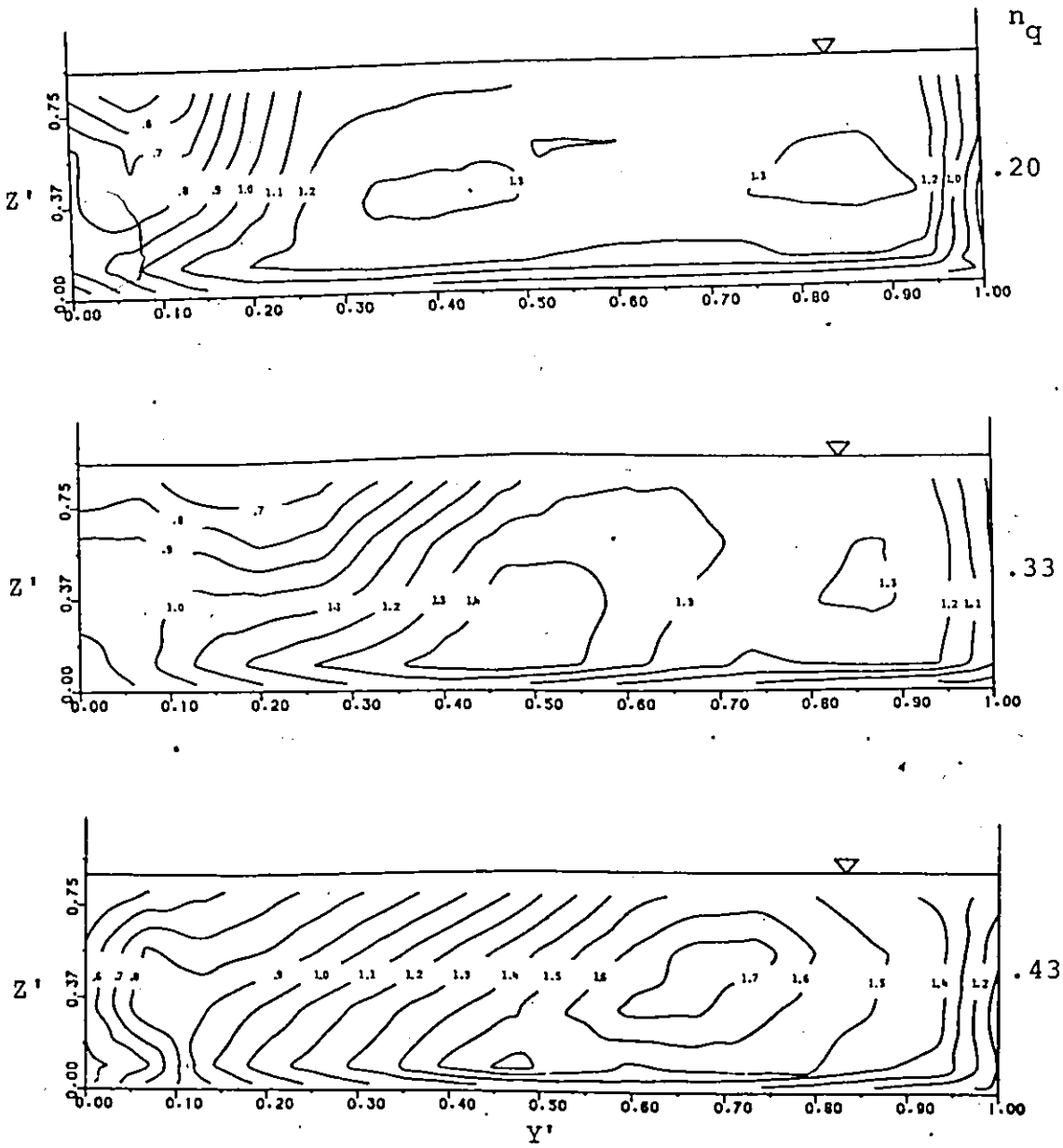

Figure 58: Isovel Patterns for Superelevated Reverse Slope (X' = 1.31)

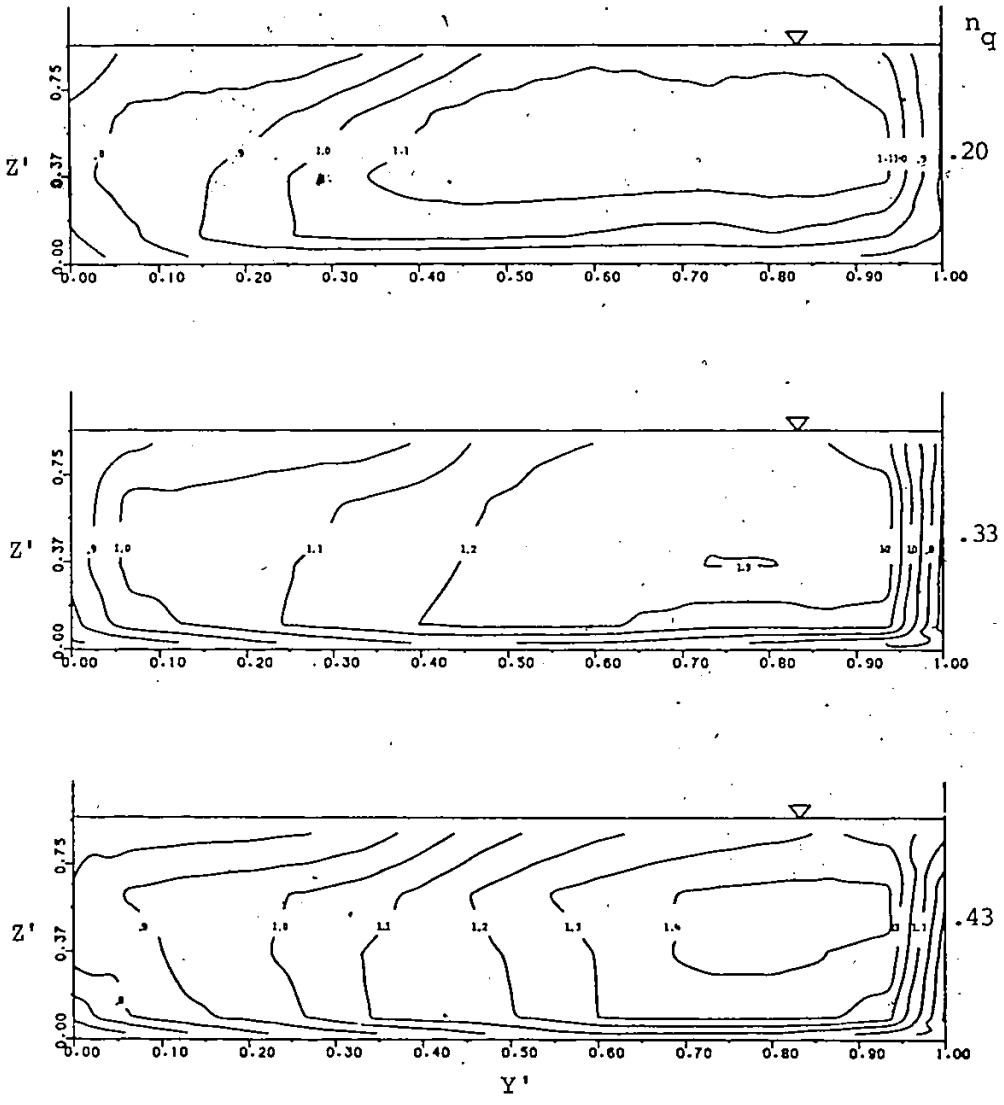

Figure 59: Isovel Patterns for Reverse Slope (X' = 2.95)

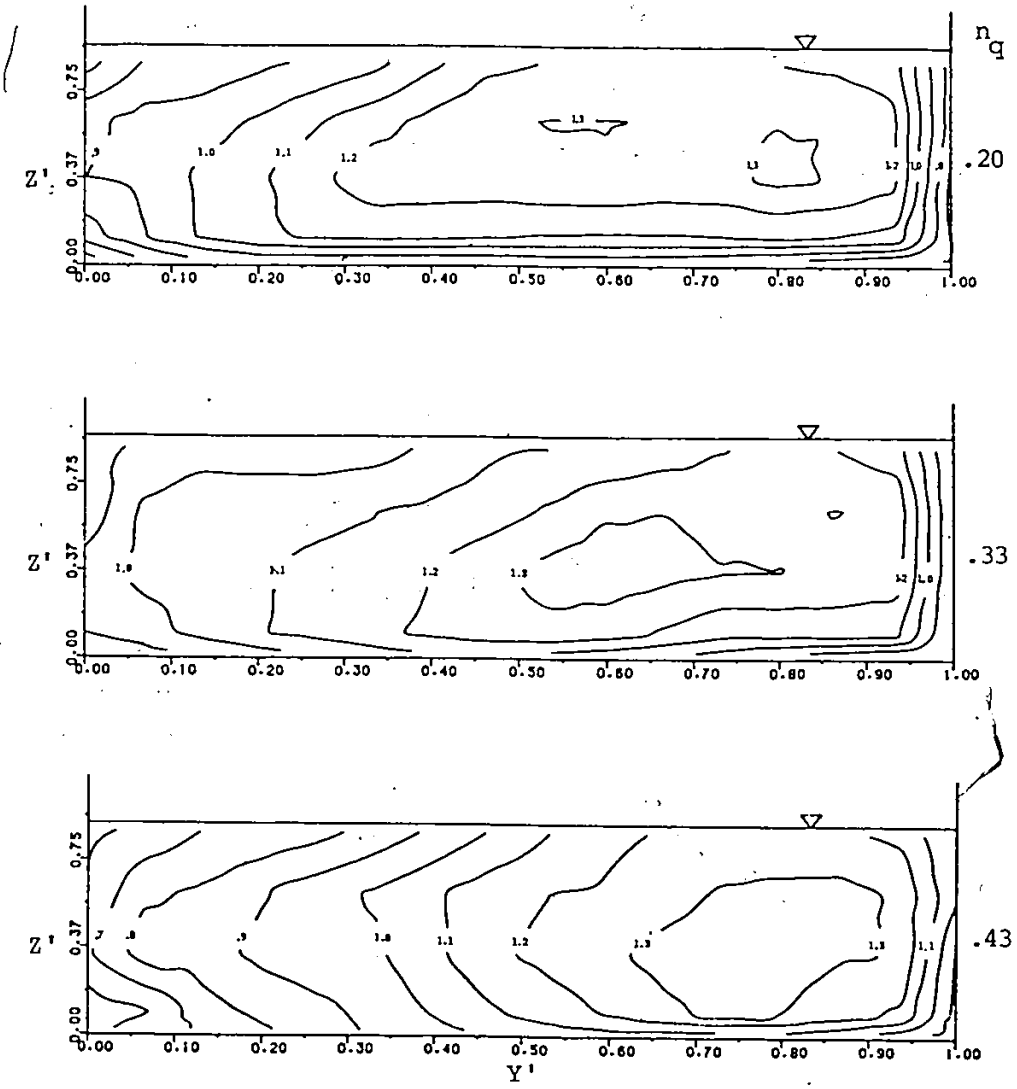

Figure 60: Isovel Patterns for Super elevated Reverse (X' = 2.95)

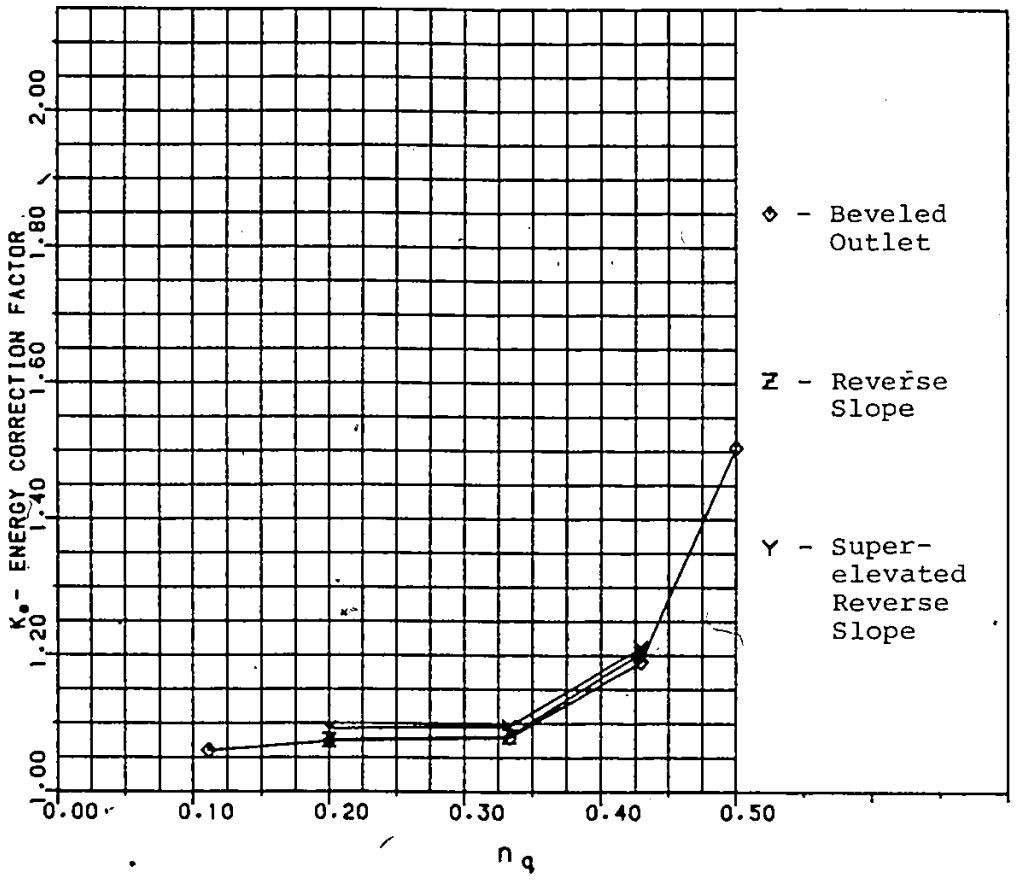

Figure 61: K_e vs n_q for Slope Modifications (X' = 1.31)

5.5.3.3 Mixing Energy Losses

The mixing energy loss coefficient, shown in Figure 66 for station 1 was very similar to that obtained for a beveled outlet, with perhaps a tendency to be somewhat higher.

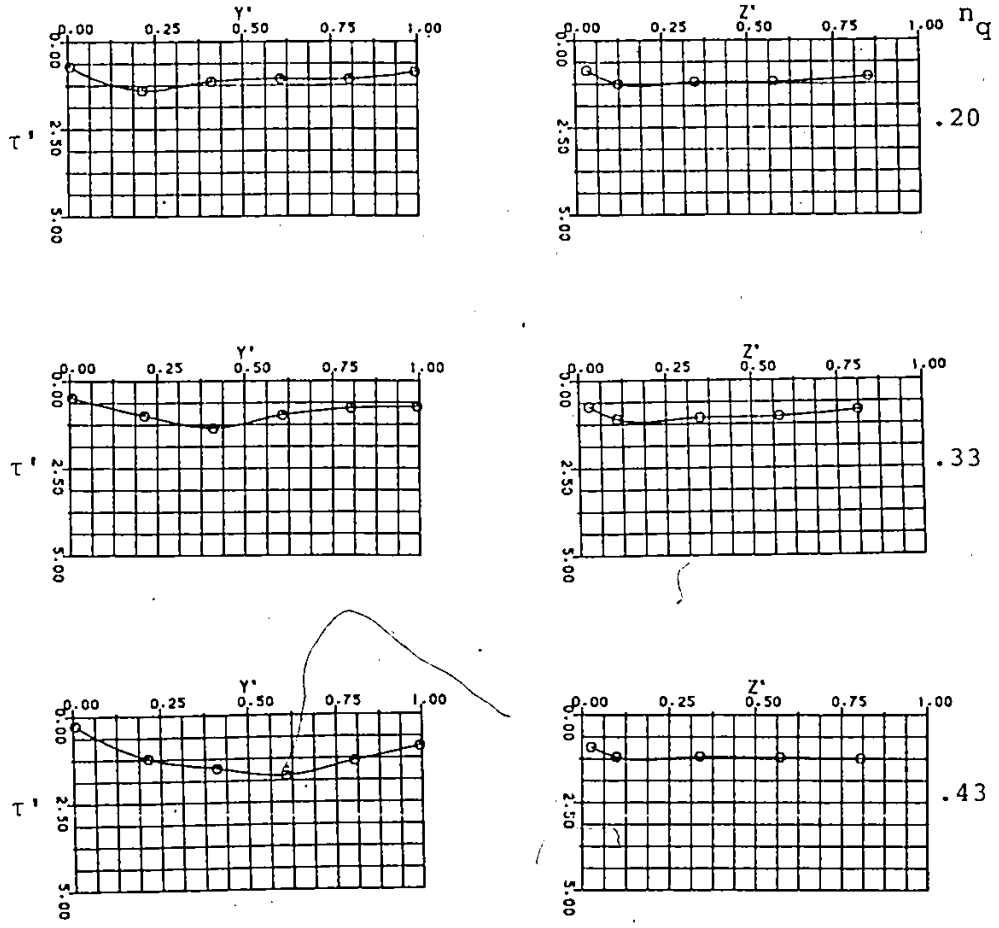

Figure 62: Shear Stress Distributions for Reverse Slope (X' = 1.31)

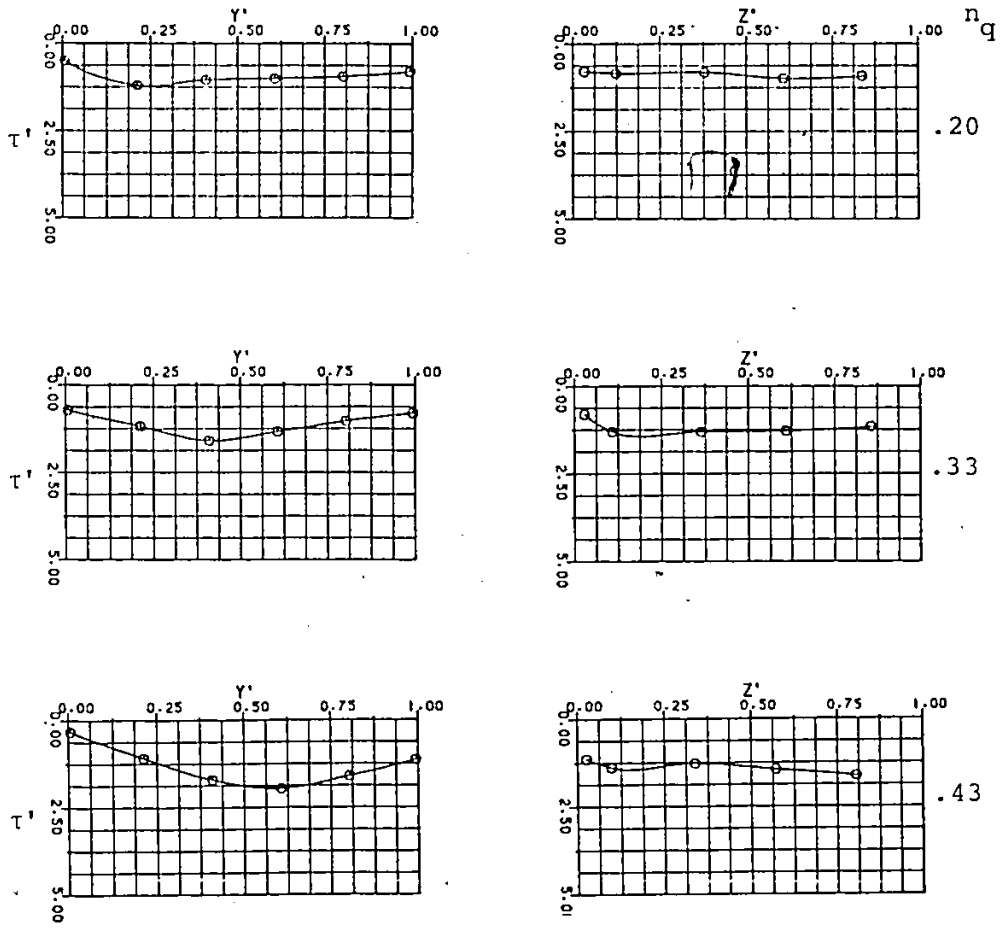

Figure 63: Shear Stress Distributions for Superelevated Slope (X'= 1.31)

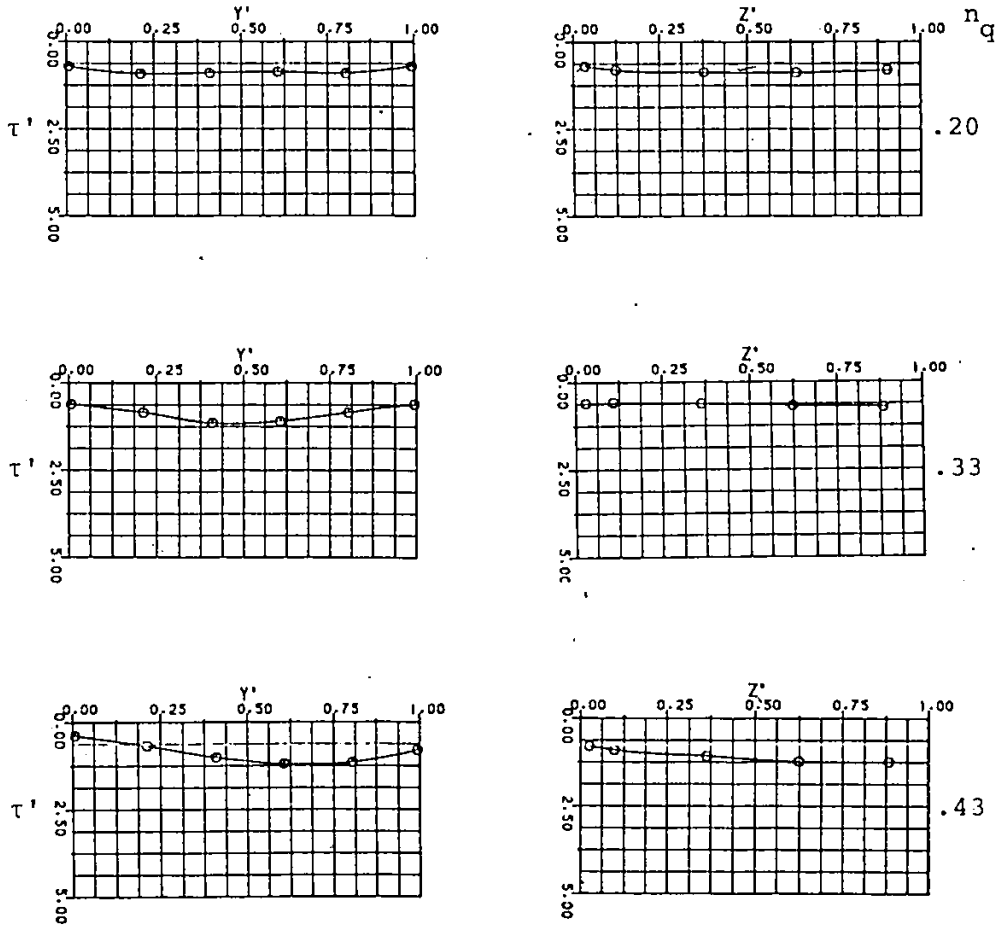

Figure 64: Shear Stress Distributions for Reverse Slope (X' = 2.95)

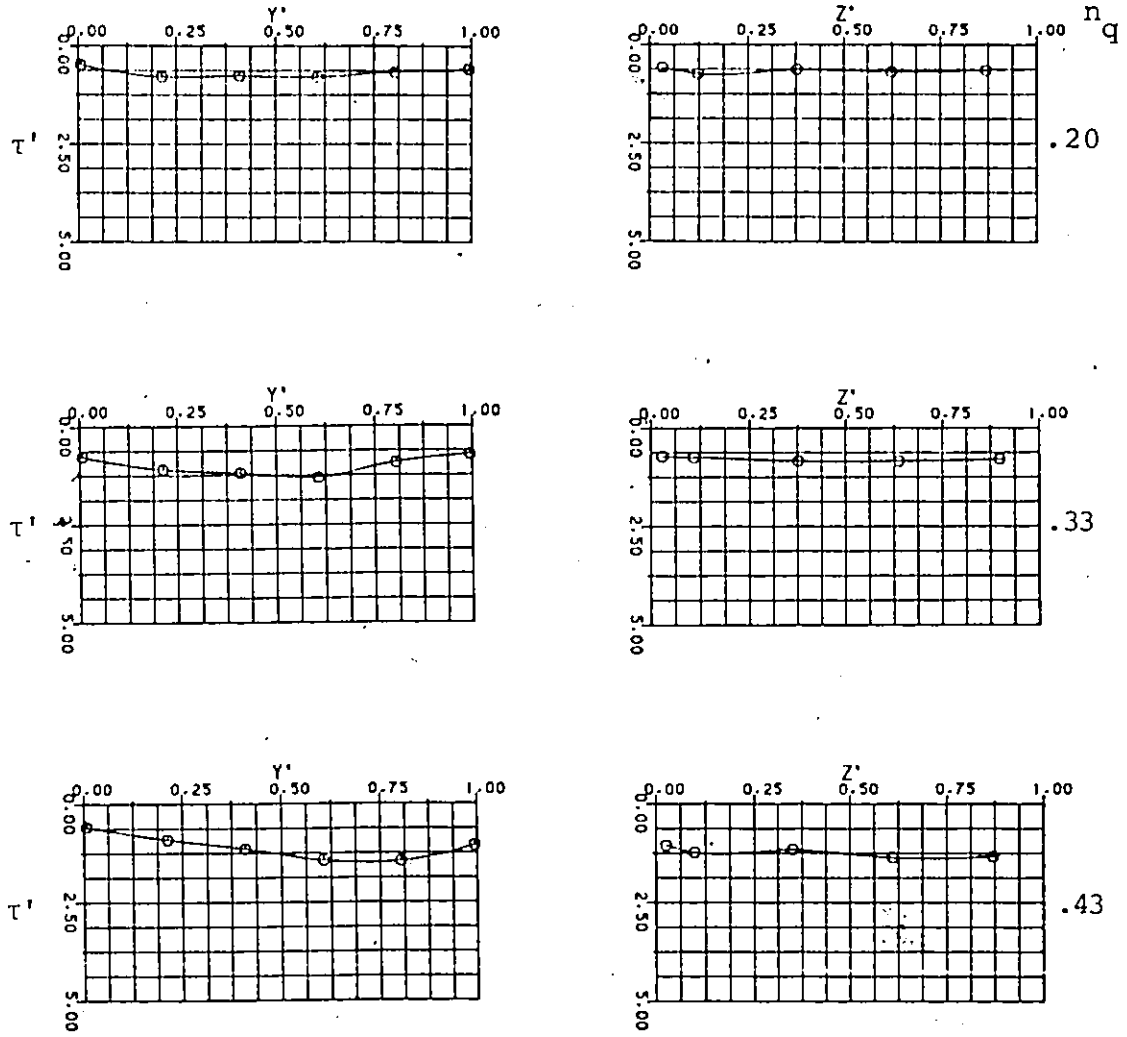

Figure 65: Shear Stress Distributions for Superelevated Slope (X' = 2.95)

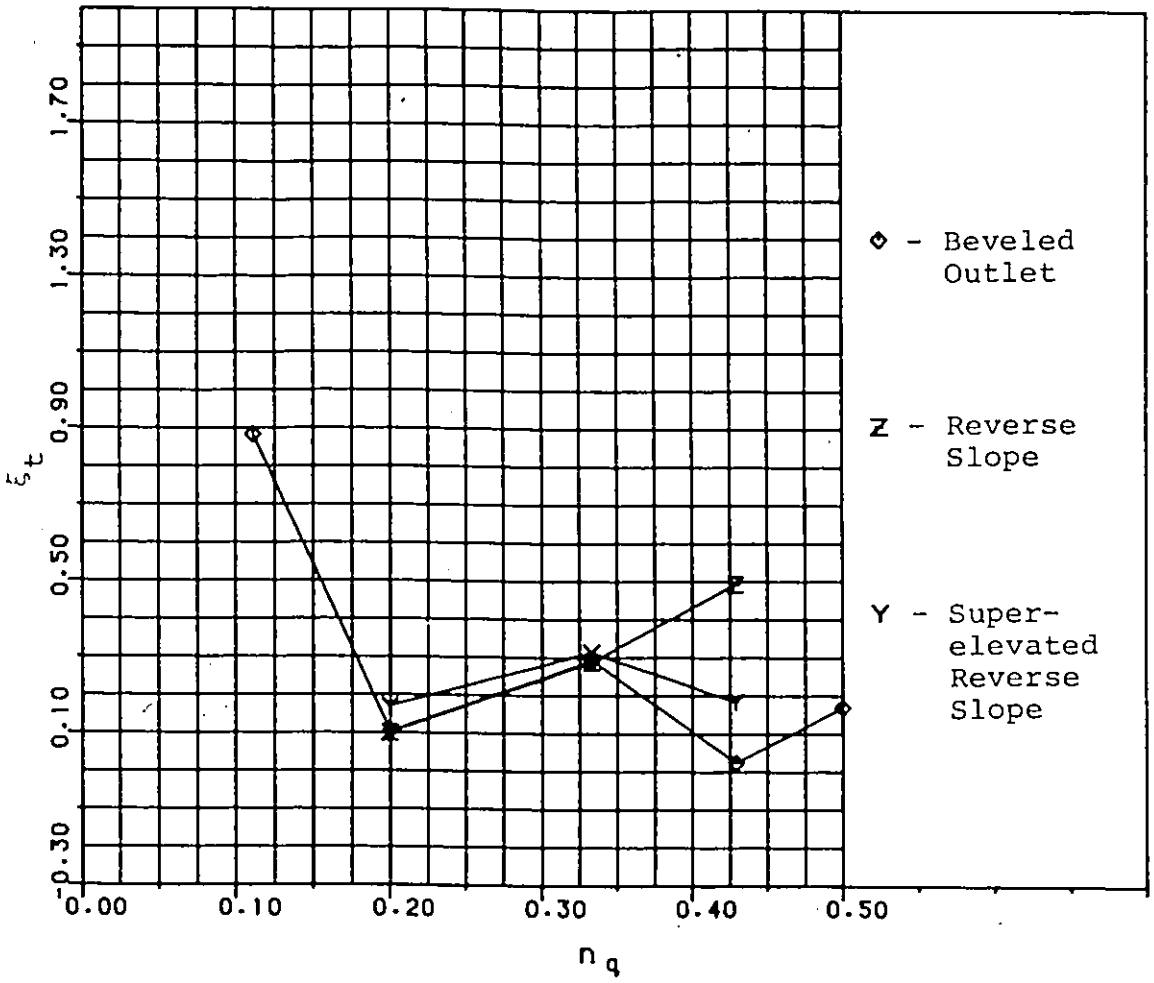

Figure 66: Mixing Energy Loss for Slope Modifications (X' = 1.31)

Chapter VI

CONCLUSIONS AND RECOMMENDATIONS

6.1 CONCLUSIONS

On the basis of the results in the previous chapter the following conclusions can be made:

1. The use of energy correction factors equal to unity when determining the kinetic energy level downstream of a confluence will lead to erroneous results. These have been found to vary from 1.95 to 1.14 for one particular plain junction just below the confluence. Thus, even when the incoming flows are small (11% of the combined flow) this correction must be made to accurately predict the downstream energy level.

2. For the design of channel junctions, allowance must be made for mixing energy losses. These have been found to be substantial, in some cases as high as the kinetic energy level downstream of the confluence, and in most cases larger than the losses to friction. Although the effects of outlet geometry on these losses have not been determined conclusively, other than to say that there is a definite effect, these losses are none-the-less substantial.

3. The outlet geometry and size of the lateral channel (or culvert) has been shown to have a marked effect on the downstream flow conditions. This has been demonstrated by the dye results, velocity and shear distributions. These velocity distributions first showed the considerable distortion of the flow field and its improvement with certain changes. Those outlet geometries that were particularly effective in improving the flow conditions were bevelling the downstream corner of the culvert outlet and the addition of a small deflection on the opposite corner, both of which helped to shift the profile closer to the center of the section. There was of course the disadvantage with the deflection wall of the backwater effect in the culvert, and thus these two effects would have to be weighed against each other for each particular installation to give the best overall culvert performance. Reverse slopes in the end of the culvert were found to have a marginal effect on the velocity distribution.

The shear stress distributions were particularly informative in that they showed up to a 330% increase in the local shear stress at the bed over that measured for uniform flow. This was reduced to a maximum of 150% by the addition of a beveled outlet, at just over one channel width downstream of the confluence. This will reduce the amount of channel boundary protection required to prevent erosion of the

natural stream. The amount of protection required for a particular installation must be evaluated based on the channel boundary material. Some reduction of these shear stresses was found possible by the addition of a reverse invert slope at the outlet of the culvert, although this was small.

6.2 RECOMMENDATIONS

Whereas time and budget constraints limited the scope of this particular study it would, never-the-less, be desirable to extend certain aspects of the work presented here. Firstly, certain portions of the laboratory investigation should be repeated using a model with non-rigid boundaries. Although the shear stress distributions presented here did indicate where abnormal scour might be concentrated, modelling with non-rigid boundaries would more conclusively answer any uncertainties as to the location, development and extent of this scour in the receiving channel. Furthermore, with non-rigid boundaries the effects of changing channel cross section (due to scour) on the hydraulic conditions could also be investigated.

Secondly, to better understand the effect of outlet geometry on the mixing head loss, it is recommended that a greater number of tests on each outlet geometry be conducted for different flow rates. While additional tests

would not reduce the spread in the data, a greater number of values would none-the-less better define the trends in these losses.

Thirdly, although it was conclusively shown that beveling of the culvert outlet improved the confluence performance, it is recommended that further work be done to determine the effect of different bevel sizes on the confluence flow characteristics. This might lead to still further improvements in hydraulic performance.

The present study, because of its basic nature, was limited to the use of rectangular-shaped cross sections for both the receiving and lateral channels. This was done to limit, as much as possible, the number of geometric variables to be considered. In light of the fact that both trapezoidal-shaped receiving channels and circular culverts are common field occurrences, it would be very informative to perform similar tests using a model with either or both of these characteristics. Such tests would increase the number of geometric variables, for instance channel side slope and bottom width for a trapezoidal section and diameter for a circular section.

BIBLIOGRAPHY

1. Atalik, A., "Hydraulic Conditions at the Confluence of Two Channels," thesis presented to the Middle East Technical University, Ankara, Turkey, in 1964, in partial fulfillment of the requirements for the degree of Master of Applied Science.

2. Barella, D.A., "Supercritical Flow at Open-Channel Junctions," U.S. Army Corps of Engineers, Los Angeles, Calif., July, 1975.

3. Behlke, C.E. and Pritchett, H., "The Design of Supercritical Flow Channel Junctions," Highway Research Record, #123, Highway Drainage and Scour Studies, Highway Research Board, NRC, Washington, D.C.

4. Bowers, C.E., "Studies of Open-Channel Junctions," (part V of Hydraulic Model Studies for Whitting Field Naval Air Station), St. Anthony Falls Hydraulic Laboratory, University of Minnisota, Technical Paper #6, Series B, January, 1950.

5. Brater, E.F. and King, H.W., Handbook of Hydraulics 6th ed, New York, McGraw-Hill, 1976.

6. Chow, V.T., Open Channel Hydraulics, New York, McGraw-Hill, 1959.

7. Daily, H.W. and Harleman, D.R.F., Fluid Dynamics, Massachusetts, Addison-Wesley, 1966.

8. French, J.L., "Tapered Inlets for Pipe Culverts," Journal of the Hydraulics Division, ASCE, Vol. 90, No. HY2, March, 1964, pp. 255-300.

9. Henderson, F.M., Open Channel Flow, New York, McMillan, 1966.

10. Karr,M.H. and Clayton, L.A., "Model Studies of Inlet Designs for Pipe Culverts of Steep Grades," Bulletin #35, Engineering Experimental Station, Oregon State College, Corvallis, 1954.

11. Kartha, V.C. and Leutheusser, H.J., "Distribution of Tractive Force in Open Channels," Journal of the Hydraulics Division, ASCE, No. HY7, July, 1970, pp. 1469-1483.

12. Lin, J.D. and Soong, H.K., "Junction Losses in Open Channel Flows," Water Resources Research, Vol. 15, No. 2, April, 1979, pp. 414-418.

13. Lorah, W.L., "Free-Surface Energy Losses in a 90° Junction Box," thesis presented to Colorado State University, Fort Collins, Colorado, in June, 1966, in partial fulfillment of the requirements of the degree of Master of Applied Science.

14. Palmer, H.K., discussion of "Flow Characteristics at Rectangular Open-Channel Junctions," by E.H. Taylor, Transactions of the American Society of Civil Engineers, No. 109, 1944, pp. 903-904.

15. Pardee, L.A., "Hydraulic Analysis of Junctions," Office Standard #115, Storm Drain Division, Bureau of Engineering, City of Los Angeles, Los Angeles, Calif., 1968.

16. Preston, J.H., "The Determination of Turbulent Skin Friction by Means of Pitot Tubes," Journal of the Royal Aeronautical Society, Vol. 58, 1954, pp. 109-121.

17. Sangster, W.M., Wood, H.W., Smerdon, E.T. and Bossy, H.G., "Pressure Changes at Open Channel Junctions in Conduits," Journal of the Hydraulics Division, ASCE, No. HY6, 1959, pp. 13-35.

18. Soong, H.K., "Effect of Lateral Inflow on Steady Open Channel Flows," thesis presented to the University of Connecticut, in 1976, in partial fulfillment of the requirements for the degree of Doctor of Philosophy.

19. Stevens, J.C., "Theoretical Energy Losses in Intersecting Pipes," Engineering News-Record, Vol. 97, No. 4, July 22, 1926.

20. Taylor, E.H., "Flow Characteristics at Rectangular Open Channel Junctions," Transactions of the American Society of Civil Engineers, Vol. 109, 1944, pp. 893-901.

Appendix A

TABLE 3-a

Maximum Bed Shear Stresses

Test#	n_q	X' = 1.31		X' = 2.95	
		τ'	Y'	τ'	Y'
Null-1	--	0.70	0.803	0.70	0.803
-2	--	0.91	0.607	0.91	0.607
-3	--	0.69	0.007	0.69	0.007
-4	--	0.76	0.410	0.41	0.410
-5	--	0.72	0.410	0.72	0.410
D1C-1	0.50	3.04	0.787	1.58	0.787
-2	0.43	3.09	0.393	1.39	0.787
-3	0.33	2.96	0.393	1.36	0.393
-4	0.20	1.70	0.393	0.92	0.393
-5	0.11	0.86	0.803	0.79	0.803
-11	0.50	2.80	0.787	1.39	0.590
-12	0.43	2.38	0.787	1.12	0.590
-13	0.33	2.10	0.993	1.36	0.393
-14	0.20	1.42	0.393	1.06	0.590
-15	0.11	1.06	0.590	0.65	0.787
-21	0.50	2.86	0.993	1.36	0.787
-22	0.43	2.87	0.393	1.07	0.787
-23	0.33	1.84	0.993	1.14	0.590
-24	0.20	1.50	0.590	0.99	0.590
-31	0.50	3.26	0.787	2.78	0.787
-32	0.43	2.94	0.607	1.70	0.803
-33	0.33	2.48	0.590	1.48	0.590
-34	0.20	1.41	0.607	1.07	0.607
-35	0.11	1.29	0.803	0.98	0.607
-41	0.50	2.95	0.590	1.58	0.803
-42	0.43	2.02	0.607	1.22	0.607
-43	0.33	1.38	0.410	0.92	0.607
-44	0.20	1.33	0.213	0.84	0.607
-45	0.11	1.98	0.410	1.49	0.410
-51	0.50	4.16	0.607	2.46	0.607
-52	0.43	3.52	0.410	1.99	0.410
-53	0.33	1.87	0.213	1.38	0.410
-54	0.20	1.46	0.213	0.99	0.213
-55	0.11	0.88	0.213	0.74	0.213

TABLE 3-a (Contd.)

Maximum Bed Shear Stresses

Test#	n_q	X' = 1.31		X' = 2.95	
		τ'	Y'	τ'	Y'
-61	0.50	2.59	0.607	1.54	0.607
-62	0.43	2.10	0.410	1.18	0.410
-63	0.33	1.66	0.410	1.09	0.410
-64	0.20	1.11	0.213	0.74	0.410
-65	0.11	0.91	0.410	0.74	0.410
-72	0.43	1.73	0.607	1.19	0.607
-73	0.33	1.35	0.410	1.14	0.410
-74	0.20	1.39	0.213	0.92	0.213
-82	0.43	1.96	0.607	1.46	0.803
-83	0.33	1.59	0.410	1.31	0.607
-84	0.20	1.20	0.203	0.79	.213/.607*
A1C-4	0.50	3.02	0.590	1.80	0.623
-3	0.43	2.92	0.590	1.59	0.590
-1	0.20	2.11	0.393	0.98	0.393
-5	0.11	1.09	0.787	0.80	0.993
D3C-2	0.43	0.91	0.410	0.85	0.393
-3	0.33	0.97	0.213	1.02	0.410
-4	0.20	0.93	0.213	0.76	0.410

* two maximums

TABLE 4-a

Turbulent Energy Loss Calculation

Test #	n_q	$H_{f_{m-t}}$ (m)	$H_{f_{l-t}}$ (m)	H_{T_m} (m)	H_{T_l} (m)	H_{T_t} (m)	$\frac{K_e V_t^2}{2g}$ (m)	ξ_t
D1C- 1	0.50	.00050	.00184	.00454	.01850	.01200	.0233	0.50
- 2	0.43	.00052	.00156	.00472	.01130	.00755	.0178	0.42
- 3	0.33	.00057	.00110	.00369	.00951	.00564	.0134	0.42
- 4	0.20	.00062	.00068	.00127	.00371	.00176	.0096	0.18
- 5	0.11	.00079	.00006	.00013	.00184	.00032	.0096	0.03
D1C-11	0.50	.00059	.00215	.00469	.01820	.01140	.0220	0.53
-12	0.43	.00053	.00154	.00422	.01510	.00890	.0146	0.61
-13	0.33	.00056	.00112	.00316	.00892	.00508	.0107	0.47
-14	0.20	.00065	.00071	.00249	.00457	.00291	.0089	0.33
-15	0.11	.00070	.00053	-.00090	-.00028	-.00083	.0064	-0.13
D1C-21	0.50	.00057	.00211	.00544	.01940	.01240	.0205	0.60
-22	0.43	.00053	.00153	.00691	.01520	.01050	.0152	0.69
-23	0.33	.00062	.00120	.00208	.00960	.00455	.0122	0.38
-24	0.20	.00072	.00078	.00096	.00446	.00166	.0090	0.18
D1C-31	0.50	.00057	.00208	.00737	.01920	.01330	.0220	0.60
-32	0.43	.00054	.00155	.00560	.01370	.00908	.0171	0.53
-33	0.33	.00059	.00113	.00325	.01100	.00583	.0120	0.49
-34	0.20	.00060	.00068	.00371	.00201	.00337	.0087	0.39
-35	0.11	.00075	.00057	.00080	.00136	.00086	.0078	0.11

$X' = 1.31$

TABLE 4-a (Contd.)

Test #	n_q	$H_{f_{m-t}}$ (m)	$H_{f_{l-t}}$ (m)	H_{T_m} (m)	H_{T_l} (m)	H_{T_t} (m)	$\frac{K_e V_t^2}{2g}$ (m)	ξ_t
D1C-41	0.50	.00051	.00281	-.00049	.00525	.00238	.0141	0.17
-42	0.43	.00053	.00214	.00080	-.00051	.00024	.0099	0.02
-43	0.33	.00053	.00116	.00197	.00279	.00224	.0077	0.29
-44	0.20	.00068	.00074	.00015	.00312	.00075	.0072	0.10
-45	0.11	.00052	.00041	.00540	.00271	.00510	.0058	0.88
D1C-51	0.50	.00064	.00189	-.00289	.03090	.01400	.0239	0.59
-52	0.43	.00059	.00153	-.00105	.02080	.00835	.0162	0.51
-53	0.33	.00062	.00113	-.00285	.01350	.00260	.0096	0.27
-54	0.20	.00061	.00067	.00076	.00335	.00128	.0068	0.19
-55	0.11	.00054	.00042	.00126	.00071	.00120	.0058	0.21
D1C-61	0.50	.00053	.00220	-.00162	.01530	.00684	.0158	0.43
-62	0.43	.00053	.00179	-.00043	.00742	.00294	.0108	0.27
-63	0.33	.00053	.00115	.00943	.00665	.00850	.0079	1.08
-64	0.20	.00064	.00071	.00078	.00135	.00089	.0072	0.12
-65	0.11	.00070	.00053	.00099	.00060	.00095	.0067	0.14
D1C-72	0.43	.00052	.00171	.00172	.00904	.00487	.0099	0.49
-73	0.33	.00057	.00121	.00103	.00484	.00230	.0080	0.29
-74	0.20	.00067	.00074	.00032	.00232	.00072	.0072	0.10
D1C-82	0.43	.00057	.00217	.00138	.00280	.00199	.0108	0.18
-83	0.33	.00055	.00118	.00150	.00439	.00246	.0079	0.31
-84	0.20	.00065	.00072	.00104	.00193	.00122	.0072	0.17

$X' = 1.31$

TABLE 4-a (Contd.)

Test #	n_q	$H_{f_{m-t}}$ (m)	$H_{f_{l-t}}$ (m)	H_{T_m} (m)	H_{T_l} (m)	H_{T_t} (m)	$\frac{K_e V_t^2}{2g}$ (m)	ξ_t
A1A- 1	0.50	.00064	.00079	.00358	.01320	.00839	.0177	0.47
- 2	0.43	.00063	.00071	.00453	.00589	.00511	.0147	0.35
- 3	0.33	.00065	.00063	.00275	.05510	.02000	.0118	1.72
- 4	0.20	.00070	.00056	.00168	.00519	.00238	.0086	0.28
A1C- 4	0.50	.00047	.00176	.00459	.01620	.01040	.0201	0.52
- 3	0.43	.00049	.00140	.00648	.01320	.00937	.0156	0.60
- 1	0.20	.00067	.00072	.00273	.00462	.00311	.0104	0.30
- 5	0.11	.00072	.00055	.00164	.00217	.00170	.0075	0.23
D3C- 2	0.43	.00061	.00200	-.00212	.00698	.00179	.0091	0.20
- 3	0.33	.00068	.00138	-.00113	.00502	.00092	.0088	0.10
- 4	0.20	.00072	.00078	-.00044	.00172	-.00001	.0070	-0.00

X' = 1.31

TABLE 4-a (Contd.)

Test #	n_q	$H_{f_{m-t}}$ (m)	$H_{f_{l-t}}$ (m)	H_{T_m} (m)	H_{T_l} (m)	H_{T_t} (m)	$\frac{K_e V_t^2}{2g}$ (m)	ξ_t
D1C- 1	0.50	.00090	.00224	.00287	.01690	.00989	.0150	0.66
- 2	0.43	.00094	.00198	.00328	.00989	.00612	.0113	0.54
- 3	0.33	.00100	.00153	.00240	.00822	.00434	.0082	0.53
- 4	0.20	.00108	.00114	.00044	.00288	.00093	.0068	0.14
- 5	0.11	.00139	.00120	.00052	.00224	.00072	.0076	0.09
D1C-11	0.50	.00107	.00263	.00443	.01820	.01130	.0139	0.82
-12	0.43	.00098	.00199	.00283	.01370	.00750	.0099	0.76
-13	0.33	.00102	.00157	.00143	.00720	.00335	.0078	0.43
-14	0.20	.00114	.00121	.00102	.00311	.00144	.0071	0.20
-15	0.11	.00123	.00105	-.00172	-.00111	-.00165	.0062	-0.27
D1C-21	0.50	.00105	.00258	.00411	.01800	.01110	.0133	0.83
-22	0.43	.00096	.00197	.00492	.01320	.00848	.0102	0.83
-23	0.33	.00112	.00170	.00067	.00820	.00318	.0083	0.38
-24	0.20	.00124	.00130	-.00127	.00220	-.00058	.0070	-0.08
D1C-31	0.50	.00101	.00252	.00543	.01730	.01140	.0134	0.85
-32	0.43	.00097	.00199	.00484	.01290	.00831	.0106	0.78
-33	0.33	.00101	.00155	.00001	.00774	.00258	.0074	0.35
-34	0.20	.00109	.00117	.00354	.00201	.00323	.0070	0.46
-35	0.11	.00124	.00106	-.00169	-.00113	-.00163	.0062	-0.26

X' = 2.95

TABLE 4-a (Contd.)

Test #	n_q	$H_{f_{m-t}}$ (m)	$H_{f_{l-t}}$ (m)	H_{T_m} (m)	H_{T_l} (m)	H_{T_t} (m)	$\frac{K_e V_t^2}{2g}$ (m)	ξ_t
D1C-41	0.50	.00099	.00328	-.00145	.00428	.00142	.0105	0.14
-42	0.43	.00101	.00262	-.00140	-.00270	-.00196	.0084	-0.23
-43	0.33	.00102	.00165	.00115	.00197	.00142	.0072	0.20
-44	0.20	.00118	.00124	-.00230	.00067	-.00171	.0063	-0.27
-45	0.11	.00096	.00084	.00541	.00272	.00511	.0057	0.90
D1C-51	0.50	.00114	.00239	-.00522	.02860	.01170	.0171	0.68
-52	0.43	.00108	.00202	-.00239	.01950	.00702	.0112	0.62
-53	0.33	.00112	.00163	-.00439	.01190	.00104	.0073	0.14
-54	0.20	.00112	.00118	.00044	.00302	.00096	.0064	0.15
-55	0.11	.00097	.00084	.00087	.00032	.00081	.0056	0.14
D1C-61	0.50	.00105	.00271	-.00075	.01620	.00772	.0112	0.69
-62	0.43	.00104	.00230	-.00057	.00728	.00281	.0084	0.33
-63	0.33	.00104	.00166	.00921	.00643	.00828	.0073	1.14
-64	0.20	.00119	.00127	.00085	.00142	.00096	.0071	0.14
-65	0.11	.00127	.00110	.00109	.00069	.00105	.0068	0.15
D1C-72	0.43	.00102	.00222	.00136	.00868	.00451	.0087	0.52
-73	0.33	.00111	.00176	.00107	.00487	.00234	.0076	0.31
-74	0.20	.00123	.00130	-.00005	.00195	.00035	.0069	0.05
D1C-82	0.43	.00114	.00274	.00155	.00297	.00216	.0094	0.22
-83	0.33	.00107	.00170	.00188	.00477	.00284	.0074	0.38
-84	0.20	.00120	.00127	.00084	.00173	.00102	.0069	0.15

$X' = 2.95$

TABLE 4-a (Contd.)

Test #	n_q	$H_{f_{m-t}}$ (m)	$H_{f_{l-t}}$ (m)	H_{T_m} (m)	H_{T_l} (m)	H_{T_t} (m)	$\frac{K_e V_t^2}{2g}$ (m)	ξ_t
A1								
A1A-1	0.50	.00108	.00123	.00250	.01210	.00730	.0114	0.64
-2	0.43	.00103	.00112	.00261	.00397	.00319	.0094	0.34
-3	0.33	.00110	.00108	.00227	.05460	.01970	.0084	2.34
-4	0.20	.00118	.00104	.00154	.00504	.00224	.0069	0.32
A1C-4	0.50	.00092	.00221	.00532	.01690	.01110	.0150	0.74
-3	0.43	.00092	.00183	.00345	.01020	.00635	.0128	0.50
-1	0.20	.00114	.00118	.00042	.00231	.00080	.0072	0.11
-5	0.11	.00121	.00104	-.00080	-.00026	-.00074	.0060	-0.12
D3C-2	0.43	.00121	.00260	-.00202	.00709	.00190	.0082	0.23
-3	0.33	.00133	.00203	-.00063	.00553	.00143	.0080	0.15
-4	0.20	.00133	.00139	-.00077	.00139	-.00034	.0068	-0.08

X' = 2.95

TABLE 5-a

Maximum Velocity Locations For Plain Junction

n_q	Z'	Y'	V_m	V_{b_m}	V_{rw_m}	%Unutilized area
0.50	.11	.53	2.0	1.9	2.0	20.
0.43	.48	.67	2.1	1.8	1.5	16.
0.33	.49	.60	1.9	1.7	1.4	7.
0.20	.51	.67	1.5	1.3	1.1	5.
0.11	.40	.67	1.5	0.9	1.0	5.
		X' = 1.31				
0.50	.49	.87	1.9	1.2	1.5	15.
0.43	.37	.80	1.7	1.2	1.1	10.
0.33	.39	.63	1.5	1.2	1.4	0.
0.20	.38	.53	1.4	0.9	1.1	0.
0.11	.50	.53	1.4	0.8	0.6	0.
		X' = 2.95				

Note: In Tables 3 to 7 Z' and Y' are the locations of the maximum velocity filament in the section and V_m, V_{b_m} and V_{rw_m} are maximum velocities in the section, on the bed and right wall respectively.

TABLE 6-a

Maximum Velocity Data For Guide Vanes - X' = 1.31

n_q	Z'	Y'	V_m	V_{b_m}	V_{rw_m}	%Unutilized area
0.50	.12	.53	2.1	1.8	1.9	15.
0.43	.37	.80	1.9	1.5	1.5	10.
0.33	.39	.47	1.6	1.4	1.5	0.
0.20	.38	.53	1.6	1.2	1.2	0.
0.11	.50	.40/.73*	1.2	1.0	1.0	0.
		Large Guide Vanes				
0.50	.65	.53	1.9	1.8	1.9	17.
0.43	.11	.40	1.8	1.7	1.7	5.
0.33	.37	.47	1.7	1.3	1.3	2.
0.20	.41	.73	1.5	1.2	1.1	0.
		Medium Guide Vanes				
0.50	.61	.80	2.1	2.0	2.1	15.
0.43	.66	.80	2.0	1.8	1.5	13.
0.33	.37	.67	1.8	1.6	1.5	4.
0.20	.37	.67	1.6	1.2	1.0	1.
0.11	.64	.53	1.4	1.0	0.9	1.
		Small Guide Vanes				

* two maximums-

TABLE 7-a

Maximum Velocity Data For Guide Vanes - X' = 2.95

n_q	Z'	Y'	V_m	V_{b_m}	V_{rw_m}	%Unutilized area
0.50	.70	.76	1.7	1.2	1.3	0.
0.43	.39	.67	1.6	1.1	1.1	0.
0.33	.39	.67	1.5	1.1	1.3	0.
0.20	.53	.80	1.3	1.0	.9	0.
0.11	.54	.73	1.2	.8	.7	0.
		Large Guide Vanes				
0.50	.37	.87	1.6	1.2	1.3	0.
0.43	.40	.93	1.5	1.0	1.2	0.
0.33	.40	.60	1.5	1.0	.9	0.
0.20	.63	.73	1.3	1.0	.8	0.
		Medium Guide Vanes				
0.50	.37	.93	1.8	1.6	1.4	0.
0.43	.38	.93	1.8	1.3	1.4	0.
0.33	.39	.80	1.4	1.2	1.1	0.
0.20	.40	.63	1.4	1.0	0.7	0.
0.11	.39	.60	1.4	1.0	.8	0.
		Small Guide Vanes				

TABLE 8-a

Maximum Velocity Location For Beveled Outlets - X' = 1.31

n_q	Z'	Y'	V_m	V_{b_m}	V_{rw_m}	%Unutilized area
0.50	.55	.53	1.9	1.7	1.4	3.
0.43	.37	.60	1.5	1.4	1.2	0.
0.33	.35	.47	1.4	1.2	0.8	0.
0.20	.46	.57	1.3	1.0	0.8	0.
0.11	.04	.40	1.4	1.4	1.2	0.
		Beveled Outlet				
0.50	.58	.53	2.3	2.2	1.7	17.
0.43	.03	.47	2.1	2.1	1.4	12.
0.33	.38	.33	1.7	1.3	0.8	2.
0.20	.39	.27	1.3	1.1	0.8	0.
0.11	.39	.60	1.3	1.0	0.9	0.
		Large Deflection Wall				
0.50	.10	.53	1.9	1.7	1.2	9.
0.43	.47	.47	1.8	1.4	1.2	0.
0.33	.11	.33	1.5	1.3	0.9	0.
0.20	.47	.60	1.5	1.0	0.8	0.
0.11	.65	.53	1.4	0.9	0.8	0.
		Small Deflection Wall				
0.43	.36	.67	1.6	1.3	1.1	0.
0.33	.37	.47	1.4	1.1	0.9	0.
0.20	.36	.73	1.4	1.1	1.0	0.
		Reverse Slope				
0.43	.63	.73	1.8	1.4	1.2	0.
0.33	.11	.47	1.5	1.3	1.0	0.
0.20	.40	.40/.87*	1.3	1.0	0.9	0.
		Superelevated Reverse Slope				

* two maximums

TABLE 9-a

Maximum Velocity Locations For Beveled Outlet - X' = 2.95

n_q	Z'	Y'	V_m	V_{b_m}	V_{rw_m}	%Unutilized area
0.50	.36	.87	1.5	1.2	1.3	0.
0.43	.36	.87	1.3	1.3	1.2	0.
0.33	.64	.67	1.2	.9	.6	0.
0.20	.63	.60	1.2	.9	.7	0.
0.11	.39	.67	1.2	1.2	1.1	0.
		Beveled Outlet				
0.50	.41	.53	1.7	1.5	0.9	0.
0.43	.43	.47	1.8	1.4	0.8	0.
0.33	.37	.33	1.3	1.1	0.6	0.
0.20	.65	.57	1.2	1.0	0.7	0.
0.11	.66	.40	1.3	0.9	0.8	0.
		Large Deflection Wall				
0.50	.38	.60	1.6	1.2	1.0	0.
0.43	.24	.50	1.4	1.1	0.7	0.
0.33	.64	.53	1.2	1.0	0.7	0.
0.20	.38	.67	1.3	0.8	0.7	0.
0.11	.66	.60	1.4	0.8	0.7	0.
		Small Deflection Wall				
0.43	.38	.77	1.4	1.1	1.1	0.
0.33	.39	.73	1.3	1.0	0.8	0.
0.20	.40	.73	1.3	0.9	0.9	0.
		Reverse Slope				
0.43	.39	.73	1.5	1.2	1.1	0.
0.33	.40	.60	1.4	1.1	0.8	0.
0.20	.66	.57	1.3	0.9	0.8	0.
		Superelevated Reverse Slope				

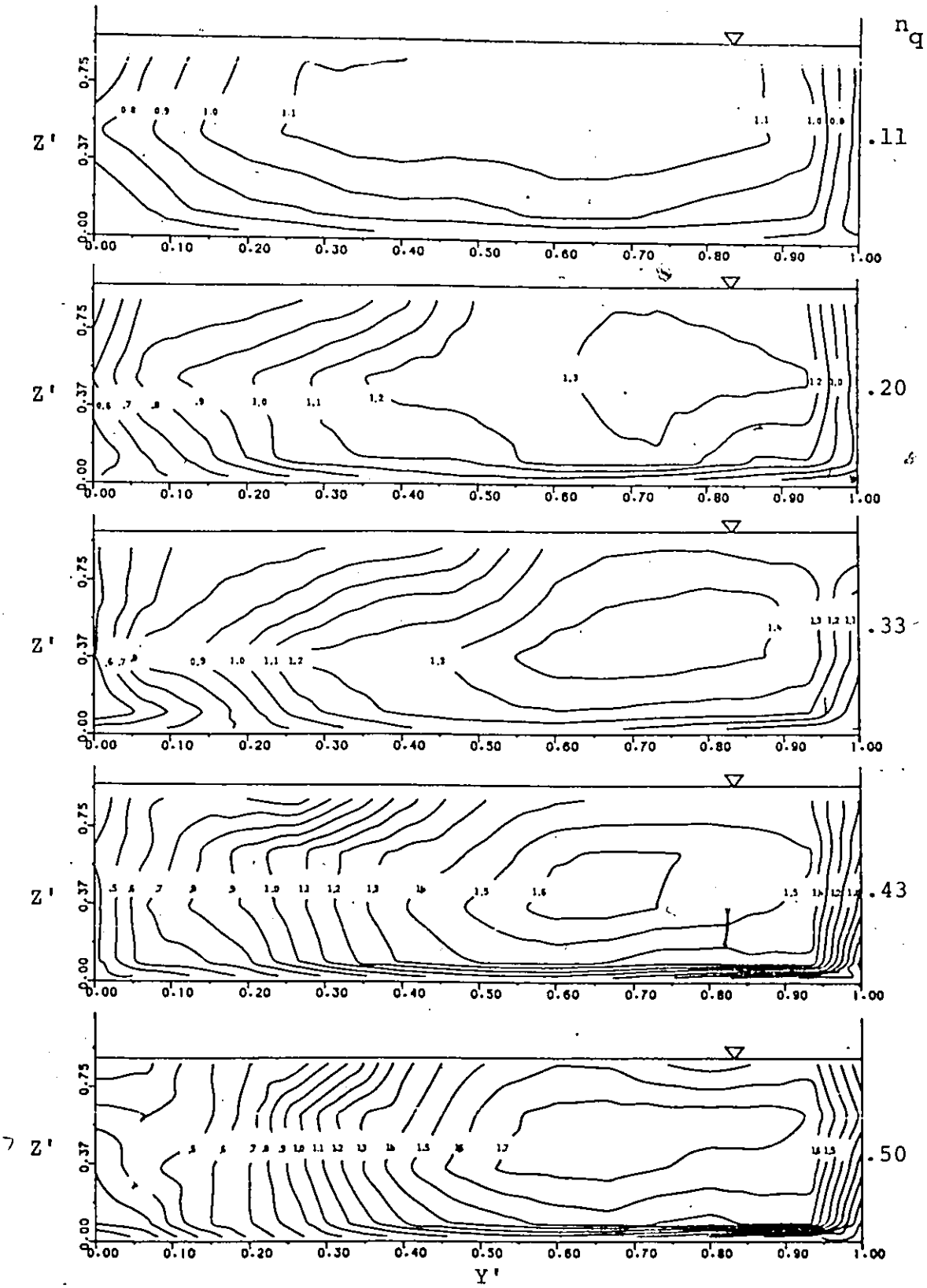

Figure 30-a: Isovel Patterns for 15.1 cm Guide Vanes (X' = 2.95)

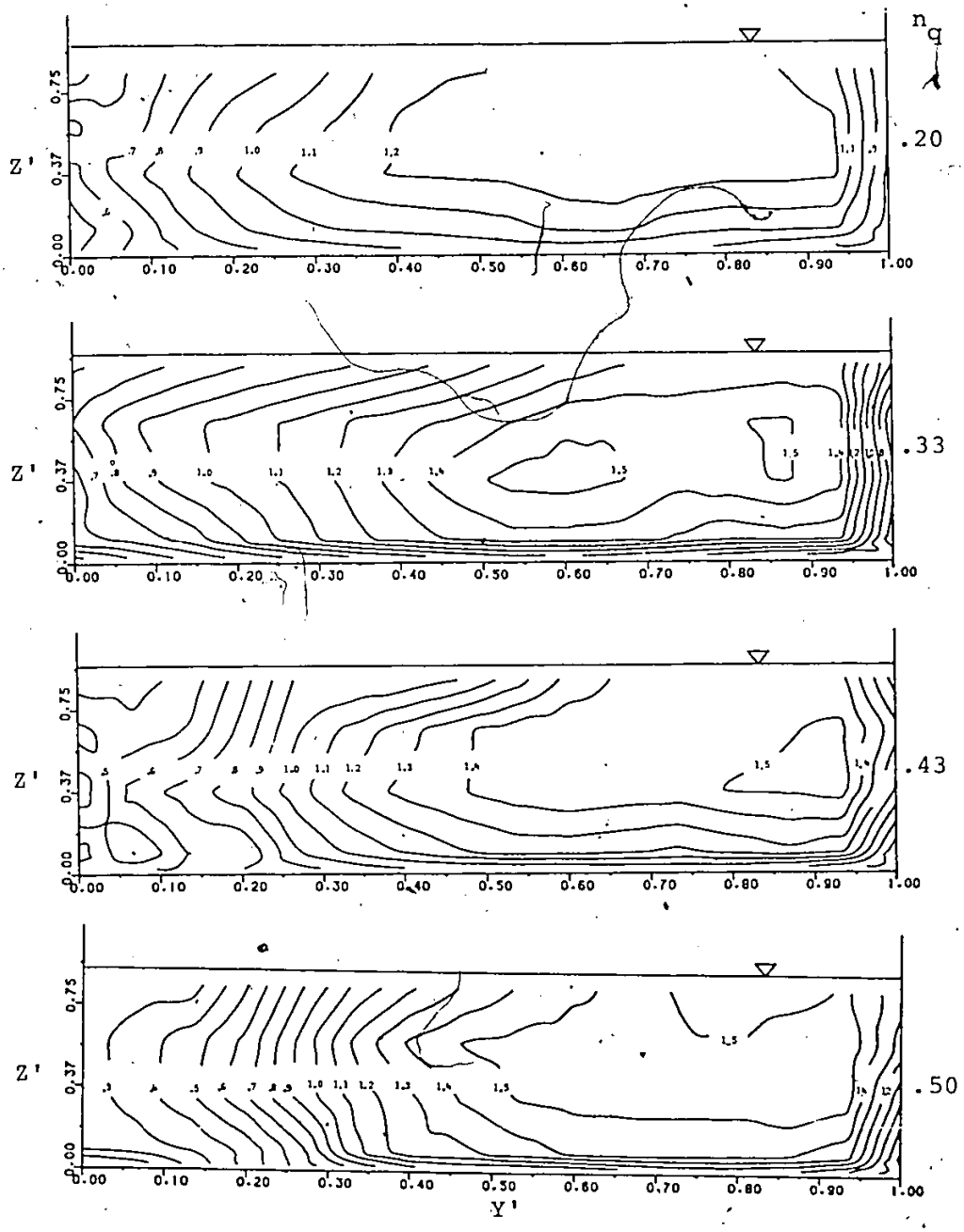

Figure 31-a: Isovel Patterns for 7.6 cm Guide Vanes (X' = 2.95)

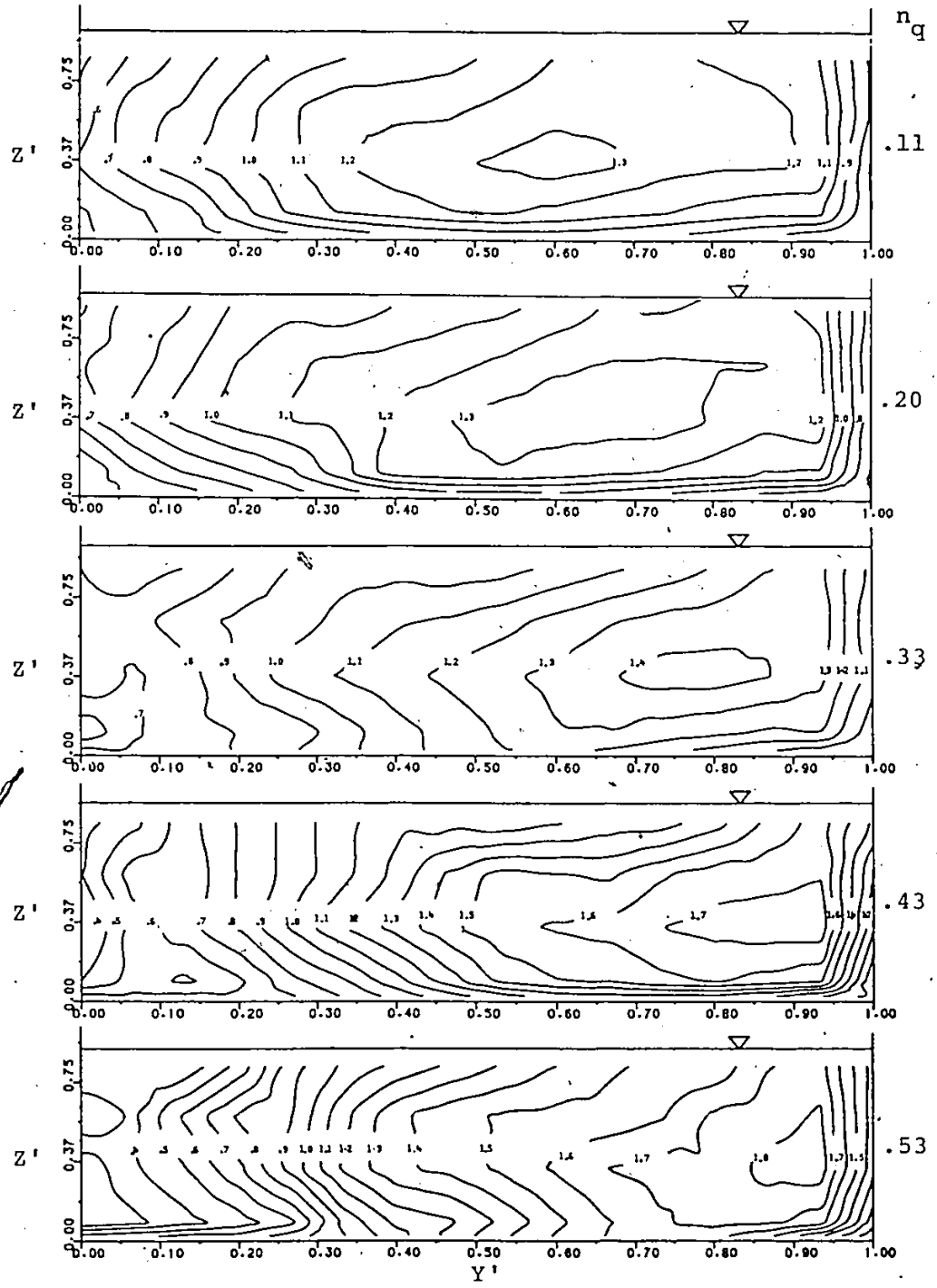

Figure 32-a: Isovel Patterns for 3.8 cm Guide Vanes (X' =2.95)

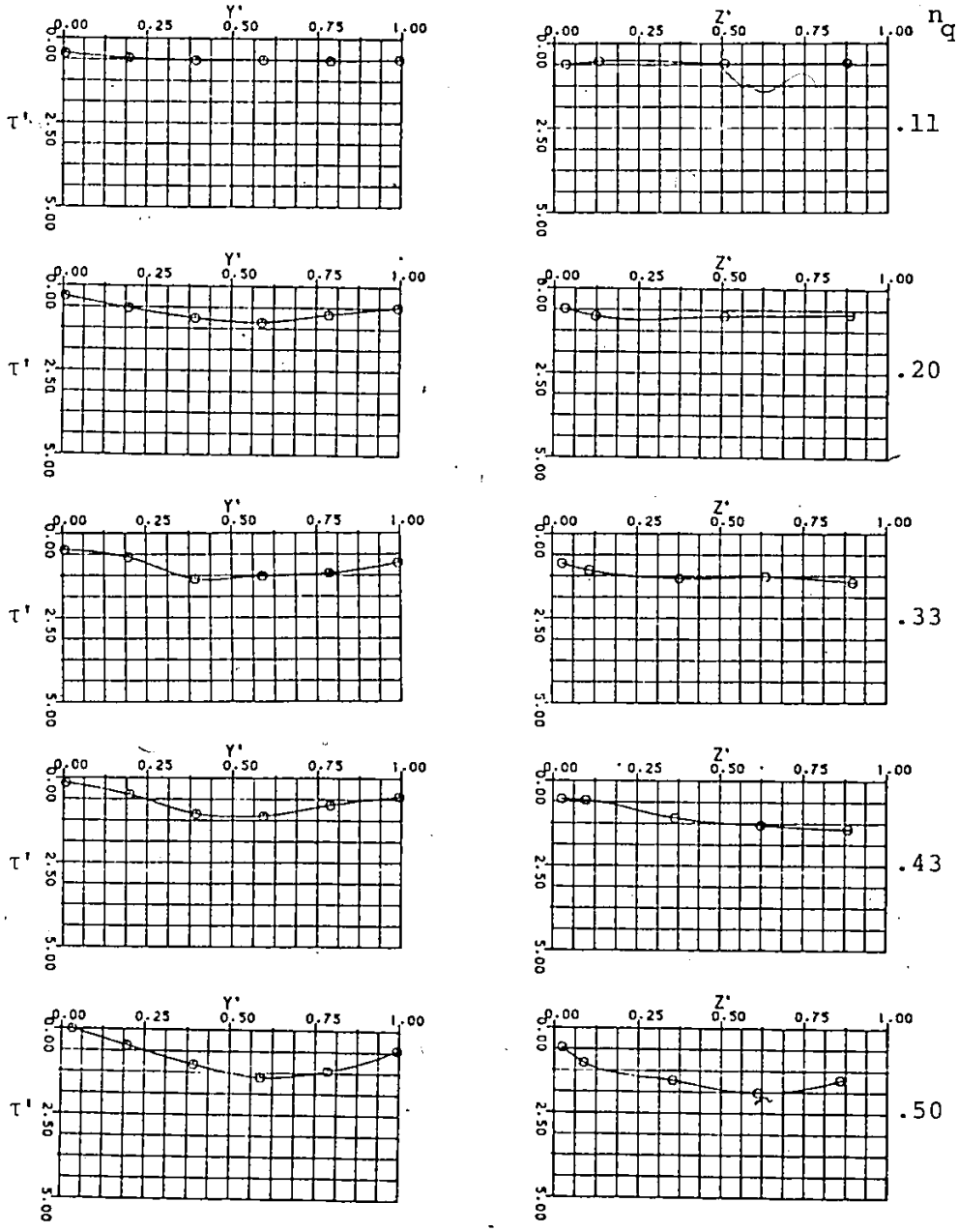

Figure 37-a: Shear Stress Distributions for 15.1 cm Guide Vanes (X' = 2.95)

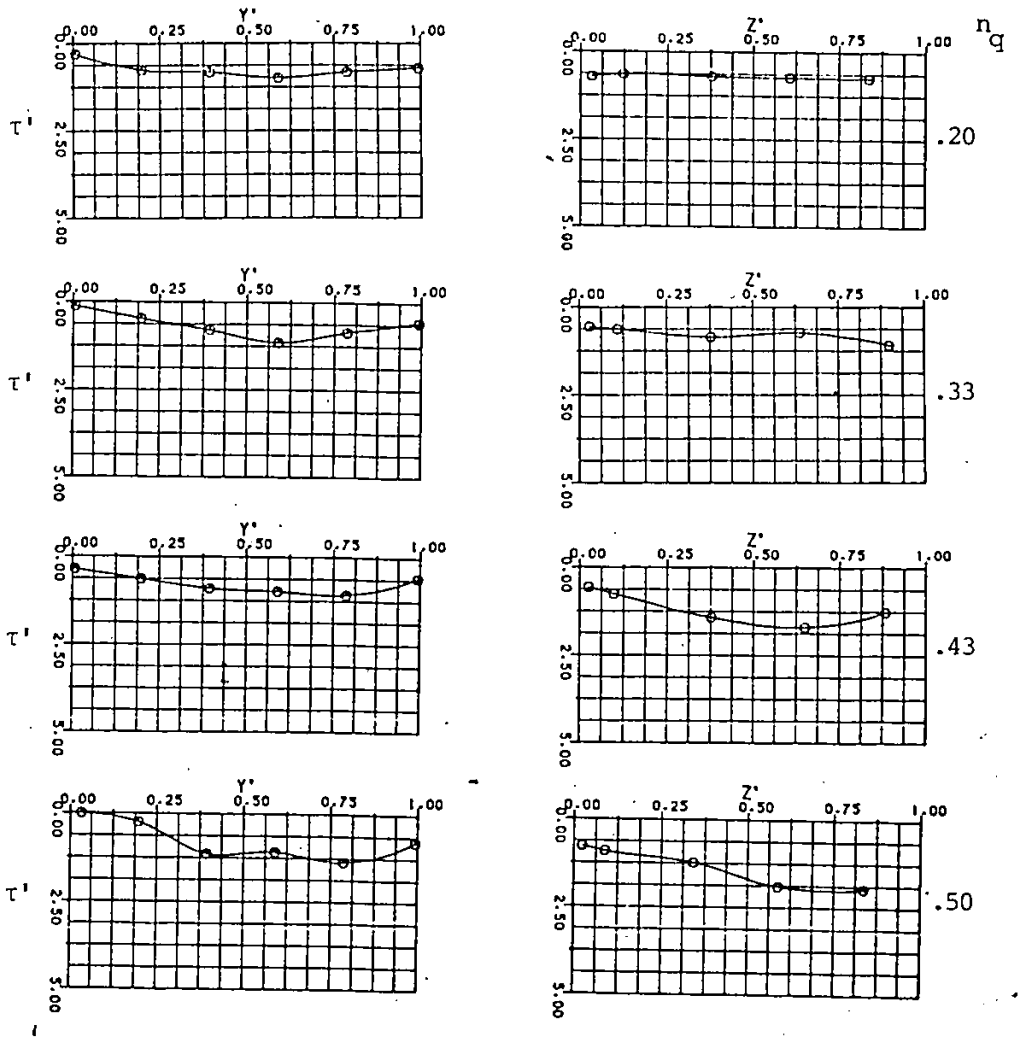

Figure 38-a: Shear Stress Distributions for 7.6 cm Guide Vanes (X' = 2.95)

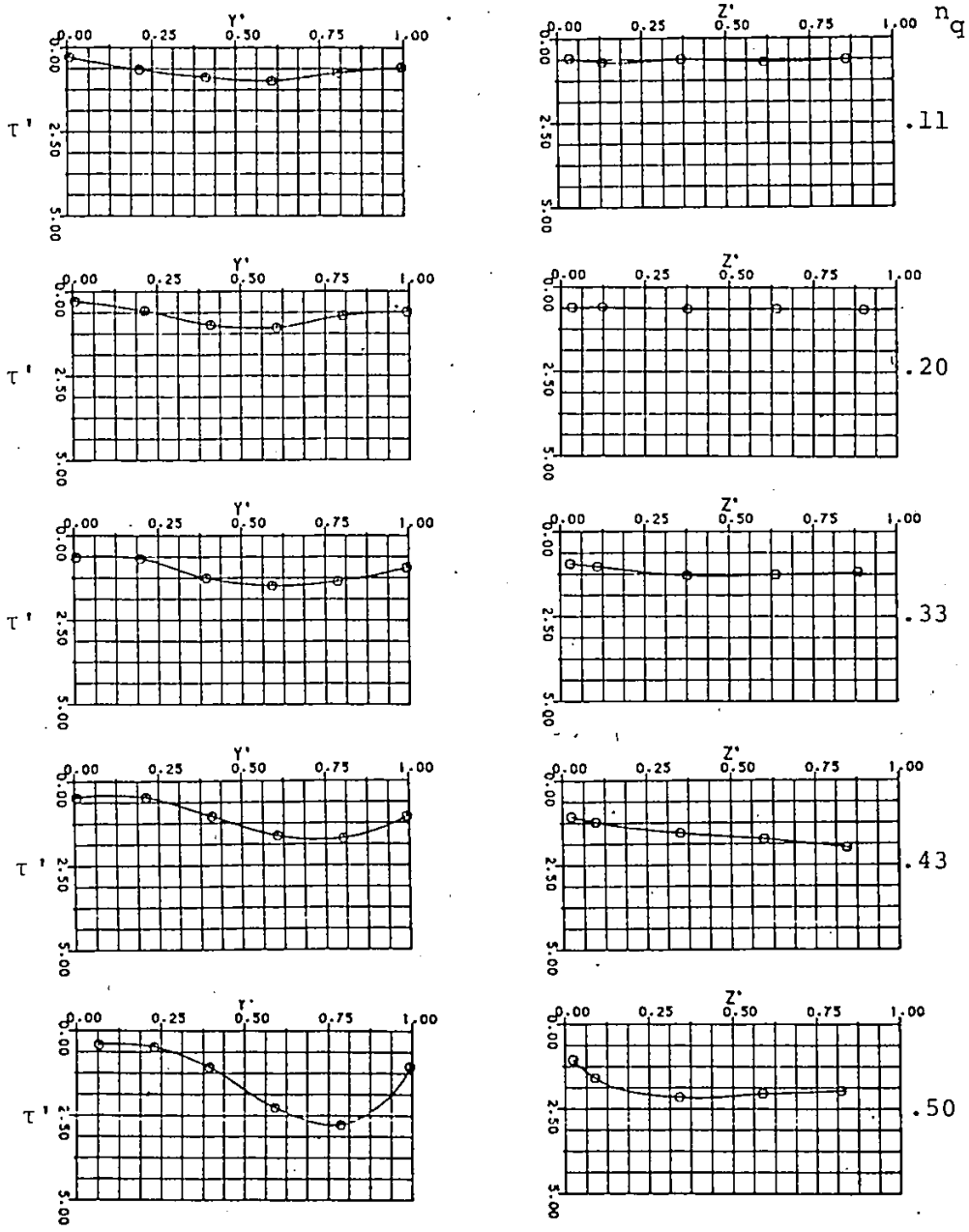

Figure 39-a: Shear Stress Distributions for 3.8 cm Guide Vanes (X' = 2.95)

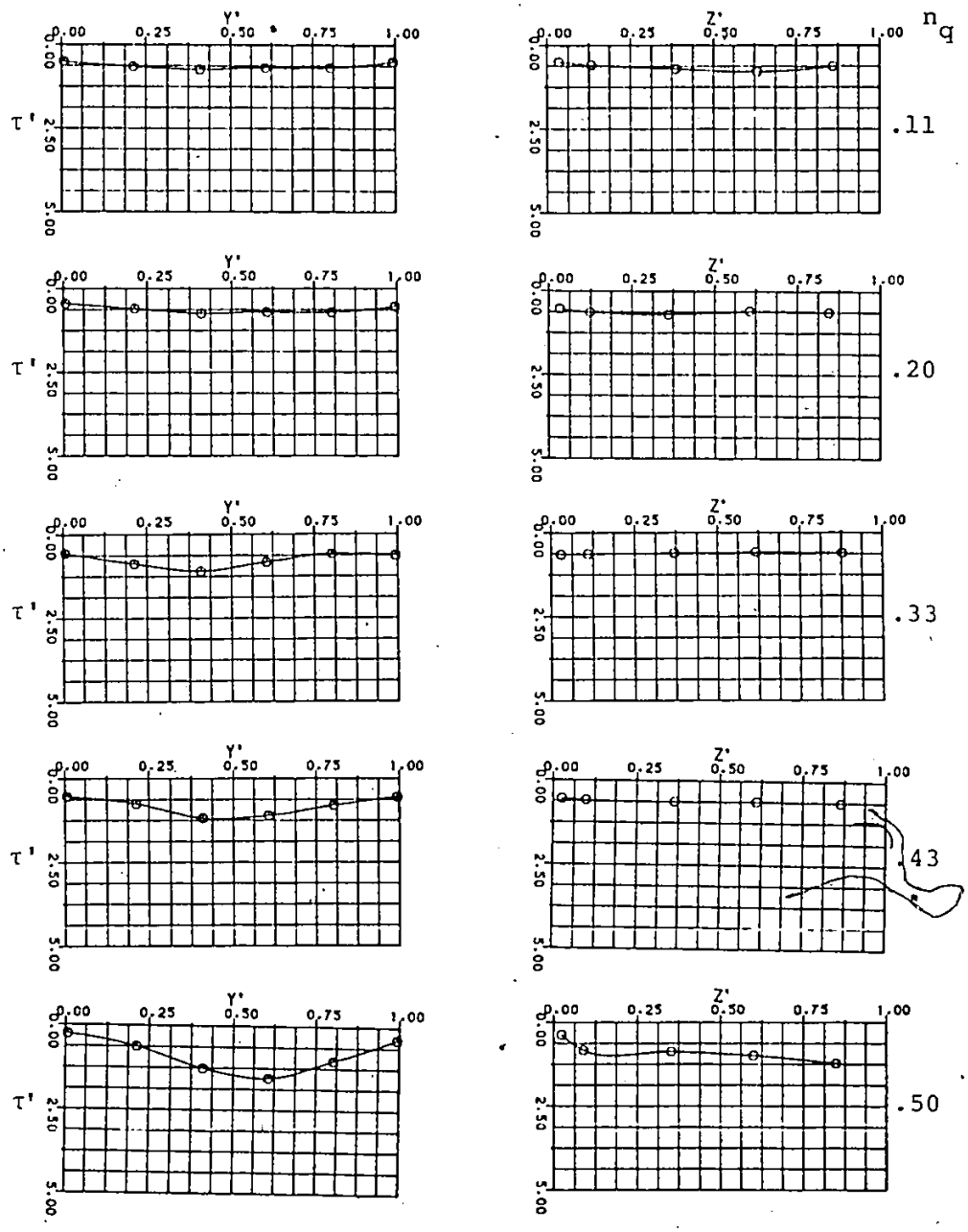

Figure 54-a: Shear Stress Distributions for Small Deflection Wall (X' = 2.95)

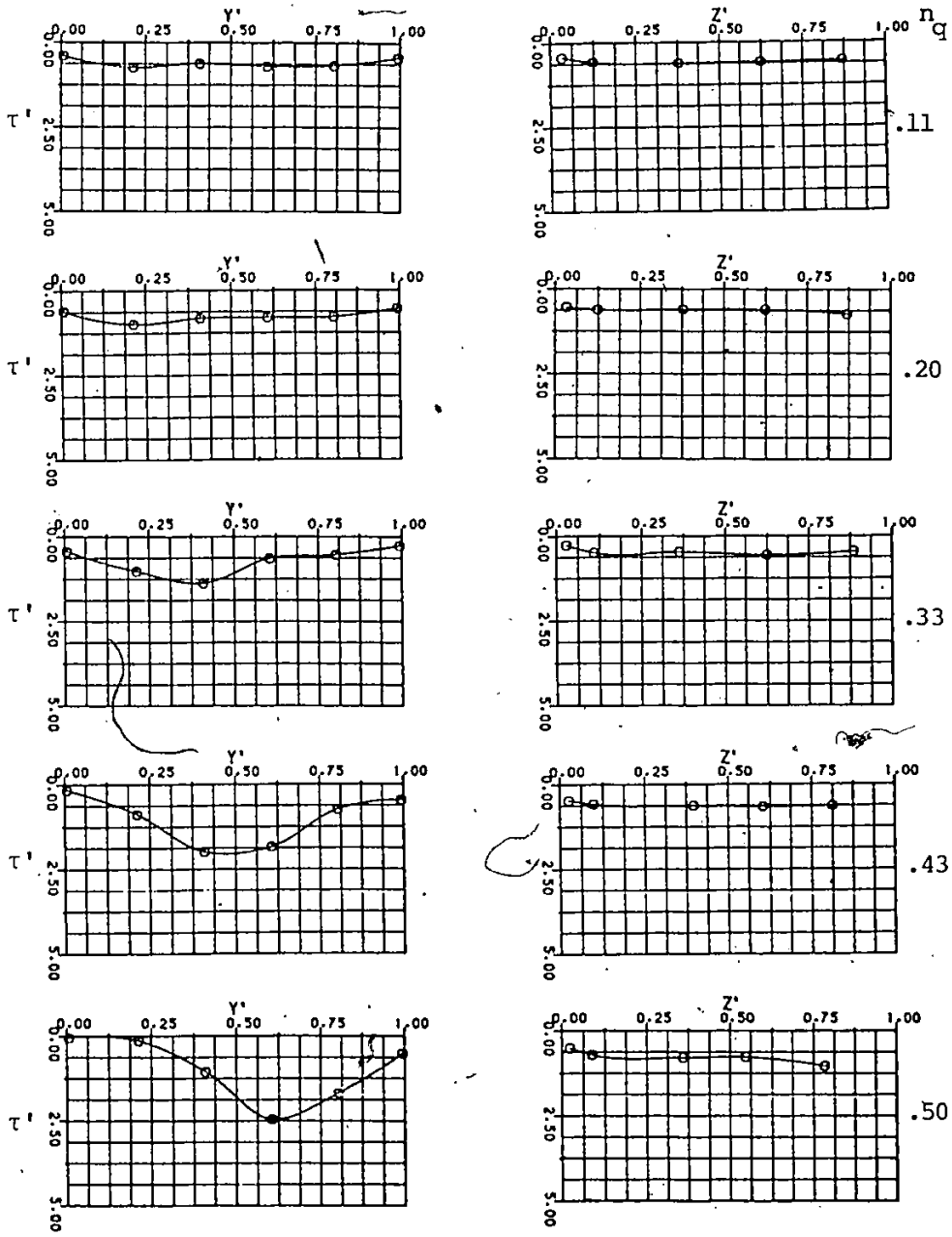

Figure 55-a: Shear Stress Distributions for Large Deflection Wall (X' = 2.95)